



UNIVERSITÀ
DEGLI STUDI
DI GENOVA



Analysis and optimization for decarbonizing a multi-energy system with geothermal storage: application to the Hönggerberg ETH Campus in Zurich

*European Master in Engineering for Energy
and Sustainable Buildings (EMESB)*

Thesis Submitted in Fulfilment of the Requirements for the
Double Degree of Master of Science
in

Energy Engineering - Università degli Studi di Genova

and

Energy and Solar Buildings - Université Savoie Mont Blanc

Thesis performed at the

Eidgenössische Technische Hochschule Zürich

Advisors

UNIGE: Prof. Stefano Bracco, Prof. Federico Delfino, Prof. Silvia Siri

ETH: Prof. Giovanni Sansavini, Paolo Gabrielli, Raphael Wu

USMB: Prof. Christophe Ménézo

Student: Alberto Acquilino

March 28, 2019

RINGRAZIAMENTI

Svolgere il lavoro descritto in queste pagine rappresenta l'esperienza formativa più piena della mia vita fino ad ora. A distanza di 7 mesi mi sento più preparato e maturo ad affrontare il mio futuro professionale.

Di questo vorrei ringraziare i miei Relatori, in primis Paolo Gabrielli, e il Reliability and Risk Engineering ETH Laboratory per la loro presenza e l'aiuto fornito in questi mesi.

Un pensiero speciale va alla mia compagna di avventura Mela, perché col sorriso si lavora meglio.

Ringrazio di cuore il Rotary Club di Genova nella persona del Presidente Giorgetta Alvigini per l'impegno a sostenere i giovani studenti a realizzare i loro sogni attraverso le loro attività e premi di studio.

M. perché è importante avere un vecchio professore che crede in quello che fai.

Giovanni che ogni giorno dimostra come si fa nella vita a seguire le proprie passioni.

Alessia, che con le splendide discussioni dei nostri momenti insieme mi spinge ogni giorno ad essere curioso e a dare il meglio di me.

Pietro, l'apripista e punto di riferimento di una vita, in cammino con un'amorevole Marta verso Santiago.

Isabella e Camillo, a cui dedico questo testo, perché i bei momenti come questo sono la vetta di un cammino che parte lontano.

28/03/2019

TABLE OF CONTENTS

<i>Abstract</i>	vii
<i>List of Tables</i>	x
<i>List of Figures</i>	xi
<i>Nomenclature</i>	xiii
<i>Introduction</i>	xv
Chapter 1: Multi-energy systems with geothermal storage	1
1.1. Why multi-energy systems	1
1.2. Multi-energy systems with seasonal geothermal storage.....	2
1.3. Geothermal systems for heating and air conditioning.....	4
1.3.1. Closed loop systems	6
1.3.2. Open loop systems	7
1.3.3. Horizontal collector systems	8
1.4. Worldwide distribution of direct-use geothermal systems.....	9
Chapter 2: State of the art of multi-energy systems optimization	11
2.1. Operational and design optimization	11
2.2. Optimization criteria	12
2.3. Literature review.....	13
Chapter 3: Description of the Anergy Grid and modeling of technologies	18
3.1. Description of the system	18
3.2. Standard auxiliary technologies	21
3.2.1. Boiler	22
3.2.2. Electrical chiller	22
3.2.3. Hot water thermal storage	23
3.3. Single node plant description.....	25
3.4. Technologies description	27
3.4.1. Heat Pump.....	27
3.4.2. Heat exchanger	29
3.4.3. Geothermal field	32
3.5. Network.....	36
3.5.1. Simple network scheme	37
<i>Mass balances</i>	38
<i>Energy balances</i>	38
3.5.2. Anergy Grid network scheme.....	39
Chapter 4: Mathematical model for the optimization of the Anergy Grid operation	42
4.1. The aim of the optimization model	42
4.2. Linearization techniques.....	43

4.2.1. Linearization through experimental data	43
4.2.2. Ordinary least squares method	45
4.2.3. Product between a binary and a continuous variable.....	46
4.2.4. McCormick envelopes linearization method	47
4.3. Input data.....	50
4.4. Decision variables	51
4.5. Constraints	52
4.5.1. Boiler	53
4.5.2. Electrical chillers	53
4.5.3. Hot water thermal storage	54
4.5.4. Heat pump	56
4.5.5. Low temperature heat exchanger	58
4.5.6. High temperature heat exchanger	59
4.5.7. Geothermal field.....	60
4.5.8. Thermal network	62
<i>Mass balances.....</i>	63
<i>Energy balances.....</i>	64
4.5.9. Energy balances at the user.....	66
4.6. Objective function	67
4.7. Time horizon representation	68
4.8. The optimization strategies.....	70
4.8.1. The optimization strategy for the single node	70
4.8.2. The optimization strategy for the Anergy Grid.....	72
Chapter 5: Analysis of results	73
5.1. Single node.....	73
5.1.1. Sensitivity on the number of typical days.....	73
5.1.2. Sensitivity on the mass flow rate.....	76
5.1.3. Optimal operation	79
<i>Winter week</i>	82
<i>Summer week</i>	83
5.1.4. Sensitivity on δ with and without HWTS	84
5.1.5. Sensitivity with temperature values at the outlet of the heat exchangers as decision variables .	85
5.2. Simple network	91
5.2.1. Sensitivity on network directions	91
5.2.2. Sensitivity on the mass flow rate.....	93
5.3. Anergy Grid	95
5.3.1. Sensitivity on the number of typical days.....	95
5.3.2. Sensitivity on the network directions and on the mass flow rate	97
5.3.3. Sensitivity on the number of hot water thermal storages and possibility of energy dissipation	101
Chapter 6: Conclusions	105
References	107
Appendix:	109

ABSTRACT

Nowadays, the issue of reducing CO₂ emissions due to energy production is spreading more and more in international political agendas. Several European programs propose guidelines with targets in the short and long term and find support and collaborations from the main universities and research centres in the field of energy engineering. Among these, the Eidgenössische Technische Hochschule of Zurich and the Università degli Studi di Genova confirm themselves to be an example of innovation and applied research, with the installation of high efficiency multi-energy systems and a polygeneration microgrid, respectively.

This project arises from a collaboration between these two important research centres and aims to formulate a linear optimization model for minimizing the CO₂ emissions of a multi-energy system, characterized by a seasonal geothermal storage with a water network at different temperature levels, to meet thermal and cooling demands. The difficulty of the work concerns the computational complexity that derives from the involvement of seasonal energy storage and the linearization of a strongly non-linear mathematical problem. This study continues the study performed at the ETH Separation Processes Laboratory on the optimal design of polygeneration systems with seasonal storage and proposes a general method to solve the optimal operation of a multi-energy system which involves a low temperature water network without predetermined flow directions and characterized by different energy levels.

The developed methodology is applied to the Anergy Grid, a multi-energy system with seasonal geothermal storage installed in the ETH Science City Campus located in

Hönggerberg, on the outskirts of Zurich. Finally, the behavior of the system is analyzed by performing a sensitivity analysis on the network configuration and on different characteristics of the multi-energy system.

LIST OF TABLES

Table 4.1: input data of the heat exchanger	45
Table 4.2: All possible products $y = ba$	47
Table 4.3: Input data of the boiler	53
Table 4.4: Input data of the electrical chiller	54
Table 4.5: Input data of the hot water thermal storage.....	55
Table 4.6: Input data of the heat pump.....	57
Table 4.7: Input data for the implementation of the McCormick envelopes linearization method.....	58
Table 4.8: Input data of the low temperature heat exchanger	59
Table 4.9: Input data of the high temperature heat exchanger	60
Table 4.10: Input data of the geothermal field	61
Table 4.11: Carbon dioxide emission factors of the energy vectors	67
Table 5.1: Utilization coefficients of the Anergy Grid	78
Table 5.2: Utilization coefficients of the Anergy Grid	86
Table 5.3: Utilization coefficients of the Anergy Grid	88
Table 5.4: Utilization coefficients of the Anergy Grid	90
Table 5.5: Utilization coefficients of the Anergy Grid	101

LIST OF FIGURES

Figure 1.1: Geothermal direct application worldwide in 2015	5
Figure 1.2: Closed loop representation (https://www.climatemaster.com/homeowner/side-links/faq)	6
Figure 1.3: Open loop representation (https://www.climatemaster.com/homeowner/side-links/faq)	7
Figure 1.4: Horizontal GT system representation (https://www.climatemaster.com/homeowner/side-links/faq)	8
Figure 1.5: Geothermal installed capacity by region	10
Figure 2.1: Optimization framework proposed by Gabrielli et al. [5]	16
Figure 3.1: View of the ETH Zurich Hönggerberg Campus	18
Figure 3.2: Anergy Grid installation at the Hönggerberg ETH Campus	20
Figure 3.3: Power technologies installed at the Science City	21
Figure 3.4: Single node plant scheme	25
Figure 3.5: counter-flow heat exchanger illustration	29
Figure 3.6: temperature diagram of the heat exchanger as a function of its length	30
Figure 3.7: Network representation of the Anergy Grid.....	36
Figure 3.8: Simple network scheme	37
Figure 3.9: plant scheme of the cluster	38
Figure 3.10: Mixing and splitting case illustration	39
Figure 3.11: Anergy Grid map with pipeline network.....	40
Figure 3.12: Anergy Grid network scheme	40
Figure 4.1: characteristic map of the heat pump installed in the HPL cluster	44
Figure 4.2: linearized curve of the exponential term. In blue: the exponential curve as a function of the mass flow rate. In red: the linearized curve adopting the OLS method. The minimized mean squared error is reported on the figure	45
Figure 4.3: bilinear surface representation	48
Figure 4.4: McCormick envelopes applied to the bilinear surface	49
Figure 4.5: Yearly profile of the g-function	62
Figure 4.6: Network MatrixA	63
Figure 4.7: Network MatrixB and mass flow vector	64
Figure 4.8: Node representation.....	64
Figure 4.9: Sensitivity analysis on the number of typical design days using M1 (blue line) and M2 (red line) methods.....	69
Figure 4.10: Optimization strategy for the single node	71
Figure 4.11: Optimization strategy for the Anergy Grid	72
Figure 5.1: Sensitivity on typical days for the single node with McCormick envelopes method	74
Figure 5.2: Current savings profile from ETH Sustainability Report.....	75
Figure 5.3: Sensitivity on typical days for the single node with the original equations	76
Figure 5.4: Sensitivity on the mass flow rate for the single node.....	77
Figure 5.5: Yearly profiles of the scheduling of technologies and mass flow rate.....	79
Figure 5.6: Heating and cooling fluxes requested (blue lines) and provided by the Anergy Grid (red lines).....	80

Figure 5.7: Yearly profiles of the borehole temperature and geothermal flux	81
Figure 5.8: Profiles of the scheduling of technologies and mass flow rate for a winter week	82
Figure 5.9: Profiles of the borehole temperature and geothermal flux for a winter week ...	82
Figure 5.10: Profiles of the scheduling of technologies and mass flow rate for a summer week	83
Figure 5.11: Profiles of the borehole temperature and geothermal flux for a summer week	83
Figure 5.12: Sensitivity analysis on δ coefficient with and without HWTS	84
Figure 5.13: Sensitivity on the mass flow rate for the single node with the new set of constraints.....	87
Figure 5.14: Yearly profiles of the scheduling of technologies and mass flow rate	88
Figure 5.15: Heating and cooling fluxes requested (blue lines) and provided by the Anergy Grid (red lines)	89
Figure 5.16: Yearly profiles of the borehole temperature and geothermal flux.....	89
Figure 5.17: Emission level with new set of constraints with addition of HWTS	90
Figure 5.18: Simple network configuration 1	91
Figure 5.19: Simple network configuration 2	92
Figure 5.20: Simple network configuration 3	92
Figure 5.21: Path sensitivity on the simple network	93
Figure 5.22: Sensitivity on the mass flow rate for the simple network.....	94
Figure 5.23: Sensitivity on typical days for the Anergy Grid with McCormick envelopes method.....	96
Figure 5.24: Selected network configuration	97
Figure 5.25: Educated solution of the network configuration.....	98
Figure 5.26: Sensitivity on the mass flow rate for the Anergy Grid	99
Figure 5.27: Strategy to increase the flow rate for the selected network configuration	100
Figure 5.28: Strategy to increase the flow rate for the educated network configuration ...	100
Figure 5.29: Sensitivity on the number of HWTS for the Anergy Grid.....	102
Figure 5.30: Anergy Grid emission level with dissipation.....	103
Figure 6.1: Ambient temperature profile.....	109

NOMENCLATURE

Abbreviations

CO ₂	Carbon dioxide
MILP	Mixed integer linear programming
MINLP	Mixed integer non-linear programming

Technologies

AG	Anergy Grid
edHP	Electrical driven heat pump
GT	Geothermal field
HTHE	High temperature heat exchanger
HWTS	Hot water thermal storage
LTHE	Low temperature heat exchanger

Superscripts

air	Ambient air
B	Boiler
CH_LT	Chiller high temperature
CH_LT	Chiller low temperature
cond	Condenser
E	Electricity
eva	Evaporator
G	Natural gas
GT	Geothermal field
H	Heating
H_D	Heating demand
HP	Heat pump
HT	High temperature cooling
HT_D	High temperature cooling demand

HTF	Heat-transfer fluid
HWTS	Hot water thermal storage
in	Inlet
LAB	Laboratory water
LM	Logarithmic mean
LT	Low temperature cooling
LT_D	Low temperature cooling demand
out	Outlet
T	Time horizon

Cluster

HPL	Cluster of buildings
HPZ	Cluster of buildings
HC0	Cluster of buildings
HWN	Cluster of buildings
HCP	Cluster of buildings

Geothermal field

GT HPL	Geothermal storage
GT HC	Geothermal storage
GT HW0	Geothermal storage

INTRODUCTION

In 2008, ETH University joined officially the “Ressourcen und Umweltmanagement der Bundesverwaltung” (RUMBA) program. Its main objective is the continuous reduction of operational and product-related environmental burdens of the civilian federal administration, which can mainly be achieved through cost savings and efficiency increase, the coordination of environmental activities of the civilian federal administration and the model role of the government in the environmental field. Each ETH department is represented in the RUMBA Commission with environmental delegates. Thus, the University departments are involved in the effort to improve the energy efficiency and sustainability of ETH facilities in order to achieve a rapid reduction of CO₂ emissions in the energy usage of its infrastructure [1]. For this reason, ETH University installed the Anergy Grid at the Science City of Hönggerberg Campus, which is in operation since 2013. It consists of a dynamic underground storage system that aims to replace the heat and cold production from fossil-based technologies. This can be realized thanks to a smart networking of heating sources and sinks in combination with a seasonal shift.

The present study aims to model the entire energy system which operates at the Science City in a linear optimization framework, to identify the most important parameters to control the system and to find their values along the year for the optimal operation of the system, minimizing annual CO₂ emissions. The work has been performed within the Reliability and Risk Engineering Laboratory of ETH in collaboration with the Naval, Electrical, Electronic and Telecommunications Engineering Department (DITEN) and the Computer Science, Bioengineering, Robotics and Systems Engineering Department

(DIBRIS) of the Università degli Studi di Genova, the “Laboratoire Optimisation de la Conception et Ingénierie de l’Environnement” (LOCIE) of the Université Savoie Mont Blanc and the Separation Processes Laboratory of ETH. The mathematical model is formulated as a mixed-integer linear programming (MILP) and the optimization is implemented in MATLAB using the academic free license of GUROBI and CPLEX solvers.

The structure of the thesis is reported in the following:

- Chapter 1, *Multi-energy systems with geothermal storage*. The concept of multi-energy systems is introduced with a focus on the integration with geothermal storage systems and the consequent implications on the dynamics of the system.
- Chapter 2, *State of the art of multi-energy systems optimization*. The main studies in the literature regarding the context of energy systems optimization are described.
- Chapter 3, *Description of the case study*. A detailed illustration of the Anergy Grid is provided. The layout of the Hönggerberg Campus, the requested power demands, the working principles of the installed conversion technologies and of the geothermal field, the hydraulic network are described. Three different configurations of the case study are reported. Moreover, a complete overview of the mathematical techniques adopted to linearize the equations of the system is made.
- Chapter 4, *Mathematical model*. The mathematical programming model developed in order to plan the operation of the Anergy Grid is illustrated in detail.

- Chapter 5, *Analysis of results*. The strategy adopted to solve the optimization problem and the solutions for the three configurations of the case study are analysed. A sensitivity analysis on relevant parameters for the operation of the system is performed and energy considerations are made. Finally, some significant graphs concerning the operation of the system are shown.
- Chapter 6, *Conclusions*. Considerations on the obtained results of this study are made and possible outlooks for future developments are proposed.

CHAPTER 1: MULTI-ENERGY SYSTEMS WITH GEOTHERMAL STORAGE

This chapter describes the benefits produced by the use of multi-energy systems, which motivate their growing development in recent years. Subsequently, the reasons justifying the growing interest in seasonal geothermal storage technologies are reported. Finally, a general description of direct-use geothermal fields is provided.

1.1. Why multi-energy systems

Concerns exist regarding the contribution of energy production to global warming, as well as other environmental problems such as air pollution, acid precipitation, ozone depletion, forest destruction, and radioactive emissions [2]. There are different alternatives to fossil fuels, such as hydropower, solar, wind, geothermal and nuclear energy. The use of many of the available natural energy resources is limited due to their reliability, quality, and energy density. Innovative technologies aimed at mitigating global warming are being proposed and tested in several countries. Among these technologies, multi-energy systems can make an important contribution thanks to their potential for high efficiencies as well as low operating costs and pollution emissions per energy output. For all these reasons, multi-energy systems can reduce greenhouse gas emissions, especially carbon dioxide. Since a multi-energy system often needs a lower amount of fuel to provide the same power output compared to a conventional power plant, a multi-energy plant typically emits less greenhouse gases. Despite this benefit, some restrictions exist to the use of multi-energy systems in a residential district because of their on-site gas emissions. Another important advantage of using multi-energy systems is that they can reduce costs and energy losses because they require shorter electricity transmission lines and fewer distribution units. The conventional

production of electrical energy typically takes place from a centralized power plant that is generally located far from the end users. Hence, the transmission and distribution electrical losses from a centralized system to the user are on average around 9%. Such advantages have motivated researchers and designers to develop suitable multi-energy systems. Often, the most significant factor in the implementation of a multi-energy system is the potential improvement in the efficiency. Further assessments before designing or selecting multi-generation plants, for instance evaluations of initial investment and operating costs, are necessary to ensure efficiency and profitability to the construction and performance of a multi-energy system [3].

Several analysis and optimization studies of multi-energy systems have been published in the recent years. Some of these systems are being considered as options for mitigating climate change. Note that various methods are available to achieve each purpose of a multi-energy system; hence the appropriate application for each case is important in meeting the system's requirements.

1.2. Multi-energy systems with seasonal geothermal storage

Multi-energy systems are increasingly based on the production of energy from renewable sources. The fluctuation and non-programmability of renewable energy make the management of a system with a strong sharing of green energy unreliable and the installation of energy storage technologies becomes an unavoidable necessity. For this reason, the development of hot water thermal storages and electric batteries are having a major development in the current market. These technologies are able to offset the imbalances due to short-term fluctuations in the production of energy from widely used sources such as solar photovoltaics and wind power. However, such renewable technologies present a more marked fluctuation over long periods, with seasonal

frequency, making the production of electricity more intense during the summer rather than during the winter or vice versa depending on the type of technology. For this reason, in recent years numerous studies and applications have been conducted to develop storage technologies capable of maintaining the energy accumulated over long periods, guaranteeing very low energy losses. This would make it possible to store the energy produced in excess during the most favorable seasons, to be able to use it months later during the most disadvantageous periods for the production of energy. Such developments have been realized for electricity with fuel cells and for thermal energy with geothermal fields. This is making seasonal geothermal fields of particular interest in current research [4]. By the way, maintaining optimal management of this technology still remains an open challenge due to the large complexity of the optimization problem, which involves numerous decisional variables and a copious set of input data due to the long time horizon that must be considered.

In 2018, Gabrielli et al. [5] of ETH have published a study on a multi-energy system with seasonal storage facing in a very detailed way the problem of large computational complexity. They take as reference the work of Pfenninger [6], in which numerous clustering methods of typical days are analyzed within long time horizons in order to make computation calculations possible. They propose two methods that simplify the problem from the computational point of view with respect to the full-scale case, however, able to faithfully follow the long dynamic dictated by geothermal storage. These methods will be described more in detail in the following chapters.

The installation of a geothermal storage to meet the thermal power and cooling power demands of a district necessarily implies the presence of a hydraulic network that connects the geothermal field with the users. The integration of a network of pipes that

transports heat from one point to another of the plant according to a linear formulation model is a problem that has already been addressed in the literature by Weber and Shah [7] and Bracco and Siri [8]. Such models allow to describe both the design and operational optimization of a district heating network linked to a multi-energy system. Nevertheless, in literature there is not a linear description for an optimization problem of a hydraulic network which is connected to a seasonal geothermal storage and considers the different temperature levels of the water flow to satisfy both thermal and cooling demands.

1.3. Geothermal systems for heating and air conditioning

Geothermal energy is a type of renewable energy which is generated within the earth and can be used directly for heating or transformed into electricity. An advantage of geothermal energy over some other renewable energy sources is that it is available year-long (whereas solar and wind energy present higher variability and intermittence) and can be found around the world. For electricity generation, medium- to high-temperature resources, which are usually close to volcanically active regions, are needed. Geothermal power has considerable potential for growth. The amount of heat within 10000 metres of the earth's surface is estimated to contain 50000 times more energy than all oil and gas resources worldwide [9].

Electricity production is the main and most important form of use of high temperature geothermal resources ($> 150 \text{ }^{\circ}\text{C}$). The resources at medium-low temperature ($< 150 \text{ }^{\circ}\text{C}$) are suitable not only for the generation of electricity with binary cycle plants, but also for a multiplicity of direct uses of heat, ranging from the heating of rooms, to refrigeration, to agricultural uses, to the aquaculture, for use in hot industrial processes

[10]. Figure 1.1 illustrates the percentage distribution of total installed capacity of geothermal direct application worldwide in 2015 [11].

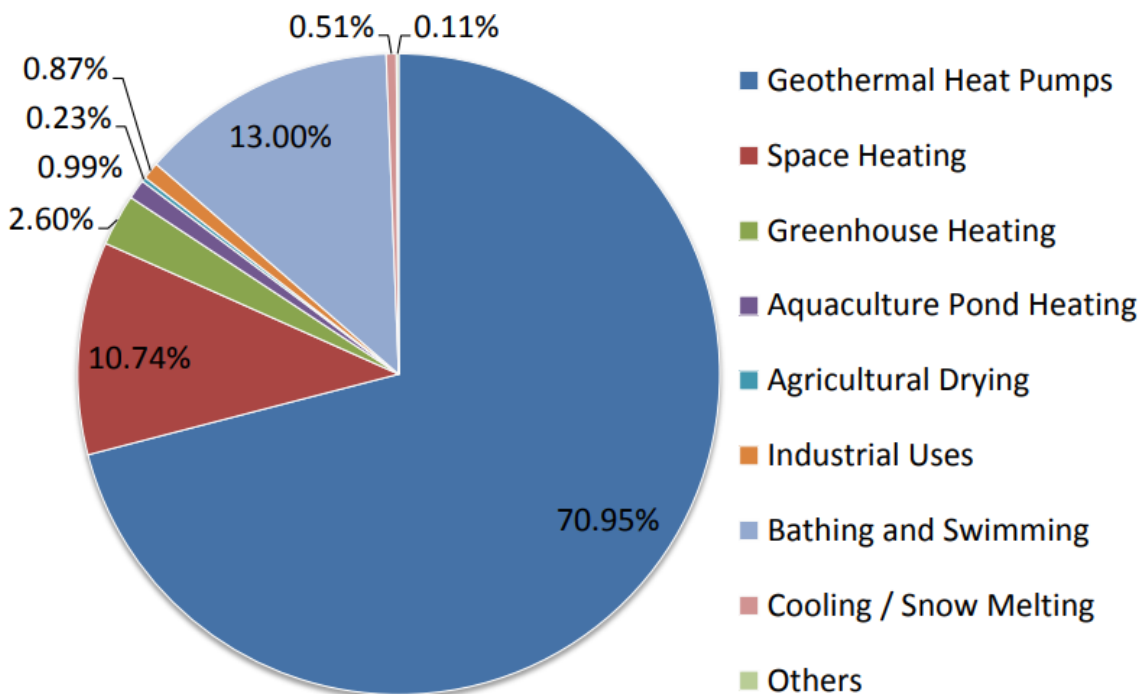


Figure 1.1: Geothermal direct application worldwide in 2015

As shown in the figure above, heat pumps are the form of direct use of geothermal heat with the greatest use of energy and the greatest installed power. The different heat pump systems available allow to extract and economically use the heat contained in low temperature bodies, such as soil, shallow aquifers, surface water masses, etc. They are machines that move heat from a colder space to a warmer one by consuming electricity. Moreover, many heat pumps are reversible and their operation can be inverted, being able to operate alternatively as heating or cooling units. Coupled with a geothermal field, heat pumps are able to achieve very high coefficients of performance (COPs), making them among the most efficient heating and air conditioning systems for reducing greenhouse gas emissions.

1.3.1. Closed loop systems

The vertical geothermal probes consist of a closed system of one or more U-connected pipes on the bottom of the well, generally at a depth of 100 - 150 m, inside which the heat transfer fluid coming from the heat pump flows, see Figure 1.2.

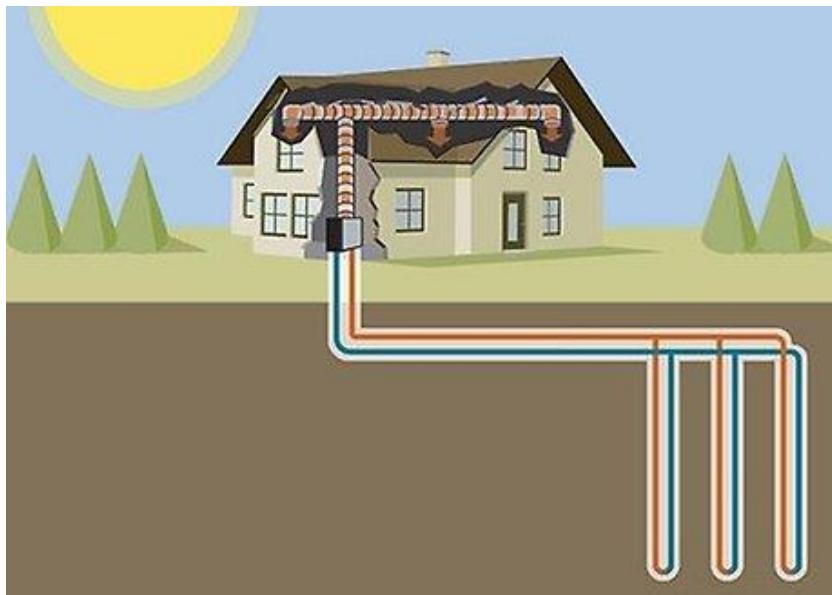


Figure 1.2: Closed loop representation (<https://www.climatemaster.com/homeowner/side-links/faq>)

The heat exchange processes take place underground, partly amplified by the thermal properties of the soil and the temperature of the undisturbed soil, which allow the extraction/dissipation in the subsoil of the thermal/cooling power generated by the heat pump. The best conditions are in the presence of fractured rock formations, with considerable groundwater flow. In fact, on the one hand rocks have in general good conductive properties, and on the other hand the permeability favors the convective component, due to the motion of the groundwater. In contrast, dry soils provide the worst yields, due not only to the lack of water, but also and above all to the presence of air between the granules.

For this type of technology, special care must be taken to avoid freezing of the fluid circulating inside the probes, due to considerable under-sizing of the geothermal heat

exchanger. The decrease of the temperature below the freezing limit imposed by the antifreeze fluid mixed with the water in the probes, even for limited time periods, involves the freezing of the heat transfer fluid, with obvious damage to the pipes and especially to the heat pump, up to when the geothermal system is completely broken.

1.3.2. Open loop systems

Geothermal wells with groundwater drawing generally provide better yield results than vertical geothermal probes. In fact, with sufficient flow rates the total thermal power required can be obtained with a much lower number of perforations than in the closed circuit solution. A geothermal extraction well usually intercepts an artesian aquifer; a pump at the bottom of the well is then prepared in order to extract the water with sufficient flow rates. For each extraction well, it is necessary to add re-injection wells for the discharge of the water leaving the heat pump in the same aquifer, as shown in

Figure 1.3

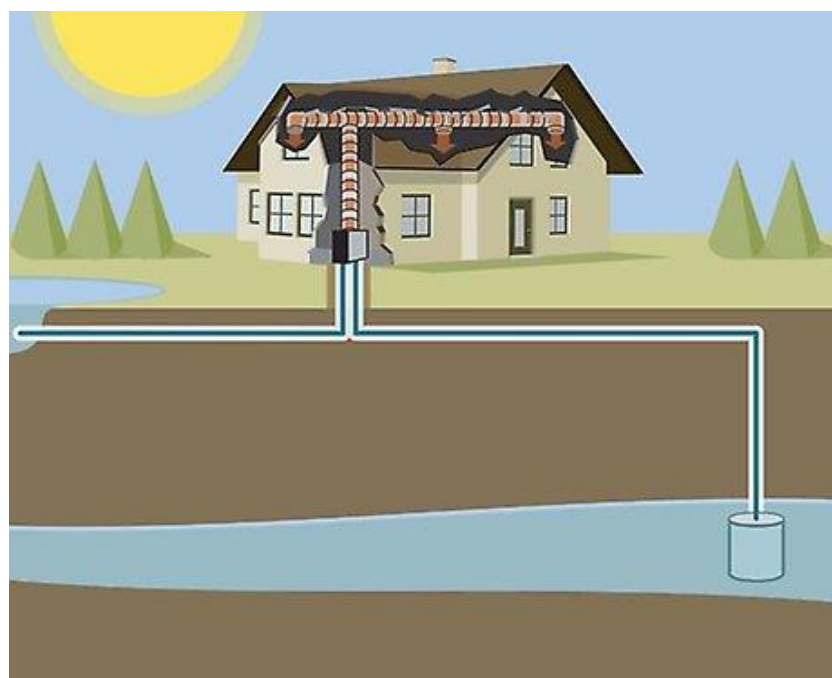


Figure 1.3: Open loop representation (<https://www.climatemaster.com/homeowner/side-links/faq>)

However, ground water cannot be used directly, due to the fine particles dissolved in it and its salt and metal content. Therefore, before entering the heat pump, it is also necessary to insert a filter in the circuit to retain the finest particles, which could damage the evaporator of the machine. Also with regard to reinjection, there are several technical problems, since the clogging of the filters at the bottom of the well can occur more frequently than in the extraction well.

Being an open circuit that does not always use the same water, the risk of fluid freezing is very low.

1.3.3. Horizontal collector systems

The solution of horizontal geothermal collectors consists in arranging, in various possible solutions (serpentine, spiral, etc.), polyethylene pipes lying on a large surface of soil, at a depth of 2-3 meters, as shown in Figure 1.4. In fact, the first 2 meters partly shield the tubes from solar radiation, so at this depth there is not an excessive temperature variability.

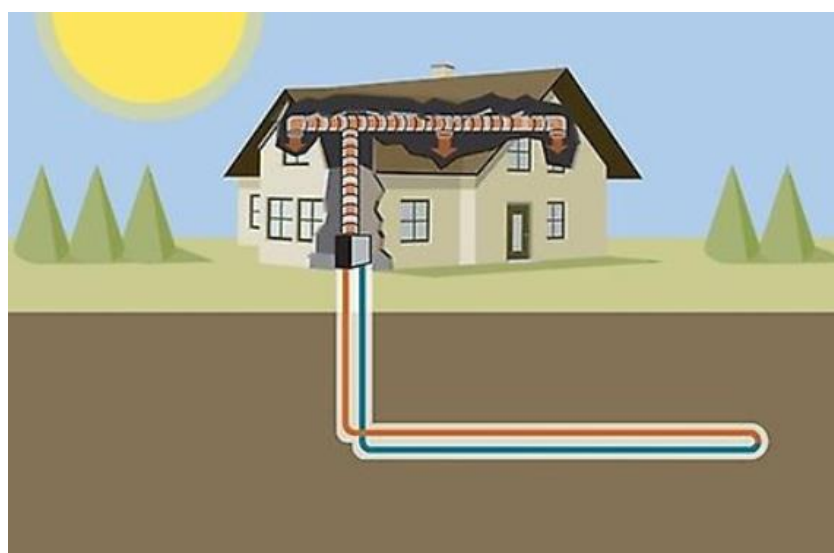


Figure 1.4: Horizontal GT system representation
[\(https://www.climatemaster.com/homeowner/side-links/faq\)](https://www.climatemaster.com/homeowner/side-links/faq)

This system has a modest thermal yield per square meter of soil. For this reason, a limitation of the system is that it requires a large extension to satisfy even relatively small powers.

Another limit to the use of this system is that the soil must have a high permeability. In fact, the installation of the collectors in dry soils leads to mediocre results which, with the operation of the heat pump over time, can also cause a complete drying up of the soil with the result of the progressive deterioration of the efficiency of the system.

1.4. Worldwide distribution of direct-use geothermal systems

The data reported are obtained from the World Geothermal Congress held in Australia and New Zealand in 2015. The growing awareness and popularity of the geothermal heat pumps has had the most significant impact on the direct use of geothermal energy. The annual energy use of these units grew 1.62 times at a compound rate of 10.3%, while the installed capacity grew 1.51 times at a compound annual rate of 8.65% compared to the situation of 2010. This is partially due to the ability of geothermal heat pumps to utilize groundwater or ground-coupled temperature anywhere in the world. Figure 1.5 illustrates the distribution of direct geothermal energy capacity installations per region.

Asia and Europe are the leaders having respectively 18 and 32 countries utilizing geothermal energy for direct-use applications. Several countries stand out as major consumers of geothermal fluids for direct uses (China, USA, Japan, Iceland and Germany); however, in most countries development is slow. This is due to the fact that fossil fuels are a major competitor as well as the initial high investment costs of geothermal projects.

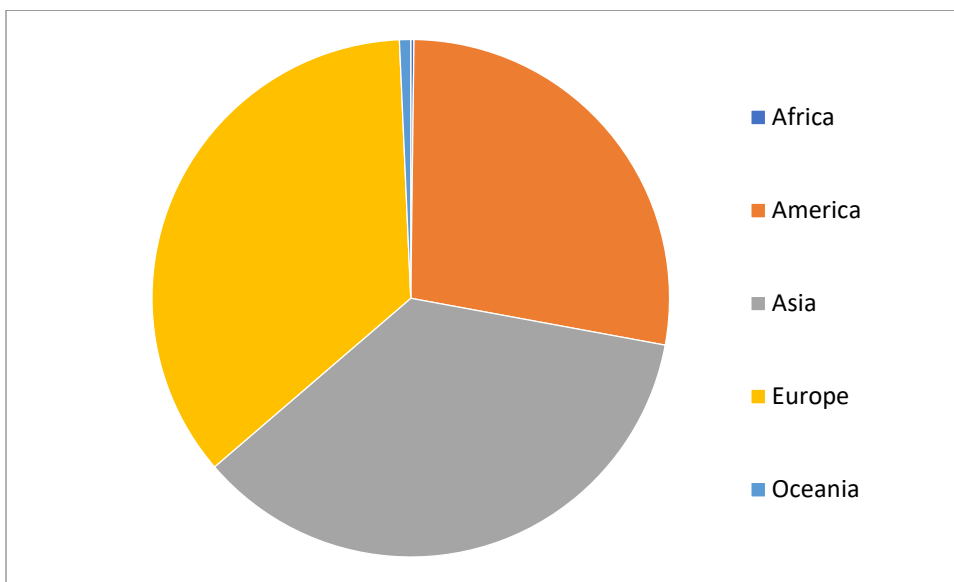


Figure 1.5: Geothermal installed capacity by region

Noteworthy in Europe are the cases of Iceland with 90% of building space heating covered by geothermal heat pumps, of Sweden with 20% of building heated using geothermal heat pumps and of Switzerland, which with 90,000 geothermal heat pumps installed, has the highest density of installation per surface ($\sim 3 \text{ units/km}^2$).

CHAPTER 2: STATE OF THE ART OF MULTI-ENERGY SYSTEMS OPTIMIZATION

This chapter presents a general overview of the state of the art on optimization of multi-energy systems. A literature review with a reference to the innovative aspects of the present study is reported.

2.1. Operational and design optimization

A first classification of multi-energy systems optimization problems can be made basing on the purpose of the formulation of the optimization problem, which can be:

- Determination of the optimal operational strategies of the plant (optimal operation)
- Determination of the optimal multi-energy system configuration (optimal design)

In the first category of problems, the operational strategies of the plant are decisional variables of the optimization problem, while typologies, number and sizes of the technologies are input data and represent part of the constraints (such as capacity constraints). In this category of problems, some are mono-objective, aimed at minimizing the costs of energy carriers in input to the system, others are multi-objective with economic, environmental, economic and exergetic criteria. The most common solution methodologies are those typical for linear programming problems.

In the second type of problems, the set of technologies, their number with the relative sizes and the related operational strategies are decisional variables of the optimization problem, and therefore represent the output of the solution. The mono-objective problems of such category have usually as objective function the minimization of the

total costs or the maximization of the net present value (NPV). On the other hand, multi-objective optimization problems use economic and environmental criteria in order to minimize the total annual costs and CO₂ emissions of the system. Even in this case, the most common solution methodologies are those typical for linear programming problems.

2.2. Optimization criteria

As mentioned before, the optimization criteria used in most of the studies present in literature are of economic, environmental and exergetic nature.

In both mono-objective and multi-objective problems of operational optimization, the economic objective is, in most cases, formulated as the total cost of energy carriers to be minimized. The cost of energy carriers depends on the fuel consumption of the involved technologies, and therefore it depends on the operational strategies of the network, which are decisional variables of the optimization problem.

The environmental objective, both in terms of operational and design optimization, is formulated as the environmental impact, in terms of total CO₂ emissions, to be minimized. As in the case of energy carrier costs, emissions depend on the operational strategies of the energy network, which are decisional variables of the optimization problem.

The exergetic analysis is normally employed in the study of multi-objective operational optimization problems of multi-energy systems. The aim is to reduce the waste of energy resources characterized by a high level of energy quality, such as fossil fuels and electricity, and the related environmental impact. The exergetic objective can be formulated as the primary exergy in input to the energy network to be minimized or as

the destruction of exergy, which occurs in primary conversion systems, to be minimized. As in the case of the cost of energy carriers, and CO₂ emissions, both the primary exergy in input and the destruction of exergy that occurs in primary conversion systems, depending on the consumption of primary sources, depend on the operational strategies of the network, which are decisional variables of the optimization problem.

In design optimization problems, whether mono-objective or multi-objective, the economic purpose is, in most cases, formulated as the total cost of the system to be minimized. This cost is given by the sum of various cost functions, such as the investment cost of the technologies to be installed, the cost associated with the consumption of energy carriers, the cost of maintenance of the technologies, and costs related to the carbon tax.

2.3. Literature review

In literature, there are numerous studies that analyse the optimization of models of multi-energy systems. Connolly et al. provided a review of different computer tools that can be used to analyse the integration of renewable energy in multi-energy systems [12]. This study allows to identify the most suitable energy tools for multi-objective analysis. An investigation on the state of the art in multi-objective distributed energy resources planning is presented by Alarcon-Rodriguez et al. [13]. Mancarella published in 2014 a comprehensive and critical overview of the latest models and assessment techniques that are currently available to analyse multi-energy systems, distributed multi-generation systems, including the concept of energy hubs, microgrids and virtual power plants [14]. He included also a description of the different approaches and criteria for energy, environmental and techno-economic assessment. In 2015, Allegrini

et al. presented a review of modelling approaches and associated software tools that address energy systems at urban district-level energy systems [15].

The coupling of multi-energy systems with accumulation technologies increases the complexity of the problem, since it is necessary to also consider the operation of the system to best use the storage technologies.

Elsido et al. proposed a MINLP (Mixed Integer Non Linear Programming) model and a two-stage optimization algorithm for determining the most profitable synthesis and design of combined heat and power units within a district heating network with thermal storage while taking into account the optimal scheduling of the units over the year [16].

In the context of MILP (Mixed Integer Linear Programming) formulations, Hawkes and Leach developed a linear programming cost minimisation model for high level system design and unit commitment of generators and storage within a microgrid [17]. Ahmadi et al. reported a multi-objective thermodynamic modeling and optimization of a polygeneration energy system for the simultaneous production of heating, cooling, electricity and hot water from a common energy source [18].

A further series of studies has been published for the optimization of multi-energy systems with the inclusion of a network for the distribution of energy vectors between the different nodes of the system.

Weber and Shah presented a district energy system design and optimization tool, based on MILP technics, to decrease the CO₂ emissions while at the same time guarantee resilience of supply [7]. Mehleri et al. published a minimising costs MILP model for the optimal design of distributed energy generation systems characterized by heating and electrical power demands [19]. The study includes the optimal design of a heating

pipeline network, that allows heat exchange among different nodes. Bracco et al. presented a multi-objective MILP model to perform design and operation optimizations of an energy system installed in an urban area with the inclusion of a heat distribution network [20].

In the aforesaid works, simplifications on models are introduced in order to deal with the high complexity of the optimization problem. Such simplifications lead to a reduction in the description of the time horizon in typical days. In this way, it is possible perform an analysis of the system dynamics over a year. This type of time horizon modeling is suitable for applications involving short-term energy storage technologies, such as hot water thermal storages or electric batteries. However, it is not suitable for the study of design and operation of seasonal storage technologies due to the lack of continuity in the decision variables between typical days.

In 2018, Gabrielli et al. published a study with a solution to this issue, still maintaining the subdivision of the time horizon in design days [21]. Two MILP formulations are proposed that allow to couple consecutive typical days. Starting from the formulation of the k-means clustering formulated by Lloyd [22] and from Pfenninger's work [6] on the analysis of the different techniques to reduce the time resolution of energy models, the time horizon is split in a set of design days organized in a sequence vector by using the MATLAB-embedded clustering algorithm k-means [23]. The algorithm receives as inputs the weather conditions, the energy prices and the load profiles, it solves a MINLP problem to find the most representative set of typical days and to assign every day of the time horizon to a specific design day among the set. Moreover, since the clustering procedure smooths the peaks of the input data making the resolution of the optimization problem less faithful to the real case, constraints on the clustering procedure are added

to maintain the minimum and maximum values of the original demand profiles. The implemented optimization framework is illustrated in Figure 2.1.

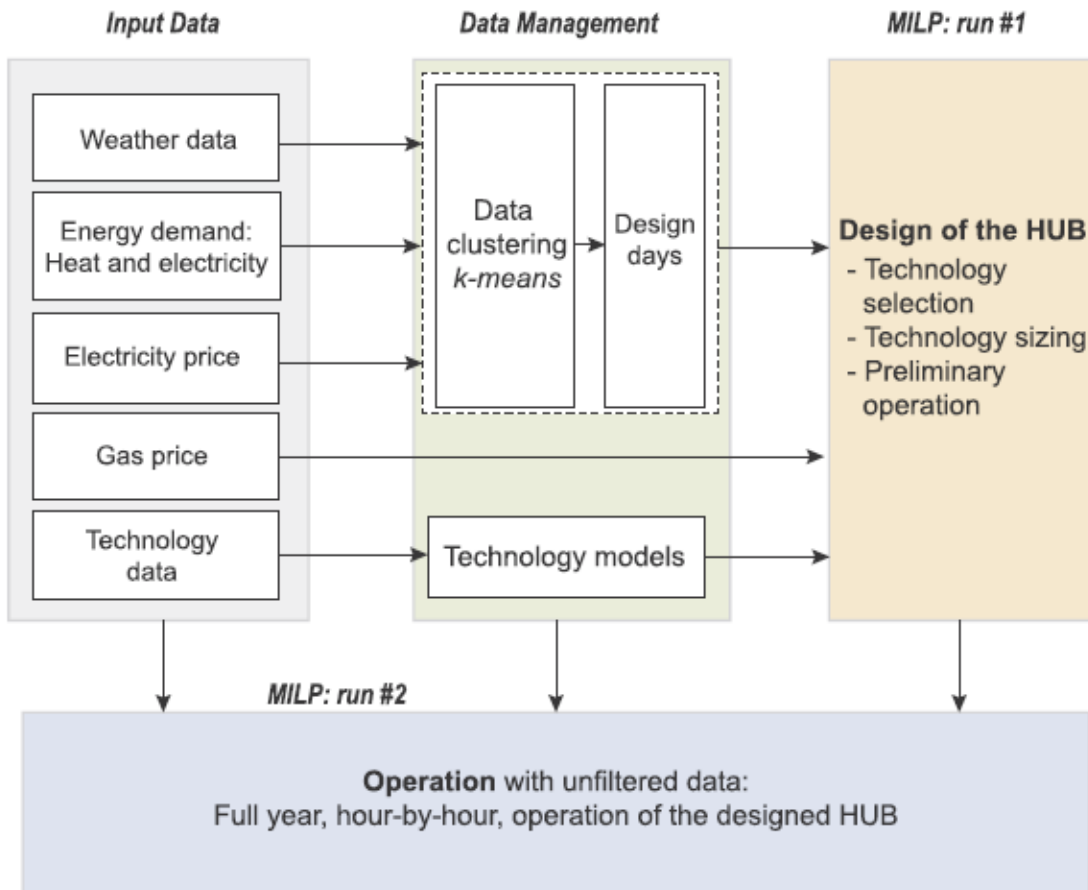


Figure 2.1: Optimization framework proposed by Gabrielli et al. [5]

As explained above, the weather data, the energy demands and the energy prices are clustered into design days by the k-means algorithm. A design optimization problem is solved basing on the selected set of typical days, on the gas price and on data provided by the models of technologies. It gives as result the selection and the corresponding size of the technologies and a preliminary operation of the system. Such solutions are used, together with the original inputs and with the models of the technologies, as input data to solve a detailed operation optimization problem.

The present work uses the optimization tool developed by Gabrielli et al. to solve an operation optimization problem of a multi-energy system with seasonal storage that

includes a low temperature water distribution network characterized by different temperature levels. A thermal demand and two required cooling loads at different temperature levels are satisfied by conversion technologies (heat pumps and heat exchangers) connected in series that exploit the energy contained in the same water flow which circulates in the network. This type of problem is strongly non-linear and is not addressed in the literature articles listed above. The non-linearities are mainly due to the products between the decision variables of mass flow rate and temperature, which are present in every energy balance.

Yliruka has addressed this problem by proposing a linear solution method based on a genetic algorithm for defining the flow profile [24]. However, this is a heuristic solution that makes it difficult to determine a general methodology for solving the problem.

In this work, the described problem is solved in a MILP formulation through an optimization strategy that makes use of the mathematical method of McCormick envelopes [25]. The model is relaxed in a linear form and the solution obtained is partially used as input data to solve the original problem by introducing a known amplitude deviation from the optimal solution.

For the formulation of the mass and energy balances of the network model, Metz's work was taken as a reference [26]. He presented a methodology applied to the same case study of this work to model the network with non-predetermined directions by assigning binary variables to the flow directions in the branches.

CHAPTER 3: DESCRIPTION OF THE ANERGY GRID AND MODELING OF TECHNOLOGIES

In this chapter, the system under study is presented and a detailed description of the installed technologies is reported. Moreover, the main assumptions and equations used to model the components of the Anergy Grid are reported.

3.1. Description of the system

The system to be investigated is the modern ETH Zurich Hönggerberg Campus, which is located on the outskirts of the city of Zurich. It represents a perfect example of the links between science, industry and the municipality. The Hönggerberg Campus not only has new buildings for research and education but also apartment blocks for students. The ETH departments of Architecture, of Civil, Environmental and Geomatic Engineering, of Materials, of Biology, of Chemistry and Applied Biosciences and of Physics are hosted in this structure. A panoramic picture of the Campus is shown in Figure 3.1.



Figure 3.1: View of the ETH Zurich Hönggerberg Campus

The Campus hosts more than 10,000 students, teachers and employees, with an energy demand of 29 GWh of heating, 23 GWh of cooling and 54 GWh of electricity [27]. The heating demand alone complies with the heating energy demand of approx. 2,000 family homes. In 2016 the University put additional residential buildings for students into operation. In order to satisfy these energy demands following the guidelines of the “Ressourcen und Umweltmanagement der Bundesverwaltung” (RUMBA) program, ETH University built at the Hönggerberg Campus the Anergy Grid, a dynamic underground storage system that shall replace the heat and cold energy production with fossil-based technologies. This is achieved by an intelligent network of heating sources and sinks in combination with a seasonal shift. This allows a significant reduction of fossil energy demands, which are associated to high CO₂ emission rate. The first phase of construction began in 2003 and was completed in 2012. ETH University has carried out this project together with the Amstein + Walther Group, one of Switzerland's leading engineering and consulting firms.

The present study investigates the potential of the Anergy Grid, which is illustrated in Figure 3.2. Three big geothermal fields are installed underground and a low temperature water network connects them with the buildings on the surface. The geothermal fields are constituted by 200 m deep vertical U-shaped probes that are exploited as seasonal energy storage [24]. The buildings of the Campus are organized into clusters, which are connected to a single substation underground. Each cluster requires both heating and cooling power demands. The cooling demand is divided in two categories: a low temperature cooling demand for the laboratories of the campus and a high temperature cooling demand for the air conditioning system. In each cluster, one heat pump and two heat exchangers are installed in order to meet the demands by exploiting the geothermal source. The heat pump absorbs electrical energy by the national grid and is used to

provide the heating power. The two different heat exchangers are installed in order to satisfy the low and high temperature cooling demands. The seasonal heat integration is achieved by exploiting the geothermal fields. The water circulating through the geothermal probes enters from the hydraulic ring circuit and it returns back to it after exchanging heat with the soil. During summer, the cooling demand in the clusters is high. Therefore, the water fed to the geothermal fields coming from the substations is warmer than the soil. Hence, the water circulating in the probes is cooled while heating up the ground. The cooled water is again able to absorb heat in the heat exchangers of the substation, providing the cooling energy required in summer. In winter, the process is reversed. The heating demand is high, so the water entering the geothermal fields is colder than the ground, which is gradually cooled while recovering the heat. The soil temperature is expected to show a cyclic behavior.

ETH Zurich, Campus Hönggerberg
Anergy Grid

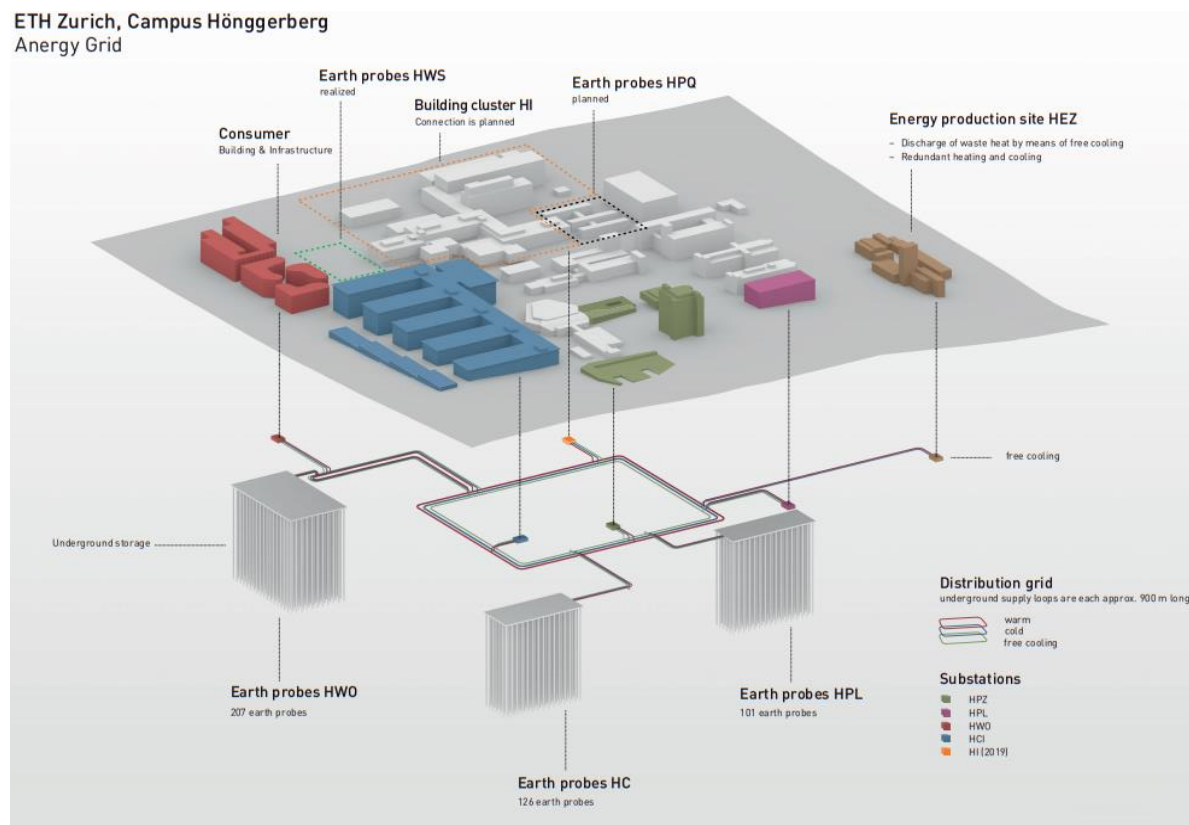


Figure 3.2: Anergy Grid installation at the Hönggerberg ETH Campus

If the Anergy Grid does not manage to satisfy the loads, auxiliary technologies, which are installed in each cluster, are put into operation to meet the demands: a boiler fed by natural gas and electrical compression chillers, which provide respectively heating and cooling power. These are the standard technologies that were present before the installation of the Anergy Grid. Figure 3.3 illustrates a representation of the Anergy Grid as a multi-energy system.

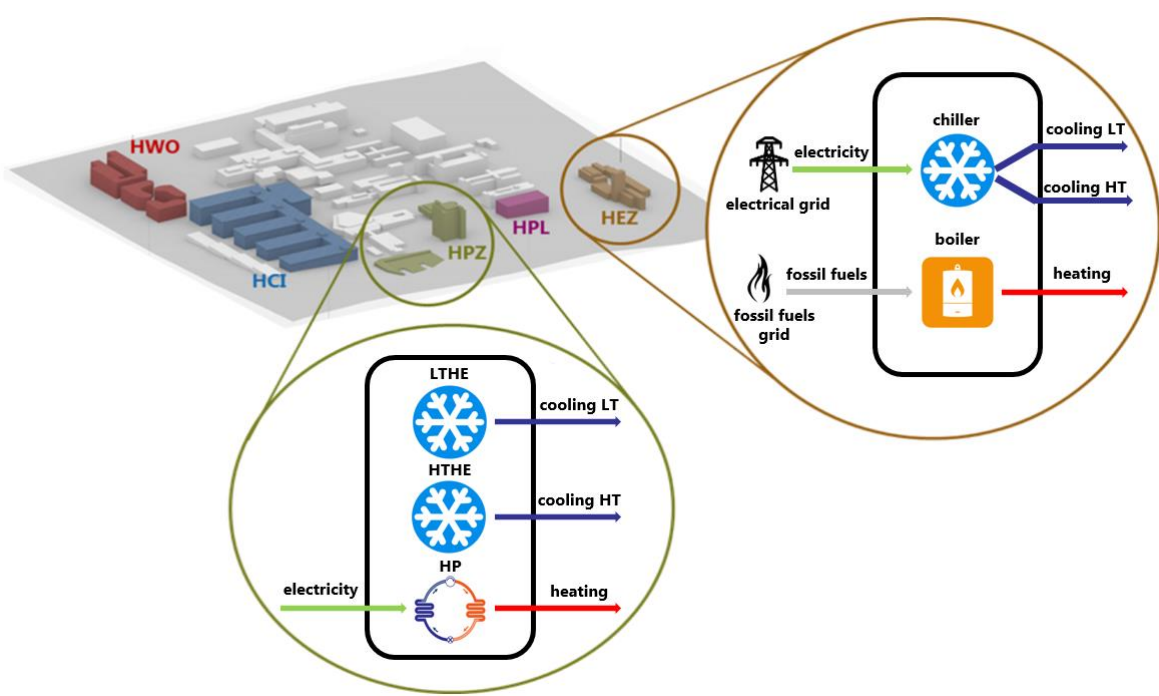


Figure 3.3: Power technologies installed at the Science City

3.2. Standard auxiliary technologies

Standard auxiliary technologies are installed in each cluster of the ETH Hönggerberg Campus in order to meet the requested power demands. As aforesaid, such components are a boiler fed by natural gas for the thermal demand and electrical compression chillers for the low temperature and high temperature cooling demands. These are the technologies that managed to satisfy the loads before the installation of the Anergy Grid.

3.2.1. Boiler

The boiler is a very common energy conversion technology, which transforms the energy contained in the chemical bonds of the input fuel into thermal energy through the combustion process. Detailed studies on boiler modeling are present in literature which take into account the dynamic behavior of the combustion reaction, but for the aim of this study a full complex description of the technology is not necessary. Thus, only a simple performance equation of the boiler is employed:

$$\dot{Q}^B = \eta^B P^G \quad (3.1)$$

where:

\dot{Q}^B : thermal power provided by the boiler [W]

η^B : thermal efficiency of the boiler [-]

P^G : chemical power of natural gas consumed by the technology [W]

The fuel is provided by the national natural gas grid.

3.2.2. Electrical chiller

Electrical chillers are installed to satisfy the two cooling demands required by the users. This type of conversion technology absorbs electrical energy by the national electrical grid and provides cooling energy through a refrigeration cycle. As the boiler, the low temperature and high temperature chiller performance are modeled through the following equations:

$$\dot{Q}^{CH_LT} = COP^{CH_LT} P^{CH_LT} \quad (3.2)$$

where:

\dot{Q}^{CH_LT} : low temperature cooling power provided by the chiller [W]

COP^{CH_LT} : coefficient of performance of the low temperature chiller [-]

P^{CH_LT} : electrical power consumed by the technology [W]

$$\dot{Q}^{CH_HT} = COP^{CH_HT} P^{CH_HT} \quad (3.3)$$

where:

\dot{Q}^{CH_HT} : high temperature cooling power provided by the chiller [W]

COP^{CH_HT} : coefficient of performance of the high temperature chiller [-]

P^{CH_HT} : electrical power consumed by the technology [W]

3.2.3. Hot water thermal storage

The hot water thermal storage is a storage technology for the accumulation of thermal energy for short periods, due to a limited capacity and relatively high thermal losses. It is a cheap, developed and commercial system. It allows to store thermal energy up to a maximum value, corresponding to its size, and to release thermal power in subsequent periods. It is not a technology installed in the Anergy Grid, but the present study intends to analyse the possible advantage that the inclusion of hot water thermal storage would provide in terms of CO₂ emissions reduction.

Assuming to consider a discretized time horizon in which t indicates a generic time instant, the energy stored inside the technology at a given time instant E_t^{HWTS} depends on its level at the previous time instant E_{t-1}^{HWTS} and it is described by the Equation (3.4).

$$E_t^{HWTS} = E_{t-1}^{HWTS}(1 - \Lambda\Delta t) + \\ -(\Pi S^{HWTS} h(T_t^{air}) - \eta^{HWTS_in} \dot{Q}^{HWTS_in} + \frac{1}{\eta^{HWTS_out}} \dot{Q}^{HWTS_out})\Delta t \quad (3.4)$$

where:

E_t^{HWTS} : energy stored inside the technology at time t [Wh]

Λ : self-discharge efficiency [h^{-1}]

Δt : duration of the time interval [h]

Π : ambient loss contribution coefficient [-]

S^{HWTS} : size of the hot water thermal storage [Wh]

η^{HWTS_in} : charging efficiency [-]

\dot{Q}^{HWTS_in} : thermal power entering in the hot water thermal storage [W]

η^{HWTS_out} : discharging efficiency [-]

\dot{Q}^{HWTS_out} : thermal power exiting from the hot water thermal storage [W]

The h function expresses the influence of the ambient temperature T^{air} on the losses of the storage technology, as described by Steen et al. [28]. It depends on the maximum T^{HWTS_max} and minimum T^{HWTS_min} temperature level of a thermal energy storage with ideal stratification and it is defined by the Equation (3.5).

$$h_t = \frac{T^{HWTS_min} - T_t^{air}}{T^{HWTS_max} - T^{HWTS_min}} \quad (3.5)$$

The thermal power entering in or exiting from the storage technology is limited to a maximum value, as expressed in Equations (3.6) and (3.7).

$$\dot{Q}^{HWTS_in} \leq \frac{S^{HWTS}}{\tau^{HWTS}} \quad (3.6)$$

$$\dot{Q}^{HWTS_out} \leq \frac{S^{HWTS}}{\tau^{HWTS}} \quad (3.7)$$

where τ^{HWTS} [h] represents the time required to fully charge or discharge the storage.

3.3. Single node plant description

A single node of the system, composed by one cluster directly connected to a geothermal field, is here analysed. The three conversion technologies of the Anergy Grid installed in the clusters are connected in series according to the scheme shown in Figure 3.4.

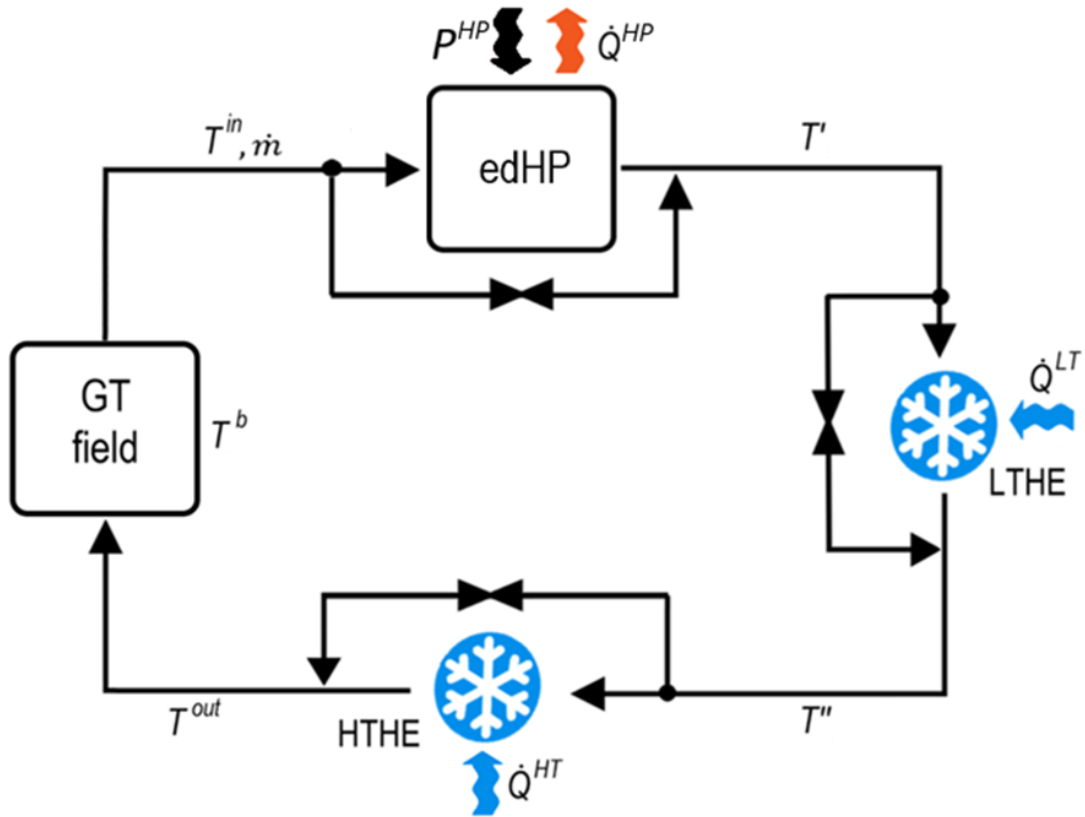


Figure 3.4: Single node plant scheme

The different quantities labeled in Figure 3.4 are:

T^b : average borehole wall temperature [K]

T^{in} : inlet temperature inside the circuit [K]

T' : temperature of the heat transfer fluid at the exit of the heat pump [K]

T'' : temperature of the heat transfer fluid at the exit of the low temperature heat exchanger [K]

T^{out} : temperature of the heat transfer fluid at the exit of the high temperature heat exchanger [K]

\dot{Q}^{HP} : thermal power provided by the HP to the cluster [W]

\dot{Q}^{LT} : low temperature cooling power extracted by the low temperature heat exchanger from the laboratory water [W]

\dot{Q}^{HT} : high temperature cooling power extracted by the high temperature heat exchanger from the air conditioning system [W]

P^{HP} : electrical power absorbed by the heat pump from the national electrical grid [W]

\dot{m} : mass flow rate of the heat transfer fluid flowing within the circuit [kg/s]

The mass flow rate coming from the geothermal field at temperature T^{in} passes through the heat pump, which provides thermal power to the cluster and decreases the temperature of the heat transfer fluid. The fluid exits the heat pump at temperature T' and enters into the first heat exchanger. There, it increases its temperature, assuming at the outlet the temperature value T'' and the same happens in the second heat exchanger. Finally, the mass flow rate comes back into the geothermal field at temperature T^{out} . The hydraulic circuit allows the mass flow rate to completely bypass the heat pump or the heat exchangers, acting on valves. Hence, the heat transfer fluid has the possibility

to bypass one, two or three technologies maintaining its temperature level and consequently the corresponding conversion technology will not provide thermal or cooling power to the user.

3.4. Technologies description

In this section, a description of the conversion technologies of the single node is provided.

3.4.1. Heat Pump

The characteristic equation of the heat pump is described by the Equation (3.8).

$$\dot{Q}^{HP} = P^{HP} \frac{T^{cond}}{T^{cond} - T^{eva}} \xi \quad (3.8)$$

where:

\dot{Q}^{HP} : thermal power provided by the heat pump [W]

P^{HP} : electrical power absorbed by the heat pump [W]

T^{cond} : temperature at the condenser of the heat pump [K]

T^{eva} : temperature at the evaporator of the heat pump [K]

ξ : ratio between real thermodynamic cycle efficiency and Carnot cycle efficiency [-]

The energy balance between the heat transfer fluid and the evaporator fluid at the user side can be evaluated through the Equation (3.9):

$$\epsilon(T^{in} - T^{eva}) = T^{in} - T' \quad (3.9)$$

where ϵ is a dimensionless number, which represents the efficiency of the heat exchanger. It is defined as the ratio between the actual heat transfer rate and the maximum possible heat transfer rate and it can be calculated with the Equation (3.10).

$$\epsilon = 1 - e^{-NTU} \quad (3.10)$$

The Number of Transfer Units NTU is another dimensionless parameter defined in the Equation (3.11).

$$NTU = \frac{UA}{(\dot{m}c)_{min}} \quad (3.11)$$

Substituting the Equations (3.10) and (3.11) in Equation (3.9), the temperature at the outlet of the heat pump T' can be calculated using Equation (3.12):

$$T' = T^{in} - (T^{in} - T^{eva})(1 - e^{-\frac{UA}{\dot{m}c}}) \quad (3.12)$$

where:

U : overall heat transfer coefficient [$W/(m^2 K)$]

A : heat exchange area [m^2]

c : specific heat of the heat transfer fluid [$J/(kg K)$]

\dot{m} : mass flow rate of the heat transfer fluid [kg/s]

The thermal power provided by the heat pump is related to the electrical power absorbed by the heat pump through the energy balance reported in Equation (3.13).

$$\dot{Q}^{HP} = P^{HP} + \dot{m}c(T^{in} - T') \quad (3.13)$$

This equation expresses the energy balance between the energy fluxes entering in and exiting from a control volume containing the whole heat pump: the sum of the electrical power and the thermal power provided by the heat transfer fluid equals the heating power delivered by the technology.

3.4.2. Heat exchanger

Heat exchangers are considered as water-to-water counter-flow heat exchangers, which provide cooling power to the user.

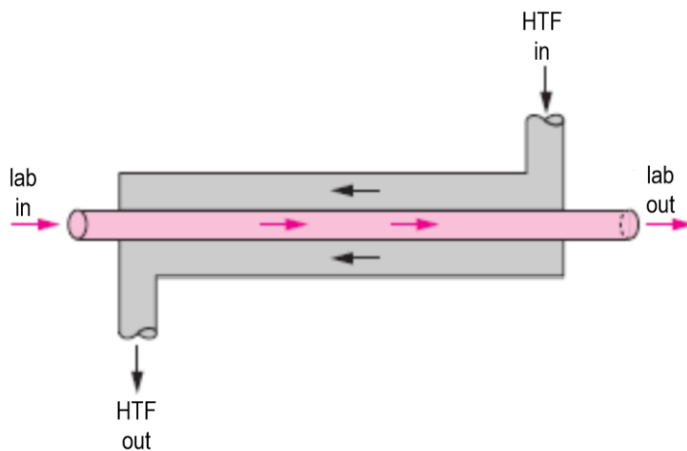


Figure 3.5: counter-flow heat exchanger illustration

In the following, the main assumptions for the description of the technology are reported:

- steady-flow
- kinetic and potential energy changes are negligible
- the specific heat of the fluids is constant
- the axial heat conduction along the tube is negligible
- the outer surface of the heat exchanger is perfectly insulated

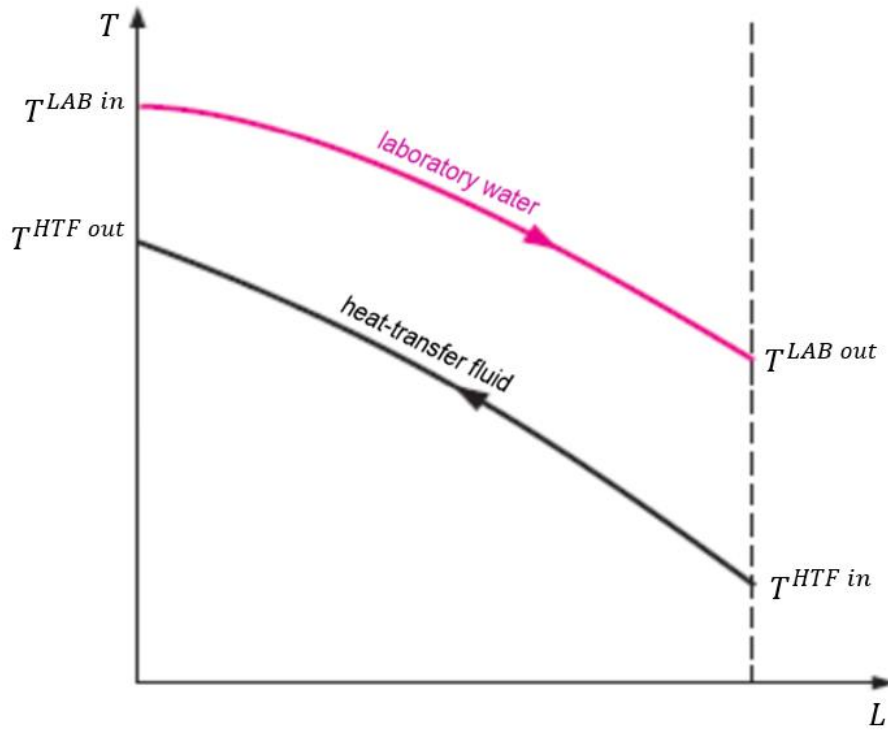


Figure 3.6: temperature diagram of the heat exchanger as a function of its length

The energy balance within the heat exchanger indicates that the rate of heat transfer from the hot fluid is equal to the rate of heat transfer to the cold one.

In this case, the transfer rate to the heat transfer fluid can be expressed by Equation (3.14):

$$\dot{Q} = \dot{m}^{HTF} c^{HTF} (T^{HTF_out} - T^{HTF_in}) \quad (3.14)$$

Similarly, the Equation (3.15) shows the transfer rate extracted from the laboratory water.

$$\dot{Q} = -\dot{m}^{LAB} c^{LAB} (T^{LAB_out} - T^{LAB_in}) \quad (3.15)$$

The temperature difference between the hot and cold fluids varies along the heat exchanger. So, it is convenient to refer to a log mean temperature difference ΔT^{LM} , which is expressed referring to Figure 3.6 in the Equation (3.16).

$$\Delta T^{LM} = \frac{(T^{LAB_in} - T^{HTF_out}) - (T^{LAB_out} - T^{HTF_in})}{\ln \left(\frac{T^{LAB_in} - T^{HTF_out}}{T^{LAB_out} - T^{HTF_in}} \right)} \quad (3.16)$$

Thus, the heat transfer rate exchanged within the heat exchanger can be defined as in the Equation (3.17).

$$\dot{Q} = UA\Delta T^{LM} \quad (3.17)$$

Low temperature heat exchanger

Considering the low temperature heat exchanger as a lumped system, the cooling power provided by the technology can be expressed through the energy balance of Equation (3.18).

$$\dot{Q}^{LT} = \dot{m}c(T'' - T') \quad (3.18)$$

The low temperature heat exchanger provides cooling power to the water used during laboratory experiments in the cluster. The heat-transfer fluid, exiting from the heat pump at temperature T' , passes through the heat exchanger decreasing the temperature of the laboratory water. The water used in the laboratory is kept at constant temperature equal to 12°C . Hence, the set point temperature of the low temperature cooled stream in the cluster is $T^{LAB_out} = 12^{\circ}\text{C}$. For this reason, the Anergy Grid is operated in order to maintain constant at 12°C the temperature T'' of the heat-transfer fluid at the exit of the low temperature heat exchanger, assuming no temperature difference between T'' and T^{LAB_out} .

$$T'' = T^{LT\text{HE}} \quad (3.19)$$

where:

T^{LTHE} : standard outlet temperature from the low temperature heat exchanger = 12 °C.

High temperature heat exchanger

The same calculation procedure for the low temperature heat exchanger can be repeated for the high temperature heat exchanger. In this case, the heat-transfer fluid provides cooling power at higher temperatures to the water of the conditioning system, which has to be kept at 16 °C at the outlet. Thus, the set point temperature of the heat transfer fluid exiting from the high temperature heat exchanger is set to 16 °C.

The main equations, which describe the technology, are:

$$\dot{Q}^{HT} = \dot{m}c(T^{out} - T'') \quad (3.20)$$

$$T^{out} = T^{HTHE} \quad (3.21)$$

where:

T^{HTHE} : standard outlet temperature from the high temperature heat exchanger = 16 °C.

3.4.3. Geothermal field

In the Anergy Grid, three geothermal fields with U-shaped vertical boreholes of 400 m length (200 m downward and 200 m upward) are installed. The geothermal field GT HPL has 101 probes, the geothermal field GT HC has 128 probes and the geothermal field GT HW0 has 200 probes. In order to determine the amount of heat to be injected or extracted from the soil, the thermal behaviour of the soil has to be modeled. In other words, the dependence of the soil temperature on the heat injected or extracted at every hour of the year has to be described. The hourly heat injections or extractions of varying

magnitude present consecutive step heat inputs. The thermal response of a single borehole is a function of time t , distance to the borehole wall r^b and the thermal diffusivity of the ground α . The thermal response function of the geothermal field results from the spatial superposition of the thermal response function of a single borehole. The temperature evolution of the soil is described by temporal superposition. The following assumptions are made in order to simplify the general partial differential equation for cylindrical heat sources:

- absence of groundwater (there is not the convection term)
- homogeneous soil (the diffusivity is not function of depth or radius)
- axial heat conduction neglected (there is no dependency on the vertical axis)
- symmetrical problem (there is no angular dependency)
- borehole connection in parallel (the temperature values at the inlet and at the outlet of each borehole are the same)
- effective undisturbed soil temperature $T^{s,0}$
- thermal equilibrium between the U-tube probe and the grout on its outside.

Due to these assumptions, the single vertical borehole heat exchanger can be modeled as an infinite line source [29]. The line source approach is in accordance with the shape of the probes of the geothermal field, their diameter being three magnitudes smaller than their length. The Equation (3.22) expresses the heat transport equation for an infinite line source.

$$T^b - T^{s,0} = \frac{q}{4\pi\lambda} \int_{\frac{(r^b)^2}{4\alpha t}}^{\infty} \frac{e^{-u}}{u} du \approx \frac{q}{2\pi\lambda} \left[\frac{1}{2} \left(\ln \frac{4\alpha t}{(r^b)^2} - \gamma \right) \right] \quad (3.22)$$

where:

T^b : average borehole wall temperature [K]

$T^{s,0}$: undisturbed soil temperature [K]

q : specific heat extraction rate [W/m]

λ : thermal conductivity of the ground [W/(m K)]

α : thermal diffusivity of the ground [m^2/s]

r^b : radius of the borehole [m]

γ : Euler-Mascheroni constant = 0.5772 [-].

The energy balance of the heat fluxes exchanged between the heat transfer fluid and the geothermal storage is expressed as:

$$\dot{Q}^{GT} = \dot{m}c(T^{in} - T^{out}) \quad (3.23)$$

The energy balance at the wall of a single borehole can be calculated as:

$$\frac{\dot{Q}^{GT}}{LN} = \frac{1}{R^b} (T^b - \bar{T}^f) \quad (3.24)$$

where:

\dot{Q}^{GT} : thermal power provided by the geothermal field to the heat-transfer fluid [W]

L : length of the borehole [m]

N : number of boreholes in the geothermal field

R^b : thermal borehole resistance [m K/W]

The temperature gradient along the U-shaped probe is neglected and its temperature is approximated by the arithmetic mean between the inlet and the outlet temperature \bar{T}^f , according to the Equation (3.25).

$$\bar{T}^f = \frac{T^{in} - T^{out}}{2} \quad (3.25)$$

The heat transport equation of the borehole is expressed as:

$$T^b = T^{s,0} + \frac{1}{2\pi\lambda LN} \sum_{i=1}^t (\dot{Q}_i^{GT} - \dot{Q}_{i-1}^{GT}) g(r^b, t-1) \quad (3.26)$$

The Equation (3.26) represents the dynamic equation for a finite line source thermal model of borehole heat exchanger. The equation contains both a temporal and a spatial superposition. The summation operator enables the temporal superposition of the step heat inputs \dot{Q}_t^{GT} . While the g -function of a geothermal field results from the spatial superposition of the individual thermal step responses [30]. The g -function is a dimensionless temperature factor that enables the quantification of the average temperature over the borehole length, in response to a step heat pulse.

Due to legal regulations, the soil temperature has to remain within the interval of $T^{GT_min} = 8 \text{ } ^\circ\text{C}$ to $T^{GT_max} = 24 \text{ } ^\circ\text{C}$ at every time instant. Therefore, also the Equation (3.27) has to be respected:

$$T^{GT_min} \leq T^b \leq T^{GT_max} \quad (3.27)$$

3.5. Network

The Anergy Grid represents a particular typology of hydraulic network. Two rings underground connect the geothermal storages to the clusters of buildings through substations, as shown in Figure 3.7. The mass flow rate flowing in the clusters is totally governed by the demands of the clusters themselves, without having fixed flow directions in the pipes. Hence, the fluid flowing in each pipe that connects two different substations can assume opposite directions in different time instants.

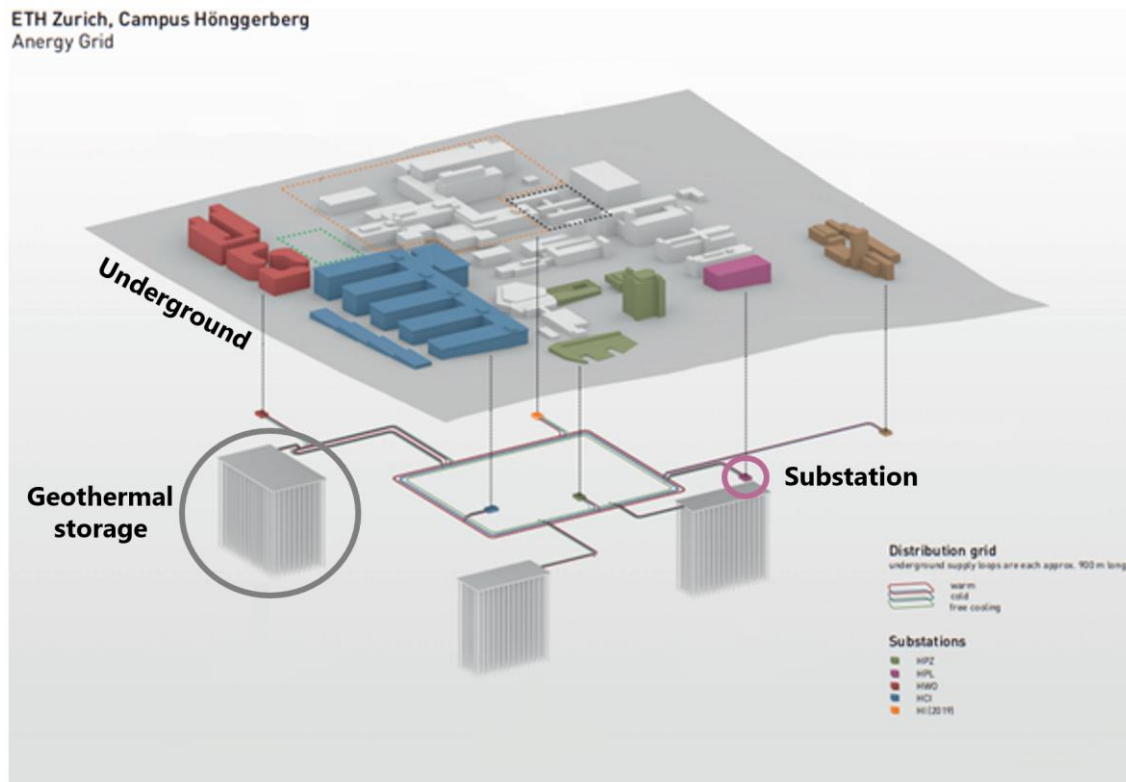


Figure 3.7: Network representation of the Anergy Grid

The following assumptions are made in order to model the low temperature water network:

- steady-state flow

- temperature losses are negligible
- extra electric power consumption for pumping is negligible

3.5.1. Simple network scheme

In order to check the correct implementation of the network model and to understand its behaviour without having a high formulation complexity of the system, a simple network configuration with two clusters and one geothermal field is here considered, as illustrated in Figure 3.8. The considered clusters are the HPL and HPZ, with different heating, low temperature cooling and high temperature cooling demands.

1 2 3 4 5 represent the nodes, while **1 2 3 4 5 6** indicate the branches.

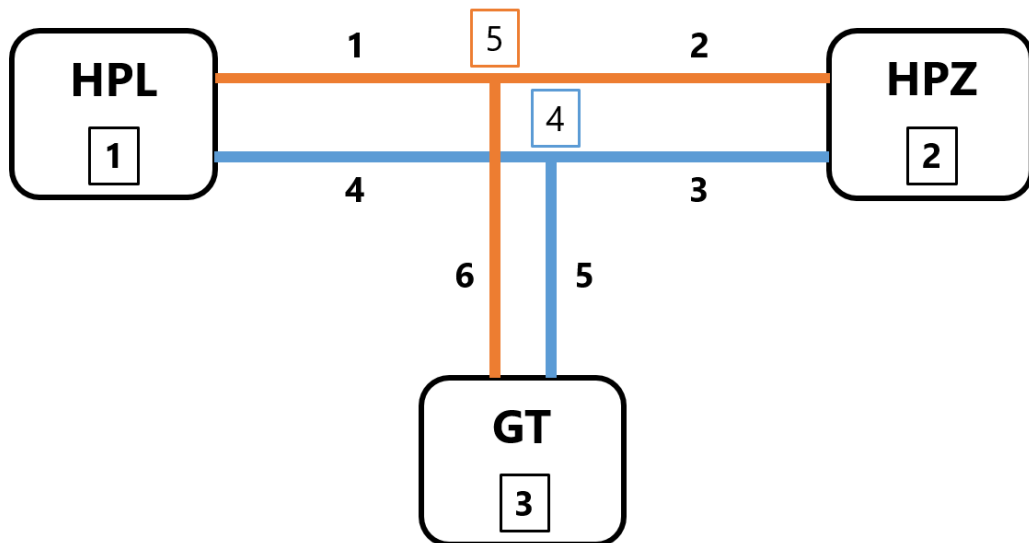


Figure 3.8: Simple network scheme

Each cluster box has a heat pump, a low temperature heat exchanger, a high temperature heat exchanger and standard technologies in order to meet the different power demands. The Anergy Grid circuit within the cluster is illustrated in Figure 3.9. Both clusters and the geothermal field are described by the same equations used for the single node.

Mass balances

The mass balances, applied to the network nodes, impose that the sum of the mass flow rates which enter in the node is equal to the sum of the mass flow rates which exit from the node, as stated by the Equation (3.28).

$$\sum_{in} \dot{m}^{in} = \sum_{out} \dot{m}^{out} \quad (3.28)$$

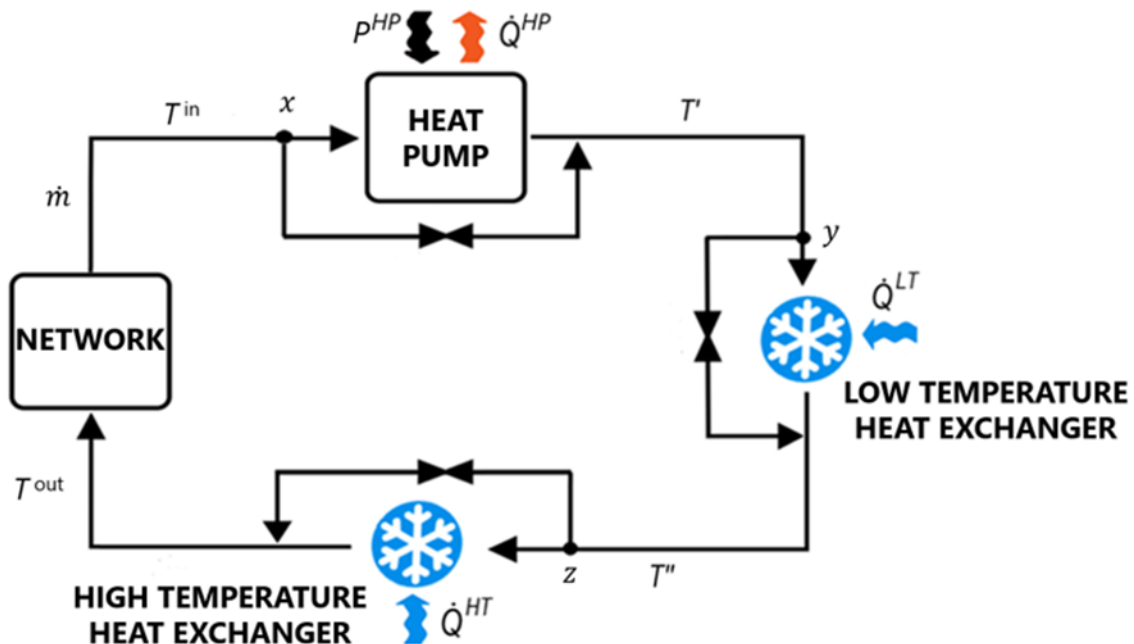


Figure 3.9: plant scheme of the cluster

Energy balances

Energy balances of the network nodes have to be applied. These are 3-way nodes and, depending on the application of mass balances, two different situations can occur, as shown in Figure 3.10.

In the first case, one mass flow is entering in and two mass flows are exiting from the node, the flow temperature at the three branches has to assume the same value, as reported in the Equation (3.29), which refers to Figure 3.10.

$$T^A = T^B = T^C \quad (3.29)$$

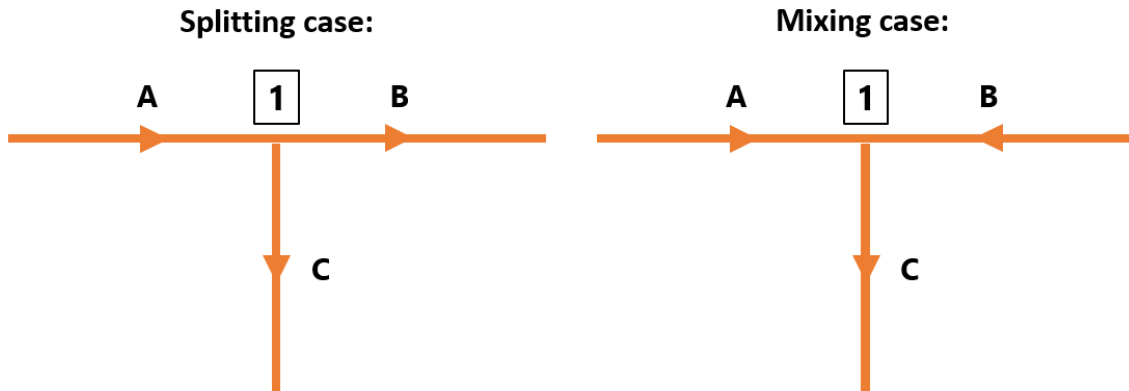


Figure 3.10: Mixing and splitting case illustration

In the second case, two mass flows are entering in and one mass flow is exiting from the node, a mixing balance has to be imposed, as in the Equation (3.30) that refers to Figure 3.10.

$$\dot{m}^A T^A + \dot{m}^B T^B = \dot{m}^C T^C \quad (3.30)$$

3.5.2. Anergy Grid network scheme

The complete Anergy Grid is finally considered. Figure 3.11 shows a top view of the ETH Campus at Hönggerberg.

Five clusters (HPL, HPZ, HC0, HWN, HCP) and three geothermal fields (GT HPL, GT HC, GT HW0) are connected to two hydraulic rings through substations. The piping network allows the clusters and geothermal storages to exchange the mass flow rate, respecting at each node the Equations (3.28), (3.29) and (3.30). Figure 3.12 illustrates the scheme of the entire Anergy Grid based on the map of Figure 3.11.

The geothermal field Optimal GT of Figure 3.12 is not considered in this study.

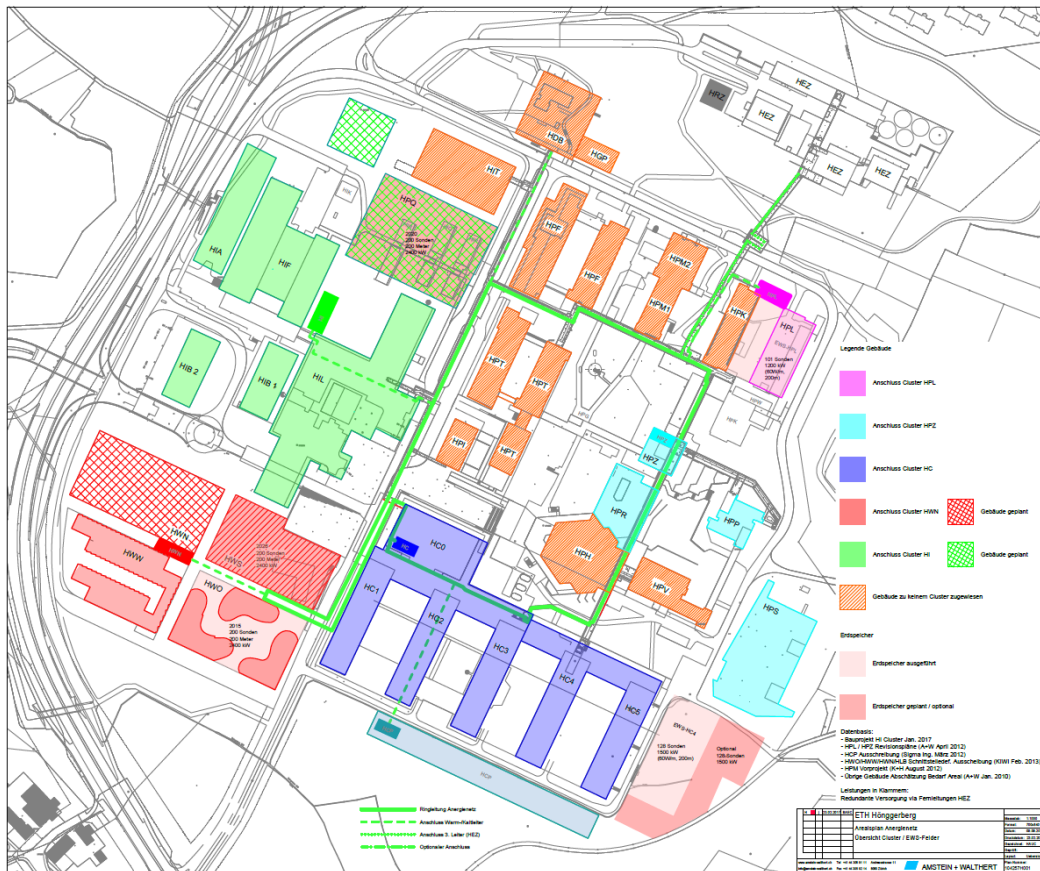


Figure 3.11: Anergy Grid map with pipeline network

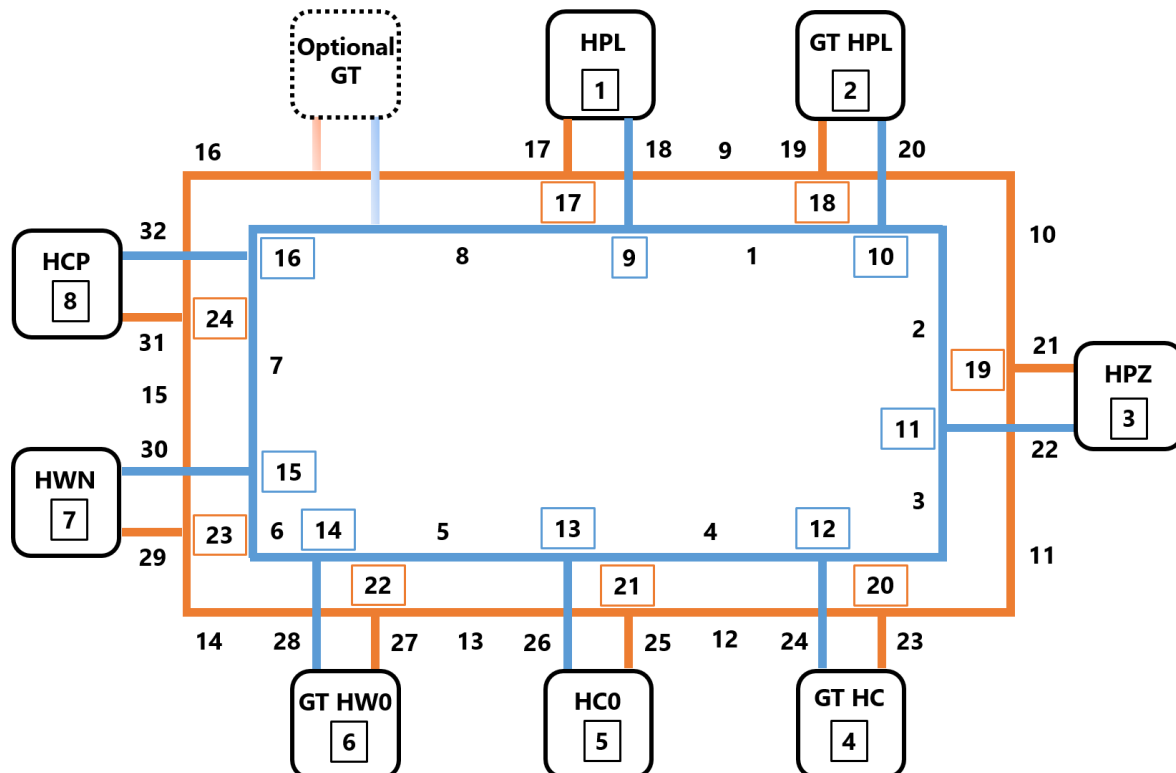


Figure 3.12: Anergy Grid network scheme

The equations used to describe the complete system are the mass and energy balances introduced for the simple network scheme.

CHAPTER 4: MATHEMATICAL MODEL FOR THE OPTIMIZATION OF THE ANERGY GRID OPERATION

In this chapter, an introduction on the aim of the study and on MILP optimization modeling is provided. Then, the linearization techniques applied to the equations of the case study are described. Later, the input data, the decision variables, the constraints and the objective function of the developed optimization model are reported and discussed. Finally, the considerations on the choice of the time horizon and on the optimization strategy are reported.

4.1. The aim of the optimization model

The aim of this study is to model the Anergy Grid in an optimization framework and to perform different analyses on the system in order to find the optimal operation of the technologies which minimizes the total annual CO₂ emissions. The considered multi-energy system has the primary objective of satisfying the energy demands of the users. It is connected to the gas and electrical national grids and composed of a set of traditional and renewable-based conversion technologies. The set of inputs of the optimization problem are the weather conditions, the load profiles, the energy prices and carbon rates and the performance characteristics of the technologies. The outputs of the optimization tool are the optimal values of the operational decision variables of the Anergy Grid.

The problem is mathematically formulated as a MILP (Mixed Integer Linear Programming), where binary variables are introduced to model the on-off status of the conversion technologies and the directions of the mass flows in the network. The MILP is presented with the general formulation:

$$\min_{\mathbf{x}, \mathbf{y}} (\mathbf{c}^T \mathbf{x} + \mathbf{d}^T \mathbf{y}) \quad (4.1)$$

s. t.

$$\mathbf{A}\mathbf{x} + \mathbf{B}\mathbf{y} = \mathbf{b} \quad (4.2)$$

$$\mathbf{x} \geq \mathbf{0} \in \mathbb{R}^{N_x}, \mathbf{y} \in \{0,1\}^{N_y} \quad (4.3)$$

where \mathbf{c} and \mathbf{d} indicate the cost vectors associated to continuous and binary decision variables, denoted respectively with \mathbf{x} and \mathbf{y} . \mathbf{A} and \mathbf{B} are the corresponding constraint coefficient matrices and \mathbf{b} is the constraint known-term. N_x and N_y represent the dimension of \mathbf{x} and \mathbf{y} respectively.

4.2. Linearization techniques

As can be seen in Chapter 3, the equations describing the technologies of the case study show numerous non-linearities, which have to be linearized in order to be implemented in a MILP formulation. The present subchapter analyses the adopted linearization techniques for the implementation of the equations listed in Chapter 3.

4.2.1. Linearization through experimental data

In the Equation (3.8), a non-linearity arises by the ratio between two operational variables of the plant, which are the electrical power absorbed by the heat pump P^{HP} and the temperature at the evaporator T^{eva} . On the other hand, the temperature at the condenser T^{cond} and the ξ parameter are considered as constant values. In order to implement the equation in a linear way, experimental data collected during the past operation of the Anergy Grid are employed. For each heat pump of the Anergy Grid, a scattering plot like the one shown in Figure 4.1 is available, which allows to extrapolate

linear relations among the provided thermal power \dot{Q}^{HP} , the consumed electrical power P^{HP} and the temperature of the heat transfer fluid at the inlet of the conversion technology T^{in} .

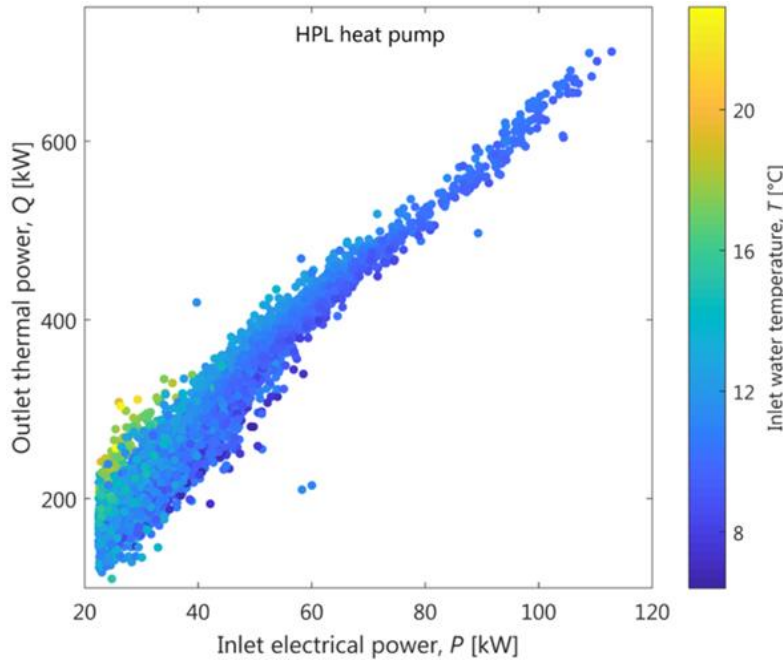


Figure 4.1: characteristic map of the heat pump installed in the HPL cluster

Each point of the map in Figure 4.1 indicates the heating power provided by the technology at a given time instant of the year with the corresponding absorbed electrical power and inlet temperature T^{in} of the heat-transfer fluid. As depicted in Figure 4.1, the trend of the points shows an almost linear behaviour. Applying the least squares method, the experimental dataset is reduced to the polynomial form:

$$\dot{Q}^{HP} = \alpha_1 P^{HP} + \alpha_2 T^{in} + \alpha_3 \quad (4.4)$$

where α_1 , α_2 and α_3 are constant coefficients. The least squares method assigns the coefficients of a linear function applying the principle of least squares: minimizing the sum of the squares of the differences between the data values of the dataset and the values predicted by the linear function.

4.2.2. Ordinary least squares method

Referring to the Equation (3.12), the exponential term represents a non-linearity given by the presence of the mass flow rate \dot{m} , which is an operational variable of the Anergy Grid, at the denominator of the exponential argument.

For this reason, it is not possible to directly implement the Equation (3.12) within a MILP formulation. Thus, the exponential term $1 - e^{-\frac{UA}{\dot{m}c}}$ is linearized using the ordinary least squares method, as shown in Figure 4.2.

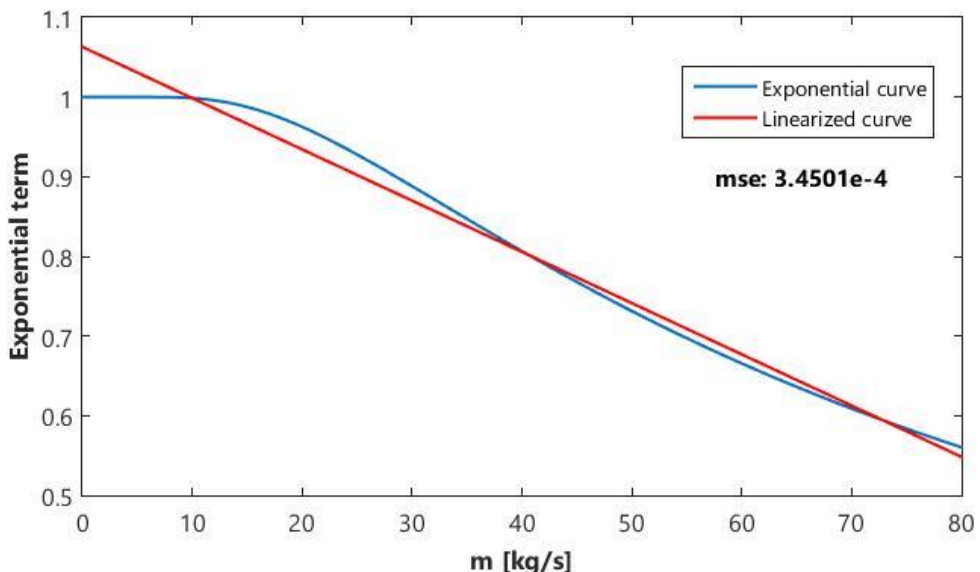


Figure 4.2: linearized curve of the exponential term. In blue: the exponential curve as a function of the mass flow rate. In red: the linearized curve adopting the OLS method. The minimized mean squared error is reported on the figure

The employed values of U , A and c are listed in Table 4.1.

Table 4.1: input data of the heat exchanger

U	1.1	$\frac{kW}{m^2 K}$
A	250	m^2
c	4.186	$\frac{kJ}{kg K}$

The ordinary least squares method is a particular type of linear least squares method for estimating a dataset in a linear regression model. Hence, the exponential term $1 - e^{-\frac{UA}{mc}}$ is reduced in the polynomial form $\beta_1 + \beta_2 \dot{m}$, and the Equation (3.12) becomes:

$$T' = T^{in} - (T^{in} - T^{eva})(\beta_1 + \beta_2 \dot{m}) \quad (4.5)$$

where β_1 and β_2 are constant coefficients. It can be seen that the equation is still non-linear, due to the multiplication between the mass flow and the temperatures. Such non-linearity is treated by applying the linearization method described in the subchapter 4.2.4.

4.2.3. Product between a binary and a continuous variable

A common problem in the formulation of MILP models arises in the implementation of equations in which the product between a continuous and a binary variable is present. This non-linearity is easily treated in literature by introducing an auxiliary variable, which represents the product indeed, and applying a set of inequalities on the variables, such that the result of the application of these constraints is the desired product [31].

If b is a binary variable and a is a continuous variable such that $0 \leq a \leq M$, the continuous variable y is introduced to replace the product $y = ba$. The following constraints are added to force y to assume the value of ba :

$$y \leq Mb \quad (4.6)$$

$$y \leq a \quad (4.7)$$

$$y \geq a - M(1 - b) \quad (4.8)$$

$$y \geq 0 \quad (4.9)$$

The validity of these constraints can be checked by examining Table 4.2 in which all possible cases are listed.

Table 4.2: All possible products $y = ba$

b	a	ba	constraints	imply
0	$a: 0 \leq a \leq M$	0	$y \leq 0$ $y \leq a$ $y \geq a - M$ $y \geq 0$	$y = 0$
1	$a: 0 \leq a \leq M$	a	$y \leq M$ $y \leq a$ $y \geq a$ $y \geq 0$	$y = a$

4.2.4. McCormick envelopes linearization method

The multiplication between two continuous variables is a bilinearity that represents a real obstacle in the linear formulation of complex problems. In fact, it describes a non-convex problem, which cannot be expressed in a linear formulation without introducing strong approximations on the result. Usually, this problem is faced by conducting a specific analysis on the variables in order to find a satisfying solution with a heuristic approach. This is often an accepted solution of this kind of problem, which is applied in different MILP applications. Nevertheless, this approach can barely be applied in this work, since a big number of non-linearities are involved. They arise in each energy balance for each technology of each cluster and in each node of the network for every time instant. For this reason, an alternative approach is adopted by introducing the

McCormick envelopes linearization method [25]. It is a mathematical method that transforms a non-convex function into a convex one by relaxing the parameters on the problem. This eliminates the possibility of having several local minima that the solver may interpret as a global minimum, which represents the weak point of MINLP problems. Relaxing the bounds through a convex relaxation decreases the computational complexity of solving the problem at the cost of introducing solutions that do not correspond to the original function. The utility of this method is that it provides a lower bound of the optimal solution of the original function that is as close as possible to the optimal solution by having a linear formulation.

Figure 4.3 shows in a three-dimensional graph the non-convex surface of products between the two continuous variables m and T .

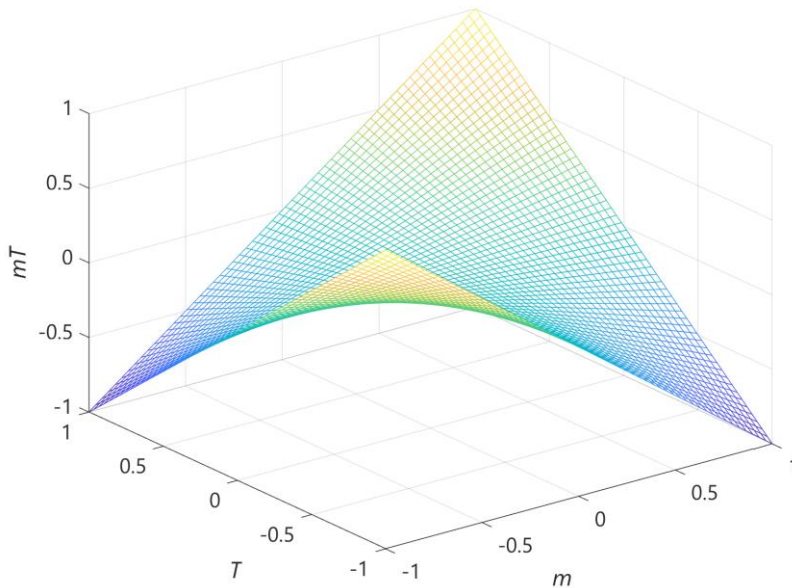


Figure 4.3: bilinear surface representation

According to the McCormick envelopes method, an auxiliary variable w , which represents the product, and the following inequalities on the continuous variables are introduced:

$$\dot{m}^L \leq \dot{m} \leq \dot{m}^U \quad (4.10)$$

$$T^L \leq T \leq T^U \quad (4.11)$$

$$w \geq \dot{m}^L T + \dot{m} T^L - \dot{m}^L T^L \quad (4.12)$$

$$w \geq \dot{m}^U T + \dot{m} T^U - \dot{m}^U T^U \quad (4.13)$$

$$w \leq \dot{m}^U T + \dot{m} T^L - \dot{m}^U T^L \quad (4.14)$$

$$w \leq \dot{m} T^U + \dot{m}^L T - \dot{m}^L T^U \quad (4.15)$$

These constraints describe a set of surfaces in the space illustrated in Figure 4.4.

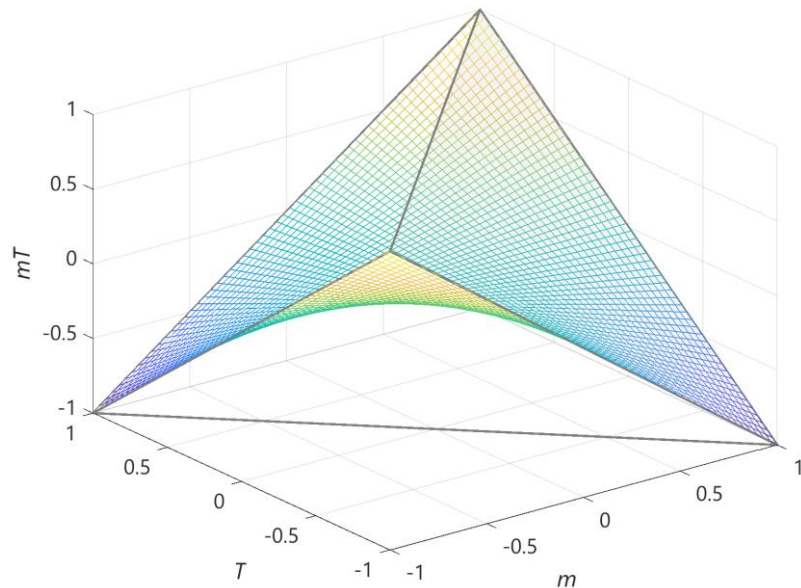


Figure 4.4: McCormick envelopes applied to the bilinear surface

McCormick envelopes introduce a convex relaxation that has the tightest bounds. An envelope is created to retain convexity while minimizing the size of the new feasible

region of solutions. This allows the lower bound obtained from using this method to be closer to the true solution than if other relaxations are used.

An upper bound of the optimal solution can be obtained by solving the original bilinear function using the results found with the relaxed problem and then checking for feasibility.

4.3. Input data

The input data of the problem are the measured 2016 time-dependent load profiles of the Anergy Grid. The input data of the optimization problem are:

- the set of clusters in the system I ;
- the set of geothermal fields in the system J ;
- the set of branches of the network V ;
- the expected thermal load, $\dot{Q}^{H-D} \in \mathbb{R}^{(I \times T)}$, low temperature cooling load, $\dot{Q}^{LT-D} \in \mathbb{R}^{(I \times T)}$, high temperature cooling load, $\dot{Q}^{HT-D} \in \mathbb{R}^{(I \times T)}$, profiles of each cluster;
- the CO₂ emission rates for electricity, f^E , and natural gas, f^G [tonCO₂/kWh];
- the environmental air temperature $T^{air} \in \mathbb{R}^T$ (see Appendix);
- the size and performance data of the installed technologies;
- the network layout.

Data are available for every hour of the year.

Other data related to the time horizon are:

- Δt , which indicates the duration of the time interval t [hours/day], with $t = 1, \dots, T$, where T represents the length of the time horizon [hours];
- D , which indicates the number of typical days in the considered time horizon.

4.4. Decision variables

Since the conversion technologies installed in each cluster can be completely by-passed, as mentioned in the subchapter 3.3, the binary variables x , y and z are introduced in the model to describe the on/off operation of the heat pump, of the low temperature heat exchanger and of the high temperature heat exchanger, respectively. Each of them is equal to 1, when the heat transfer fluid goes through the corresponding technology, otherwise when the fluid by-passes the technology, which consequently does not provide any heating or cooling power.

The decision variables of the optimization problem are listed here below.

- The on/off status of the heat pump, $x \in \{0,1\}^{I \times T}$, of the low temperature heat exchanger, $y \in \{0,1\}^{I \times T}$ and of the high temperature heat exchanger, $z \in \{0,1\}^{I \times T}$. They are equal to 1 if the technology installed in the cluster $i \in I$ is working at time t , $\forall t = 1, \dots, T$.
- The mass flow rate that flows in each cluster or geothermal field $\dot{m} \in \mathbb{R}^{(I+J) \times T}$ and in each branch of the network $\dot{m} \in \mathbb{R}^{V \times T}$ [kg/s].
- The inlet temperature in the cluster $T^{in} \in \mathbb{R}^{I \times T}$, the temperature at the outlet of the heat pump $T' \in \mathbb{R}^{I \times T}$, the temperature at the evaporator $T^{eva} \in \mathbb{R}^{I \times T}$, the temperature at the outlet of the low temperature heat exchanger $T'' \in \mathbb{R}^{I \times T}$, the temperature at the outlet of the high temperature heat exchanger $T^{out} \in \mathbb{R}^{I \times T}$,

the inlet temperature in the geothermal field $T^{GT_in} \in \mathbb{R}^{J \times T}$, the average borehole wall temperature $T^b \in \mathbb{R}^{J \times T}$, the outlet temperature of the geothermal field $T^{GT_out} \in \mathbb{R}^{J \times T}$, the temperature of the mass flow in each branch of the network $T \in \mathbb{R}^{V \times T}$ [K].

- The primary power of the boiler $P^G \in \mathbb{R}^{I \times T}$; the thermal powers provided by the heat pump $\dot{Q}^{HP} \in \mathbb{R}^{I \times T}$, by the boiler $\dot{Q}^B \in \mathbb{R}^{I \times T}$ and by the geothermal field to the heat transfer fluid $\dot{Q}^{GT} \in \mathbb{R}^{J \times T}$; the thermal power absorbed $\dot{Q}^{HWTS_in} \in \mathbb{R}^{I \times T}$ and provided $\dot{Q}^{HWTS_out} \in \mathbb{R}^{I \times T}$ by the hot water thermal storage; the electrical power absorbed by the heat pump $P^{HP} \in \mathbb{R}^{I \times T}$ and by the chiller $P^{CH_LT} \in \mathbb{R}^{I \times T}$ and $P^{CH_HT} \in \mathbb{R}^{I \times T}$; the low temperature cooling powers provided by the low temperature heat exchanger $\dot{Q}^{LT} \in \mathbb{R}^{I \times T}$ and by the electrical chiller $\dot{Q}^{CH_LT} \in \mathbb{R}^{I \times T}$; the high temperature cooling powers provided by the high temperature heat exchanger $\dot{Q}^{HT} \in \mathbb{R}^{I \times T}$ and by the electrical chiller $\dot{Q}^{CH_HT} \in \mathbb{R}^{I \times T}$ [W].
- The binary variables $d \in \{0,1\}^{V \times T}$ that indicate the flow direction in each branch of the network.
- The stored thermal energy $E^{HWTS} \in \mathbb{R}^{I \times T}$, the initial stored energy $E_0^{HWTS} \in \mathbb{R}^I$ and the capacity $S^{HWTS} \in \mathbb{R}^I$ of the hot water thermal storage [Wh].

4.5. Constraints

In the following the constraints of the optimization problem related to the performance of the technologies and to the energy balances are reported. Most of the performance equations of the technologies are described in the Chapter 3.

4.5.1. Boiler

The boiler generates thermal energy from the combustion of natural gas. Constraints on the performance of the technology are derived from Equation (3.1).

$$\dot{Q}_{i,t}^B = \eta^B P_{i,t}^G \quad (4.16)$$

with $i \in I$ and $t = 1, \dots, T$.

Moreover, the primary power of the boiler is limited by the size of the technology S^B .

$$0 \leq P_{i,t}^G \leq S^B \quad (4.17)$$

with $i \in I$ and $t = 1, \dots, T$.

Note that all the installed boilers are characterized by the same values of thermal efficiency and size.

Table 4.3: Input data of the boiler

η^B	0.92	-
S^B	900	kW

4.5.2. Electrical chillers

The electrical chiller provides cooling energy by absorbing electrical energy. Constraints on the performance of the technology are derived from Equations (3.2) and (3.3).

$$\dot{Q}_{i,t}^{CH_LT} = COP^{CH_LT} P_{i,t}^{CH_LT} \quad (4.18)$$

$$\dot{Q}_{i,t}^{CH_HT} = COP^{CH_HT} P_{i,t}^{CH_HT} \quad (4.19)$$

with $i \in I$ and $t = 1, \dots, T$.

The electrical power absorbed is limited by the sizes of the technologies S^{CH_LT} and S^{CH_HT} .

$$0 \leq P_{i,t}^{CH_LT} \leq S^{CH_LT} \quad (4.20)$$

$$0 \leq P_{i,t}^{CH_HT} \leq S^{CH_HT} \quad (4.21)$$

with $i \in I$ and $t = 1, \dots, T$.

Note that all the installed chillers are characterized by the same values of coefficient of performance and size.

Table 4.4: Input data of the electrical chiller

COP^{CH_LT}	3.5	-
COP^{CH_HT}	3.5	-
S^{CH_LT}	300	kW
S^{CH_HT}	300	kW

4.5.3. Hot water thermal storage

The hot water thermal storage allows to accumulate thermal energy. Due to the fairly high energy losses and the low energy density, this technology is mainly used to overcome short-term mismatch between thermal energy generation and use. The hot water thermal storage is not installed in the Anergy Grid, but this study intends to evaluate the inclusion of this technology as a possible solution to reduce the total annual CO₂ emissions. For this reason, it is the only technology for which a design optimization strategy is applied, in which its different sizes and initial stored energy are decision variables. Constraints on the performance of the technology are derived from Equations (3.4), (3.5), (3.6) and (3.7).

$$E_{i,t}^{HWTS} = E_{i,t-1}^{HWTS}(1 - \Lambda\Delta t) + \\ - \left(\Pi S_i^{HWTS} h_t - \eta^{HWTS_in} \dot{Q}_{i,t}^{HWTS_in} + \frac{1}{\eta^{HWTS_out}} \dot{Q}_{i,t}^{HWTS_out} \right) \Delta t \quad (4.22)$$

$$h_t = \frac{T^{HWTS_min} - T_t^{air}}{T^{HWTS_max} - T^{HWTS_min}} \quad (4.23)$$

$$\dot{Q}_{i,t}^{HWTS_in} \leq \frac{S_i^{HWTS}}{\tau^{HWTS}} \quad (4.24)$$

$$\dot{Q}_{i,t}^{HWTS_out} \leq \frac{S_i^{HWTS}}{\tau^{HWTS}} \quad (4.25)$$

with $i \in I$ and $t = 1, \dots, T$. In this analysis a Δt of 1 h is fixed.

A periodicity constraint imposes the same storage level at the beginning and at the end of the year:

$$E_{i,0}^{HWTS} = E_{i,T}^{HWTS} \quad (4.26)$$

The stored thermal power is limited by the sizes of the technologies S_i^{HWTS} , which are in turn limited by minimum and maximum input values:

$$0 \leq E_{i,t}^{HWTS} \leq S_i^{HWTS} \quad (4.27)$$

$$S^{HWTS_min} \leq S_i^{HWTS} \leq S^{HWTS_max} \quad (4.28)$$

with $i \in I$ and $t = 1, \dots, T$.

Note that all the installed heat pumps have the same input data.

Table 4.5: Input data of the hot water thermal storage

Λ	0.005	h^{-1}
Π	0.0005	-

η^{HWTS_in}	0.95	-
η^{HWTS_out}	0.95	-
T^{HWTS_min}	55	°C
T^{HWTS_max}	90	°C
τ^{HWTS}	3	h
S^{HWTS_min}	0	kWh
S^{HWTS_max}	28 000	kWh

4.5.4. Heat pump

The heat pump is used to produce thermal energy by exploiting the energy contained in the heat transfer fluid and absorbing electricity. Constraints on the performance of the technology are derived from Equations (3.13), (4.4) and (4.5).

$$\dot{Q}_{i,t}^{HP} = \alpha_1 P_{i,t}^{HP} + \alpha_2 T_{i,t}^{in} x_{i,t} + \alpha_3 x_{i,t} \quad (4.29)$$

$$T'_{i,t} = T_{i,t}^{in} - (T_{i,t}^{in} - T_{i,t}^{eva})(\beta_1 + \beta_2 \dot{m}_{i,t})x_{i,t} \quad (4.30)$$

$$\dot{Q}_{i,t}^{HP} = P_{i,t}^{HP} + \dot{m}_{i,t} c (T_{i,t}^{in} - T'_{i,t})x_{i,t} \quad (4.31)$$

with $i \in I$ and $t = 1, \dots, T$.

The binary variable x is introduced in the constraints so that if the mass flow bypasses the conversion technology (and therefore $x_{i,t}=0$), there is no thermal flux exchanged with the user and the flow temperature remains equal to the inlet temperature to the heat pump.

The electric power absorbed by the heat pump is limited by its size S^{HP} and by a minimum technical value, which is a percentage of the size.

$$\delta S^{HP} x_{i,t} \leq P_{i,t}^{HP} \leq S^{HP} x_{i,t} \quad (4.32)$$

with $i \in I$ and $t = 1, \dots, T$.

Note that all the installed heat pumps have the same input data.

Table 4.6: Input data of the heat pump

α_1	6.493	-
α_2	5.285	-
α_3	-36.1	-
β_1	-0.0064	-
β_2	1.063	-
c	4.186	$\frac{kJ}{kg K}$
δ	0.1	-
S^{HP}	120	kW

Equations (4.29), (4.30), (4.31) and (4.32) present non-linearities due to the product between a continuous and a binary variable and between two continuous decision variables. Such non-linearities are treated by applying the additional constraints of the linearization techniques described in subchapter 4.2 by Equations (4.6), (4.7), (4.8), (4.9) and Equations (4.10), (4.11), (4.12), (4.13), (4.14), (4.15) respectively. In the implementation of the McCormick envelopes method, it is necessary to provide minimum and maximum values of the involved continuous variables. The decision variables to which this linearization method is applied are the mass flow rates and the temperatures or variables derived from them. Therefore, minimum and maximum values of temperature (T^{min} and T^{max}) and mass flow (\dot{m}^{min} and \dot{m}^{max}) are defined. Since for legal regulations the temperature of the geothermal field must be kept between $8^{\circ}C$ and $24^{\circ}C$, this restriction is applied to all the temperature variables on which the McCormick envelopes method is applied. For the mass flow rate, conservative experimental values between 0 kg/s and 80 kg/s are applied.

Table 4.7: Input data for the implementation of the McCormick envelopes linearization method

T^{min}	8	$^{\circ}C$
T^{max}	24	$^{\circ}C$
\dot{m}^{min}	0	kg/s
\dot{m}^{max}	80	kg/s

4.5.5. Low temperature heat exchanger

The low temperature heat exchanger exploits the energy contained in the heat transfer fluid exiting the heat pump in order to cool the laboratory water of the clusters, generating low temperature cooling power. Constraints on the performance of the technology are derived from Equations (3.18) and (3.19).

$$\dot{Q}_{i,t}^{LT} = \dot{m}_{i,t} c (T''_{i,t} - T'_{i,t}) y_{i,t} \quad (4.33)$$

$$T''_{i,t} = T^{LTHE} y_{i,t} + T'_{i,t} (1 - y_{i,t}) \quad (4.34)$$

with $i \in I$ and $t = 1, \dots, T$.

Analogously to the heat pump, the binary variable y is introduced in the constraints so that if the mass flow bypasses the conversion technology (and therefore $y_{i,t}=0$), there is no low temperature cooling flux exchanged with the user and the flow temperature remains equal to the inlet temperature to the low temperature heat exchanger.

The provided low temperature cooling power is limited by the size of the technology S^{LTHE} .

$$0 \leq \dot{Q}_{i,t}^{LT} \leq S^{LTHE} y_{i,t} \quad (4.35)$$

with $i \in I$ and $t = 1, \dots, T$.

Also in this case, the non-linearities present in the Equations (4.33), (4.34) and (4.35) are treated by applying the additional constraints of the linearization techniques described in subchapter 4.2.

Note that all the installed low temperature heat exchangers have the same input data.

Table 4.8: Input data of the low temperature heat exchanger

T^{LTHE}	12	$^{\circ}C$
S^{LTHE}	1000	kW

4.5.6. High temperature heat exchanger

Similarly to the low temperature heat exchanger, the technology provides cooling energy, but at higher temperature for the air conditioning system of the clusters. Constraints on the performance of the technology are derived from Equations (3.20) and (3.21).

$$\dot{Q}_{i,t}^{HT} = \dot{m}_{i,t} c (T_{i,t}^{out} - T''_{i,t}) z_{i,t} \quad (4.36)$$

$$T_{i,t}^{out} = T^{HTHE} z_{i,t} + T''_{i,t} (1 - z_{i,t}) \quad (4.37)$$

with $i \in I$ and $t = 1, \dots, T$.

As for the two previous technologies, the binary variable z is introduced in the constraints so that if the mass flow bypasses the conversion technology (and therefore $z_{i,t}=0$), there is no high temperature cooling flux exchanged with the user and the flow temperature remains equal to the inlet temperature to the high temperature heat exchanger.

The provided high temperature cooling power is limited by the size of the technology S^{HTHE} .

$$0 \leq \dot{Q}_{i,t}^{HT} \leq S^{HTHE} z_{i,t} \quad (4.38)$$

with $i \in I$ and $t = 1, \dots, T$.

Analogously to the heat pump and to the low temperature heat exchanger, the nonlinearities present in the Equations (4.36), (4.37) and (4.38) are treated by applying the additional constraints of the linearization techniques described in subchapter 4.2.

Note that all the installed low temperature heat exchangers have the same input data.

Table 4.9: Input data of the high temperature heat exchanger

T^{HTHE}	16	$^{\circ}\text{C}$
S^{HTHE}	1000	kW

4.5.7. Geothermal field

The geothermal field consists of a big storage of water which is insulated by the external air temperature. Constraints on the performance of the technology are derived from Equations (3.23), (3.24), (3.25), (3.26) and (3.27).

$$T_{j,t}^b = T^{s,0} + \frac{1}{2\pi\lambda LN_j} \sum_{i=1}^t (\dot{Q}_{j,i}^{GT} - \dot{Q}_{j,i-1}^{GT}) g(r_j^b, t-i) \quad (4.39)$$

$$\dot{Q}_{j,t}^{GT} = \dot{m}_{j,t} c (T_{j,t}^{GT_out} - T_{j,t}^{GT_in}) \quad (4.40)$$

$$\frac{\dot{Q}_{j,t}^{GT}}{LN_j} = \frac{1}{R^b} (T_{j,t}^b - \bar{T}_{j,t}^f) \quad (4.41)$$

$$\bar{T}_{j,t}^f = \frac{T_{j,t}^{GT_in} + T_{j,t}^{GT_out}}{2} \quad (4.42)$$

$$T^{GT_min} \leq T_{j,t}^b \leq T^{GT_max} \quad (4.43)$$

with $j \in J$ and $t = 1, \dots, T$.

An additional constraint is inserted for the soil temperature. It is imposed that at the end of the considered time horizon, the borehole temperature has to remain close to its temperature at the beginning of the simulation. Such constraint forces the system to have a sustainable operation also for period longer than the considered time horizon.

$$T_{j,0}^b - \Delta T^b \leq T_{j,T}^b \leq T_{j,0}^b + \Delta T^b \quad (4.44)$$

with $j \in J$.

Similarly to the conversion technologies described above, the non-linearities present in the Equation (4.40) are treated by applying the additional constraints of the McCormick envelopes linearization method described in subchapter 4.2.4.

The input data of the geothermal fields are reported in Table 4.10.

Table 4.10: Input data of the geothermal field

$T^{s,0}$	14	$^{\circ}\text{C}$
λ	2.9	$\frac{\text{W}}{\text{m K}}$
L	400	m
N_{HPL}	101	-
N_{HC}	128	-
N_{HW0}	200	-
R^b	88	$\frac{\text{m K}}{\text{W}}$
$g(r_j^b, t - i)$	See Figure 4.5	-
T^{GT_min}	8	$^{\circ}\text{C}$
T^{GT_max}	24	$^{\circ}\text{C}$
ΔT^b	0	$^{\circ}\text{C}$

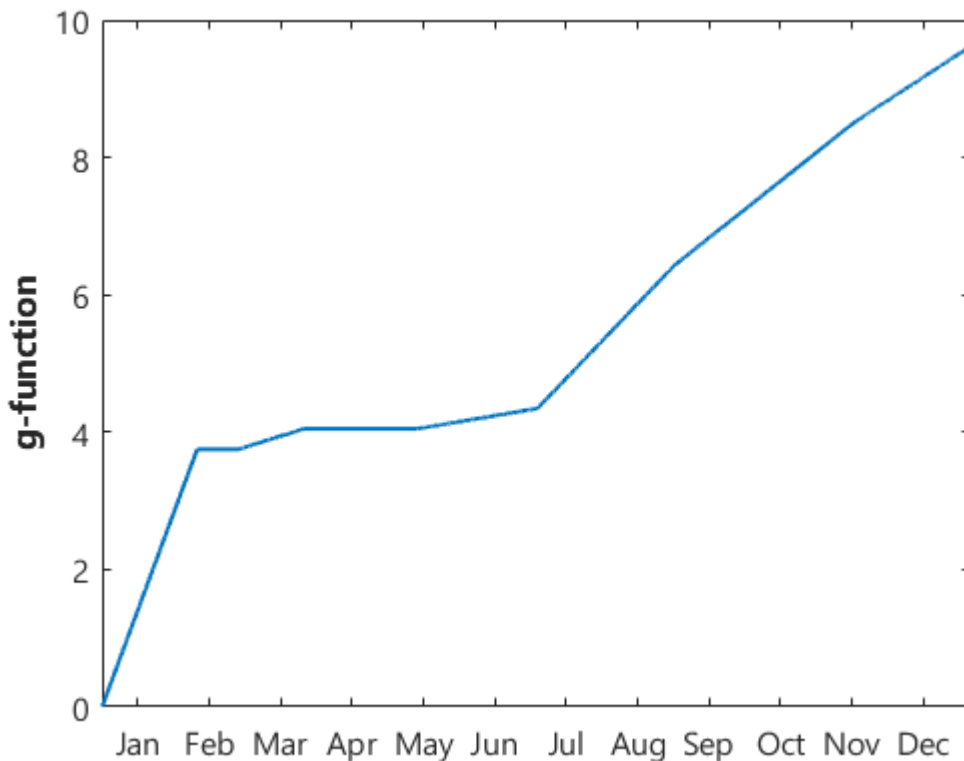


Figure 4.5: Yearly profile of the g-function

Due to lack of data, the same value of the g -function (relative to the geothermal storage GT HPL) is applied to the three geothermal fields. However, this fact does not affect the validity of this analysis.

4.5.8. Thermal network

A general formulation for the thermal network is implemented, for which mass flow rates, temperatures and flow directions in the branches are decision variables of the optimization problem. The fact that directions are not predetermined increases the complexity of the problem formulation. In the following, the network constraints are listed for simplicity only for the simple network configuration, since the implementation on the complete Anergy Grid network is analogous.

Mass balances

Two matrices of the network with binary variables are defined and the values of mass flow rate circulating in the branches are inserted into a column vector, as shown in Figure 4.6 and Figure 4.7. The formulation of these matrices and of this vector refers to the simple network with the values of nodes and branches, as they are represented in Figure 3.8.

		BRANCHES					
		1	2	3	4	5	6
NODES	1	$d_{1,1,t}$	0	0	$d_{1,4,t}$	0	0
	2	0	$d_{2,2,t}$	$d_{2,3,t}$	0	0	0
	3	0	0	0	0	$d_{3,5,t}$	$d_{3,6,t}$
	4	0	0	$d_{4,3,t}$	$d_{4,4,t}$	$d_{4,5,t}$	0
	5	$d_{5,1,t}$	$d_{5,2,t}$	0	0	0	$d_{5,6,t}$

Figure 4.6: Network MatrixA

The binaries $d_{l,v,t}$ are determined so that they can assume either the value 1 if the corresponding flow is entering in the node l from the branch v or 0 if it is exiting.

The binaries $b_{l,v,t}$ are defined as:

$$b_{l,v,t} = 2(d_{l,v,t} - 0.5) \quad (4.45)$$

with $l \in (I + J)$, $v \in V$ and $t = 1, \dots, T$.

In this way, $b_{l,v,t}$ is equal to +1 if the corresponding flow is entering in the node l from the branch v or -1 if it is exiting. On the other side, $\dot{m}_{v,t}$ is defined as the value of the mass flow rate flowing in the branch v and it is equal or greater than 0. This last constraint is indirectly applied by the implementation of the Equation (4.10) of the McCormick envelopes method, where $\dot{m}^L = \dot{m}^{min} = 0 \text{ kg/s}$.

		BRANCHES						
		1	2	3	4	5	6	
NODES	1	$b_{1,1,t}$	0	0	$b_{1,4,t}$	0	0	$\dot{m}_{1,t}$
	2	0	$b_{2,2,t}$	$b_{2,3,t}$	0	0	0	$\dot{m}_{2,t}$
	3	0	0	0	0	$b_{3,5,t}$	$b_{3,6,t}$	$\dot{m}_{3,t}$
	4	0	0	$b_{4,3,t}$	$b_{4,4,t}$	$b_{4,5,t}$	0	$\dot{m}_{4,t}$
	5	$b_{5,1,t}$	$b_{5,2,t}$	0	0	0	$b_{5,6,t}$	$\dot{m}_{5,t}$

Figure 4.7: Network MatrixB and mass flow vector

The mass balance of the network is defined by imposing equal to 0 the product between the network matrix and the mass flow vector:

$$\text{MatrixB}_t \times \text{FlowVector}_t = 0 \quad (4.46)$$

The non-linearities present in the Equation (4.46) are linearized by applying the additional constraints of the product between a binary and a continuous variable described in subchapter 4.2.3.

Energy balances

In order to apply energy balances at the nodes without having predetermined directions, the following methodology is implemented. As explained in the subchapter 3.5.1, two different types of constraints have to be imposed: splitting and mixing constraints.

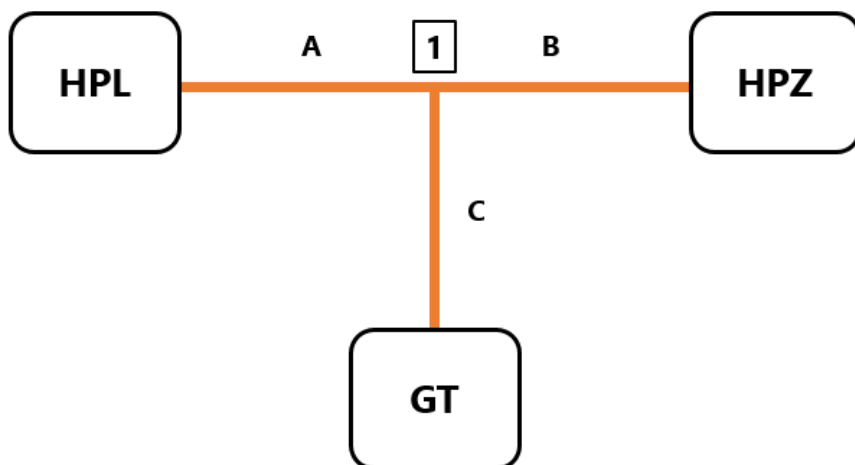
**Figure 4.8: Node representation**

Figure 4.8 illustrates the scheme of one node of the simple network. In order to distinguish if in the considered node either a splitting or a mixing constraint has to be applied, a binary parameter is introduced, defined as:

$$bin_{l,t} = 2 - \sum_{idx=A,B,C} d_{l,idx,t} \quad (4.47)$$

with $l \in (I + J)$ and $t = 1, \dots, T$.

By the definition of the binary variables that determine the flow direction $d_{l,v,t}$, $bin_{l,t}$ is equal to 1 if mass flow is entering the node l from one branch and exiting from the other two branches, while it is equal to 0 if mass flow is entering the node l from two branches and exiting from the other branch. In this way, the splitting constraint for the example of Figure 4.8 is imposed as in the Equation (4.48).

$$\begin{aligned} bin_{1,t} [d_{1,A,t} T_{HPL,t}^{out} + (1 - d_{1,A,t}) T_{HPL,t}^{in}] &= \\ = bin_{1,t} [d_{1,B,t} T_{HPZ,t}^{out} + (1 - d_{1,B,t}) T_{HPZ,t}^{in}] &= \\ = bin_{1,t} [d_{1,C,t} T_{GT,t}^{out} + (1 - d_{1,C,t}) T_{GT,t}^{in}] \end{aligned} \quad (4.48)$$

The Equation (4.49) shows the implementation of the mixing constraint.

$$\begin{aligned} d_{1,A,t} \dot{m}_{A,t} T_{HPL,t}^{out} + d_{1,B,t} \dot{m}_{B,t} T_{HPZ,t}^{out} + d_{1,C,t} \dot{m}_{C,t} T_{GT,t}^{out} &= \\ = (1 - d_{1,A,t}) \dot{m}_{A,t} T_{HPL,t}^{in} + (1 - d_{1,B,t}) \dot{m}_{B,t} T_{HPZ,t}^{in} + (1 - d_{1,C,t}) \dot{m}_{C,t} T_{GT,t}^{in} \end{aligned} \quad (4.49)$$

with $l \in (I + J)$ and $t = 1, \dots, T$.

It is worthy to point out that if the node 1 has a splitting configuration, the constraint of Equation (4.49) is automatically verified by the application of Equations (4.46) and (4.48).

The constraints reported above for the example of Figure 4.8 are implemented for every node of the simple network and of the complete Anergy Grid network.

The non-linearities present in the Equations (4.48) and (4.49) are treated by applying the additional constraints of the linearization techniques described in subchapter 4.2.

4.5.9. Energy balances at the user

In this subchapter, the constraints that impose the fulfillment of the power demands by the users are described.

Thermal demand

The conversion technologies that provide thermal power are the heat pumps, the boilers and the hot water thermal storages, if installed. The energy balance at the node without the installation of the hot water thermal storages is expressed by Equation (4.50).

$$\dot{Q}_{i,t}^{H,D} = \dot{Q}_{i,t}^{HP} + \dot{Q}_{i,t}^B \quad (4.50)$$

If the hot water thermal storages are installed in the clusters, the energy balance at the nodes becomes:

$$\dot{Q}_{i,t}^{H,D} + \dot{Q}_{i,t}^{HWTS,in} = \dot{Q}_{i,t}^{HP} + \dot{Q}_{i,t}^B + \dot{Q}_{i,t}^{HWTS,out} \quad (4.51)$$

with $i \in I$ and $t = 1, \dots, T$.

Low temperature cooling demand

The installed conversion technologies that provide low temperature cooling power are the low temperature heat exchangers and the electrical chillers. The energy balance at the nodes is given by the Equation (4.52).

$$\dot{Q}_{i,t}^{LT,D} = \dot{Q}_{i,t}^{LT} + \dot{Q}_{i,t}^{CH,LT} \quad (4.52)$$

with $i \in I$ and $t = 1, \dots, T$.

High temperature cooling demand

The installed conversion technologies that provide high temperature cooling power are the high temperature heat exchangers and the electrical chillers. The energy balance at the nodes is expressed by the Equation (4.53).

$$\dot{Q}_{i,t}^{HT_D} = \dot{Q}_{i,t}^{HT} + \dot{Q}_{i,t}^{CH-HT} \quad (4.53)$$

with $i \in I$ and $t = 1, \dots, T$.

4.6. Objective function

The objective function to be minimized is the total annual CO₂ emissions of the system C , measured in $tonCO_2$. It derives from the sum of two terms:

- emissions associated to the electrical energy imported from the national grid (and used by heat pumps and electrical chillers);
- emissions related to the natural gas consumption of boilers.

Table 4.11 reports the relative CO₂ rates, which are considered constant along the year [32].

Table 4.11: Carbon dioxide emission factors of the energy vectors

Carbon dioxide emission factor f [$tonCO2/kWh$]:	
Electricity	3e-05
Natural gas	2.37e-04

The electricity emission factor value reported in Table 4.11 is quite unusual compared to the European standard values. This is due to the fact that ETH University buys only

electricity from renewable sources [33], above all hydroelectric power plants. Thus, a very low CO₂ emission factor is associated to the electrical energy withdrawn from the national grid.

No CO₂ emissions are linked to the heat exchangers and to the geothermal fields.

By the definition of the emission factors, the total annual CO₂ emissions of the system can be calculated as:

$$\begin{aligned} C = f^E \Delta t & \left(\sum_{i=1}^I \sum_{t=1}^T P_{i,t}^{HP} + \sum_{i=1}^I \sum_{t=1}^T P_{i,t}^{CH_LT} + \sum_{i=1}^I \sum_{t=1}^T P_{i,t}^{CH_HT} \right) + \\ & + f^G \Delta t \sum_{i=1}^I \sum_{t=1}^T P_{i,t}^G \end{aligned} \quad (4.54)$$

4.7. Time horizon representation

The considered time horizon for the present study is one year with hour resolution. Because of the huge number of decision variables and constraints, a time discretization has to be applied to the model in order to reduce the computational complexity of the problem. Recently, a specific study on time discretization methods applied to energy models has been proposed by Pfenninger [6], who analysed different techniques to decrease the time resolution based on k-means clustering algorithm proposed by Lloyd [22]. For the present work, the M0, M1 and M2 methods proposed by Gabrielli et al. [21] are adopted.

- Method M0 represents the traditional methodology, in which the sequence of design days along the year is formulated independently for each design day D . In this way, each day is decoupled from the previous and the following one. For

this reason, such method is not suitable to the present study, which involves the installation of a geothermal storage with a seasonal dynamics.

- Method M1 allows the full-scale (hour-by-hour) description of the geothermal storage while still describing the time horizon through typical design days. It introduces a vector σ that represents the sequence of typical design days, which allows to couple successive days of the year.
- Method M2 is based on the fact that binary variables are mainly responsible for the increase in computational complexity. Thus, the binary decision variables are clustered into typical design days, like for the method M1, while the continuous variables are described hour-by-hour.

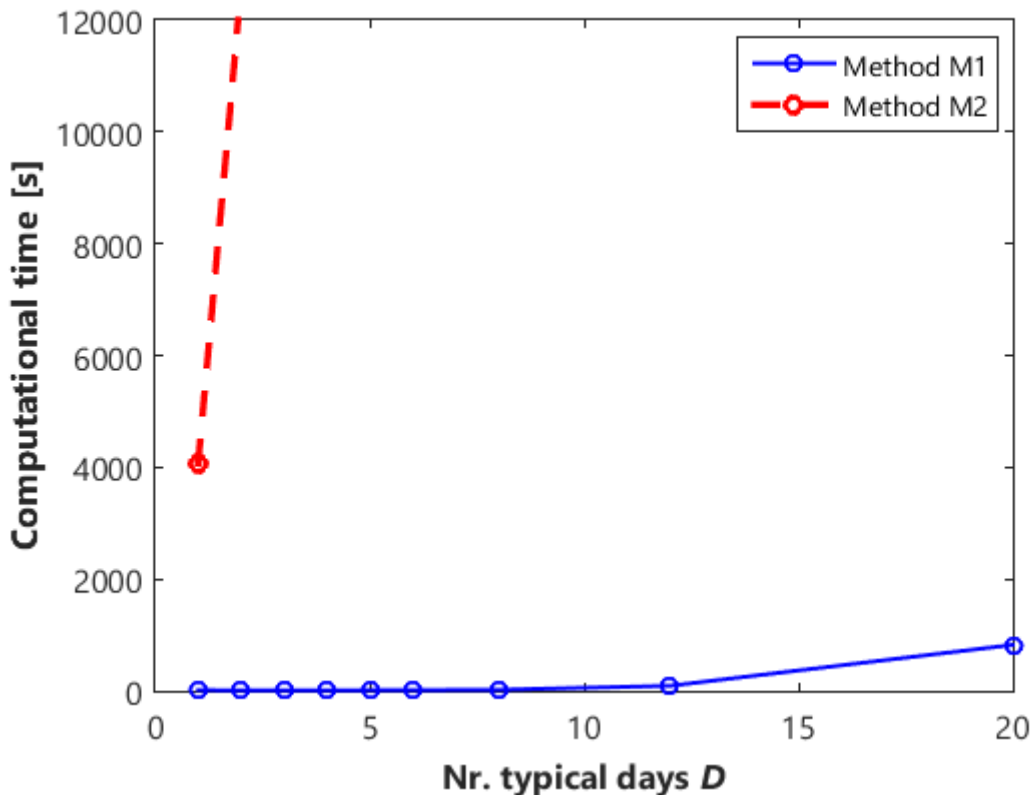


Figure 4.9: Sensitivity analysis on the number of typical design days using M1 (blue line) and M2 (red line) methods

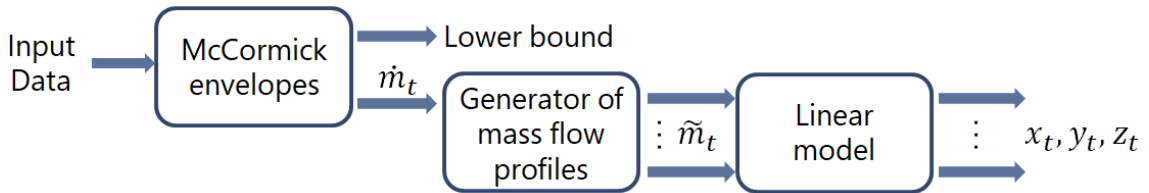
In the present study, a sensitivity analysis is performed on M1 and M2 time discretization methods in order to evaluate the computational complexity of the optimization problem for different number of typical design days D . Figure 4.9 shows the difference in computational time between the two methods for the calculation of the single node configuration. Based on the results of this analysis, the discretization method M1 is adopted for this study, since it allows to strongly reduce computational time of the performed simulations, still remaining sufficiently close to the full scale solution.

4.8. The optimization strategies

The most important decision variables for the operation of the real system are the mass flow rates \dot{m}_t , the scheduling of the technologies x_t , y_t and z_t and the directions of the flows in the branches. The values of the other decision variables (fluid temperature along the circuit and exchanged power or the power exchanged with the users) are a consequence of the performance equations of the conversion technologies. For this reason, the focus of this study is on finding the optimal values of the flow rate, of the binary variables x_t , y_t and z_t and of the network directions, that solve the problem while minimizing the total CO₂ emissions of the system.

4.8.1. The optimization strategy for the single node

Given the configuration of the single node, there are no constraints on the network, thus the variables that determine the flow directions are not involved. The strategy adopted to solve the optimization problem for the single node configuration is shown in Figure 4.10.

**Figure 4.10: Optimization strategy for the single node**

Since the equations of the model present bilinearities, the problem is firstly solved by using the McCormick envelopes linearization method. The solution provides an indication on the lower bound of the solution. It represents a lower limit for the emissions of the real system.

Note that the found solution gives also a reference mass flow rate profile along the year. Applying the McCormick envelopes method, this mass flow rate profile settles in “low” values. This is due to the fact that this linearization method introduces auxiliary variables that substitute the product between mass flow rate and temperature, chosen in their respective domains (see Equations (4.10) – (4.15) and Table 4.7). Such auxiliary variables are employed in the energy balance equations to satisfy the requested power demands, expressed as $\dot{Q} = \dot{m}c\Delta T$. While the mass flow rate that flows along the circuit is the same, the temperature values for each technology are less constrained. Hence, when at the same time instant the user requires a high thermal demand and a low cooling demand (or vice versa), the relaxed model has a domain of the decision variables large enough to satisfy all the loads, by choosing a low mass flow rate, suitable to satisfy the lower demand, and a high temperature difference to satisfy the higher demand. Thus, the mass flow rate profile found with the McCormick envelopes linearization method is under-estimated compared to the real one.

Therefore, a generator of mass flow profiles is employed, which produces new flow curves starting from the one found with McCormick envelopes. Such profiles are used

as input data to eliminate the non-linearities of the model and to solve the linear model without introducing the approximations deriving from the McCormick method. In this way, for each mass flow profile generated, the optimal solution is obtained, providing the scheduling profile of the conversion technologies. Among the obtained solutions, the one with the lowest level of total CO₂ emissions is the best solution proposed for the optimal operation of the system.

4.8.2. The optimization strategy for the Anergy Grid

For the simple network and the Anergy Grid configurations, the network constraints have to be included and consequently the decision variables on the direction of the flows in the branches have to be taken into account. In order to reduce the computational complexity of the problem, the binary variables that determine the flow direction in each branch can only assume one value for the whole year. In this way, the model can choose only one possible configuration of the network. The new optimization strategy is shown in Figure 4.11.

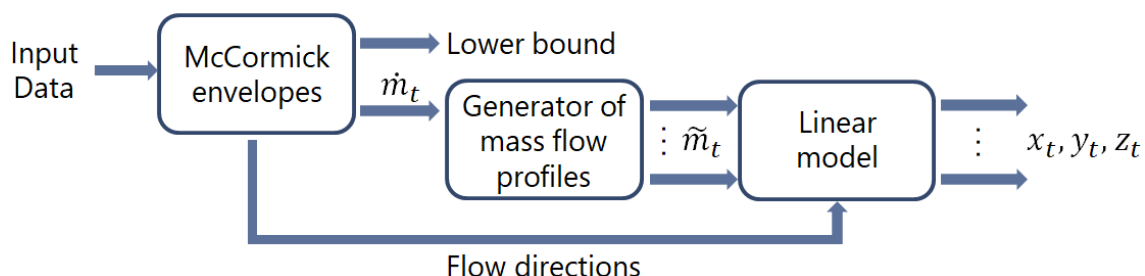


Figure 4.11: Optimization strategy for the Anergy Grid

The strategy is the same as for the single node, but in this case the solution found with the McCormick envelopes method also provides the flow directions in the branches. This network configuration is fixed and set as input to the linear model.

CHAPTER 5: ANALYSIS OF RESULTS

In this chapter, the results obtained with the optimization problem formulated in Chapter 4 are reported and discussed. As previously mentioned, three different configurations of the Anergy Grid are analysed: single node scheme, simple network scheme and the entire Anergy Grid. The optimization model is implemented in MATLAB using the academic free license of GUROBI and CPLEX solvers.

5.1. Single node

A simple case study is here considered in order to understand the behaviour of the mathematical model under different operating conditions. It consists of the single node configuration, explained in detail in the subchapter 3.3, in which one cluster is directly connected to one geothermal field. Therefore, network constraints are not considered: the cluster shares the same mass flow rate with the geothermal field and it is imposed that the temperature of the fluid exiting from the geothermal field is equal to the temperature at the inlet of the heat pump and the temperature of the fluid entering in the geothermal field is equal to the temperature at the exit of the high temperature heat exchanger, according to Figure 3.4. Simulations have been launched for the GT HPL geothermal storage and the HPL cluster, without the installation of the hot water thermal storage. The system is characterized by 0.97 GWh heating, 0.38 GWh low temperature cooling and 0.71 GWh high temperature cooling annual demands. This first study allows to understand the system dynamics and to determine the feasible operating conditions of the system.

5.1.1. Sensitivity on the number of typical days

A first analysis is conducted on the number of typical days D that is able to describe with a good approximation the operation of the system along the year. Different

solutions of the model linearized through the McCormick envelopes method are calculated for different values of D . Figure 5.1 shows the obtained results (*McCormick curve*):

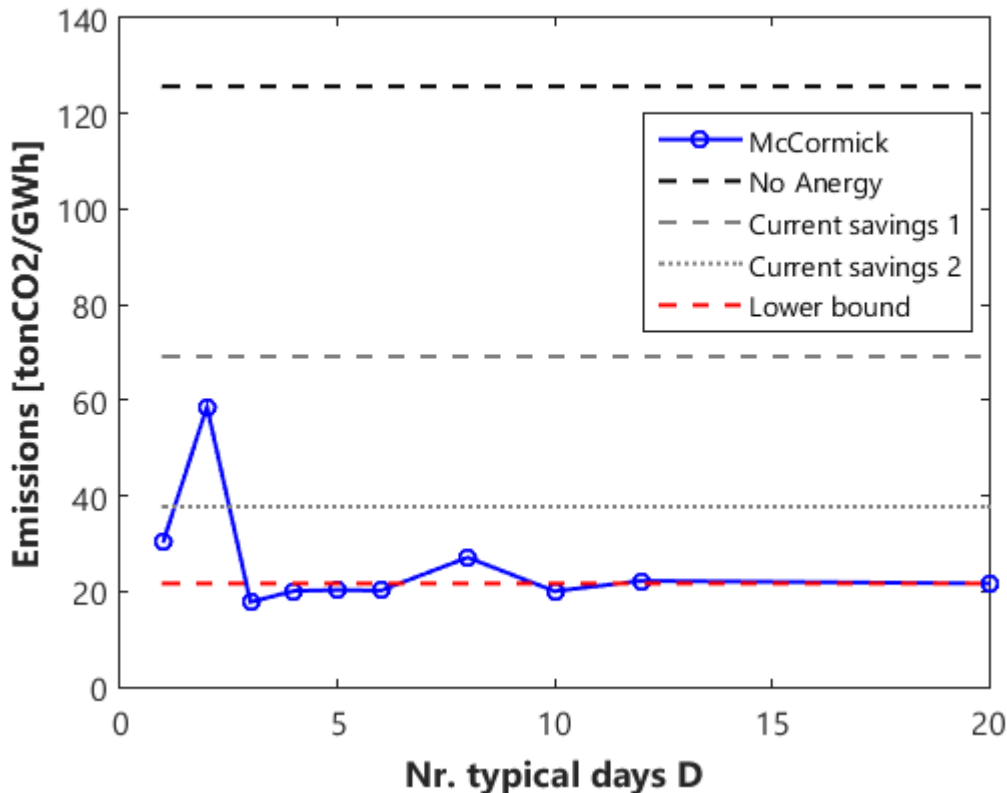


Figure 5.1: Sensitivity on typical days for the single node with McCormick envelopes method

On the x -axis the number of typical days is reported, while in the y -axis there is the normalized emission level \bar{e} [$\text{tonCO}_2/\text{GWh}$], defined as the ratio between the total annual emissions e [tonCO_2] and the sum of the thermal, low temperature cooling and high temperature cooling energy demands [GWh], as expressed in the Equation (5.1).

$$\bar{e} = \frac{e}{\Delta t \left(\sum_{i=1}^I \sum_{t=1}^T \dot{Q}_{i,t}^{H-D} + \sum_{i=1}^I \sum_{t=1}^T \dot{Q}_{i,t}^{LT-D} + \sum_{i=1}^I \sum_{t=1}^T \dot{Q}_{i,t}^{HT-D} \right)} \quad (5.1)$$

with $i \in I$ and $t = 1, \dots, T$.

The dashed horizontal red line represents the lower bound of the full-scale solution obtained with the McCormick envelopes method, for which the number of typical days D is equal to the number of days of the considered time horizon. The dashed horizontal black line (*No Anergy*) indicates the value of the CO₂ emissions for the configuration without the Anergy Grid, for which all the demands are satisfied by the auxiliary technologies. The dashed horizontal grey line (*Current savings 1*) represents the level of the CO₂ emissions for the current operation of the Anergy Grid, as reported in the ETH Sustainability Report [33]. Figure 5.2, which is extracted from the ETH Sustainability Report, refers a measured value of saved CO₂ emissions of about 45% for the year 2016.

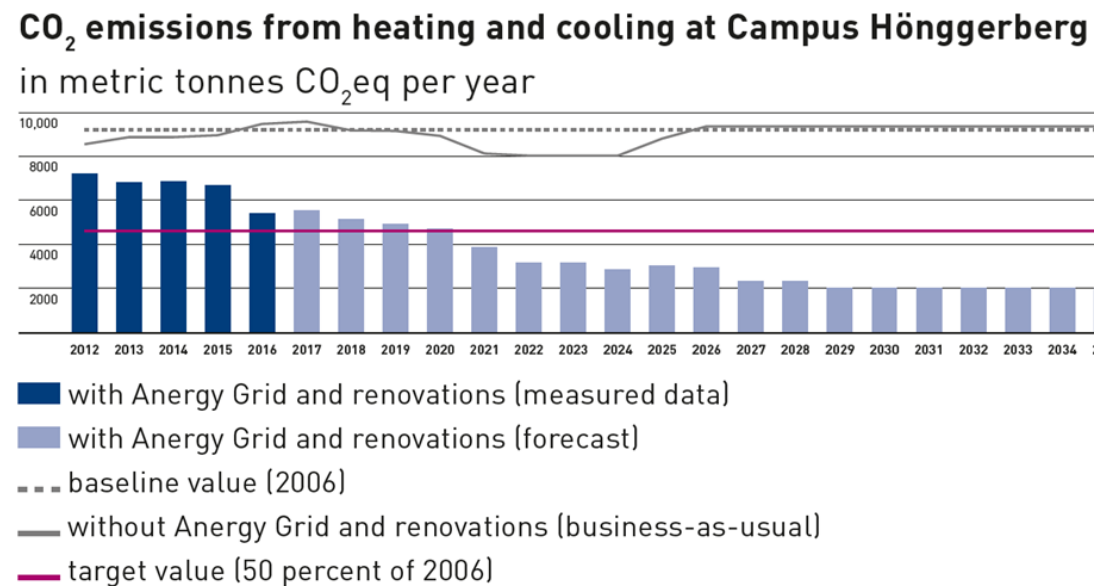


Figure 5.2: Current savings profile from ETH Sustainability Report

The dotted grey curve of Figure 5.1 (*Current savings 2*) represents the level of the CO₂ emissions for the operation of the Anergy Grid, as reported in [34]. This value is related to the Anergy Grid system in which hot water thermal storages are installed in each cluster and there is the possibility of dissipating thermal and cooling energy into the environment. It allows to save 70% of the total annual CO₂ emissions.

The results of Figure 5.1 show that the curve of the solutions reaches convergences with a small number of typical days. Solutions for $D = 4, 5, 6, 10, 12, 20$ are within a range of $\pm 3\%$ with respect to the full-scale value.

The same analysis is performed with the original equations of the system for a fixed input mass flow rate of 8 kg/s flowing in the circuit at every hour of the year, according to the values proposed by Yliruka [24]. Results of the optimization are shown in Figure 5.3.

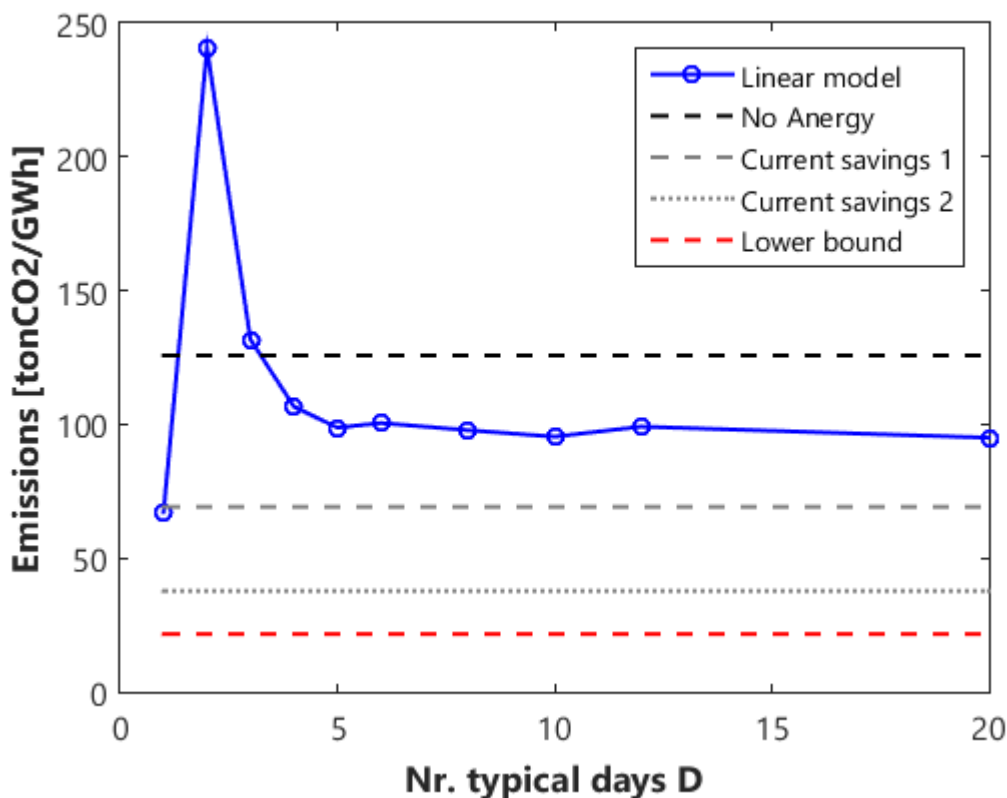


Figure 5.3: Sensitivity on typical days for the single node with the original equations

Also in this case, the results reach convergence for more than 4 typical days.

5.1.2. Sensitivity on the mass flow rate

The analysis performed on the number of typical days led to fix $D = 12$, to which a very good approximation of the full scale behaviour of the system is associated. Following

the optimization strategy explained in the subchapter 4.8.1, a sensitivity analysis on the mass flow rate is performed. Figure 5.4 shows the obtained results.

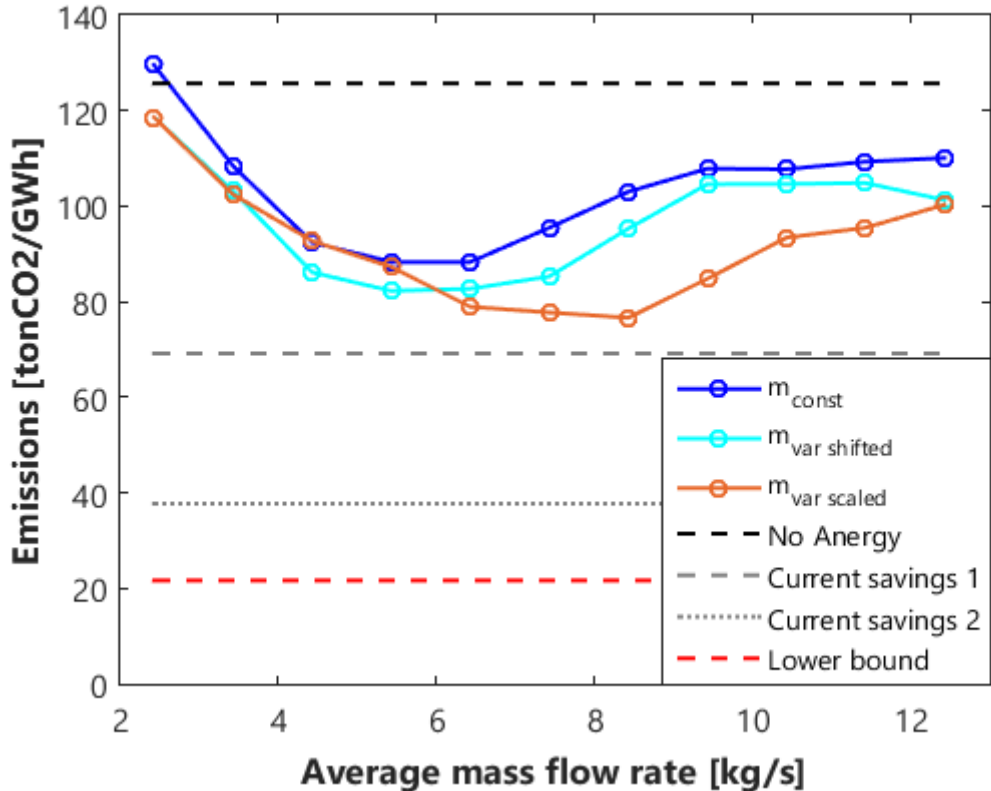


Figure 5.4: Sensitivity on the mass flow rate for the single node

On the x -axis the average value of the mass flow rate profile flowing in the cluster HPL is reported. The solutions are obtained implementing the original equations with the input data of the mass flow derived from the optimization using the McCormick envelopes method with $D = 12$. Three different approaches are adopted to generate the mass flow profile. The blue curve indicates results obtained with a fixed mass flow rate for all the time steps of the time horizon. The first solution on the left of the blue curve in Figure 5.4 is obtained by imposing as constant mass flow rate for each time step of the year the average value obtained with the McCormick envelopes method. Such value is then increased of 1 kg/s progressively, obtaining the other solutions reported in the figure. The cyan and the orange curves specify results obtained imposing the variable

mass flow rate profile obtained by the McCormick envelopes method solution. It allows to better follow the demand by supporting the conversion technologies of the Anergy Grid with a higher mass flow when higher demands are requested. The first solution on the left of the cyan and orange curves in Figure 5.4 is obtained by imposing exactly the values of the variable mass flow rate found with the McCormick envelopes method. As for the blue curve, the values of the mass flow rate of the cyan line are progressively increased by summing 1 kg/s to the mass flow for each time step, obtaining the other solutions reported in the figure. Instead, the orange curve is obtained by increasing the mass flow profile through a multiplication factor. This solution would accentuate the variations in the mass flow profile allowing it to support in a different way the conversion technologies.

As explained in the subchapter 4.8.1, increasing the values of the mass flow rate with respect to the profile indicated by the solution using the McCormick method leads to a reduction in CO_2 emissions. The performance of the system increases up to a few kg/s more than the value of the McCormick method and then starts to get worse. This occurs for all the three curves.

The best solution corresponds to a variable mass flow rate profile increased with the multiplication factor for an average mass flow of 8.4 kg/s . It allows the Anergy Grid to save the 39% of CO_2 emissions and to satisfy more than 42% of the total energy demand, according to Table 5.1.

Table 5.1: Utilization coefficients of the Anergy Grid

Anergy Grid Coverage Fraction [%]	
Heating	39.6

Low temperature cooling	15.1
High temperature cooling	60.1
Global	42.3

The Anergy Grid Coverage Fraction $AGCF$ represents the percentage of heating and cooling (low and high temperature) demands satisfied by the Anergy Grid and it is defined as the ratio between the demand satisfied by the Anergy Grid $AGSD$ [kWh] and the load demand LD [kWh], according to the Equation (5.2):

$$AGCF^{idx} = \frac{AGSD^{idx}}{LD^{idx}} \quad (5.2)$$

with idx : heating, low temperature cooling, high temperature cooling and total energy.

5.1.3. Optimal operation

The profiles of the most important decision variables related to the operation of the real system are shown in Figure 5.5.

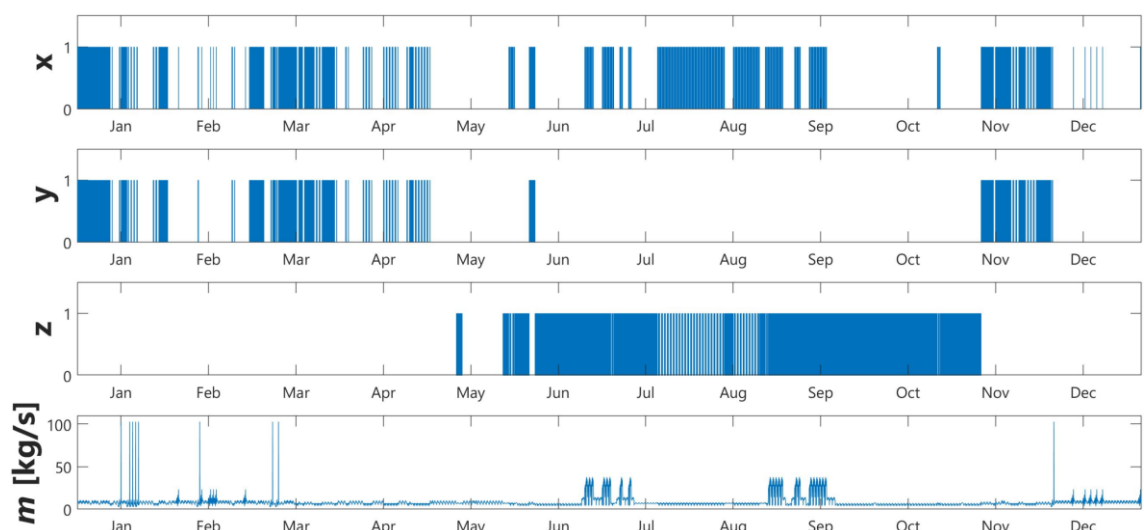


Figure 5.5: Yearly profiles of the scheduling of technologies and mass flow rate

The first three graphs above illustrate the on/off status of the heat pump and of the heat exchangers for each hour of the year. The profiles of x , y and z follow the curves of the corresponding demands. The fourth plot of Figure 5.5 illustrates the profile of the mass flow rate along the year. Despite having an average value less than 10 kg/s , it presents strong fluctuations during summer, due to very high cooling demands for the air conditioning system. During the winter, there are peak values of the mass flow profile due to strong gradients in the thermal demand, as shown in the Figure 5.6. These values of the heating demand derive from experimental measurements of the real system.

Figure 5.6 illustrates the power provided by the heat pump and the two heat exchangers (red lines) compared to the load demands (blue lines). As aforementioned, the part of demand not met by the Anergy Grid is satisfied by auxiliary technologies.

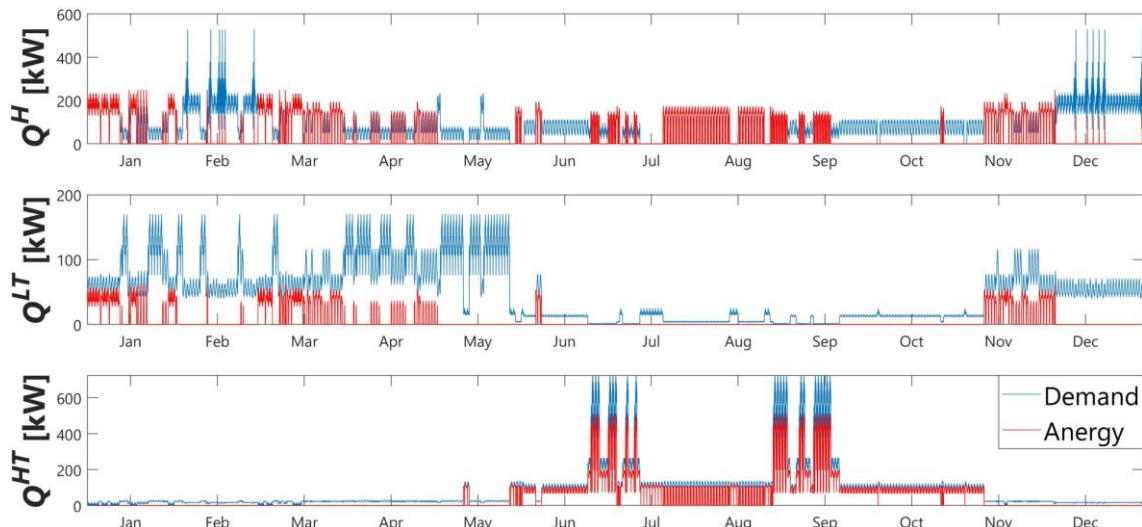


Figure 5.6: Heating and cooling fluxes requested (blue lines) and provided by the Anergy Grid (red lines)

The model keeps a balance between the exchanged thermal and cooling powers in order to maintain the borehole wall temperature at end of the year at the same value of the beginning. Figure 5.7 shows the borehole temperature profile and the heat flux provided by the ground to the heat transfer fluid in the probes along the year. As shown in Figure

5.7, the model keeps the borehole temperature T^b very close to the initial value with a maximum deviation of about $0.7\text{ }^\circ\text{C}$. The geothermal field presents a thermal inertia of about one month, confirming its seasonal behavior. The system can modify T^b deciding whether satisfying the thermal or the cooling demand. The priority of the optimization tool is to firstly satisfy the thermal demand because it is associated with a higher CO₂ emission rate. Since the cluster requires more thermal than cooling energy, the system would operate exploiting the geothermal energy stored in the ground to satisfy the thermal demand while decreasing T^b . Since it is imposed that $T_T^b = T_0^b$, the model tries to satisfy all the possible thermal energy that can be compensated by the fulfilment of the cooling demand. For this reason, the Anergy Grid Coverage Fraction is higher for cooling than for heating.

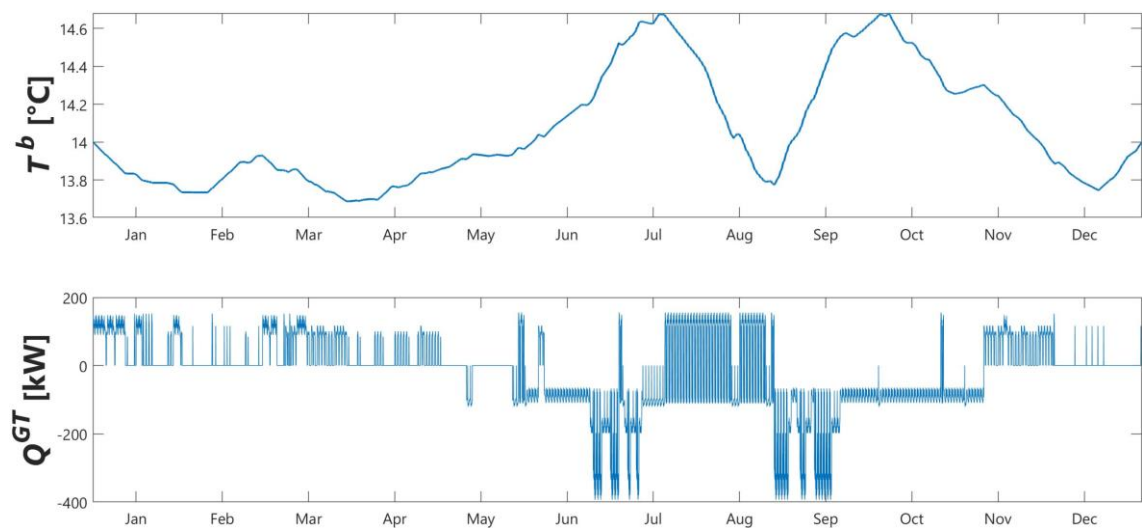


Figure 5.7: Yearly profiles of the borehole temperature and geothermal flux

In order to observe the operation of the system in detail, the same graphics are illustrated during a winter week (Figure 5.8, Figure 5.9) and a summer week (Figure 5.10, Figure 5.11).

Winter week

During winter periods, there is a low cooling demand for the air condition system, while the thermal and the low temperature cooling demands are high. The found solution of the optimization problem operates the technologies to meet almost the whole heating demand and to partially cover the low temperature cooling load. On the other hand, the high temperature heat exchanger is kept off for the whole period, leaving the corresponding electrical chiller to satisfy the demand.

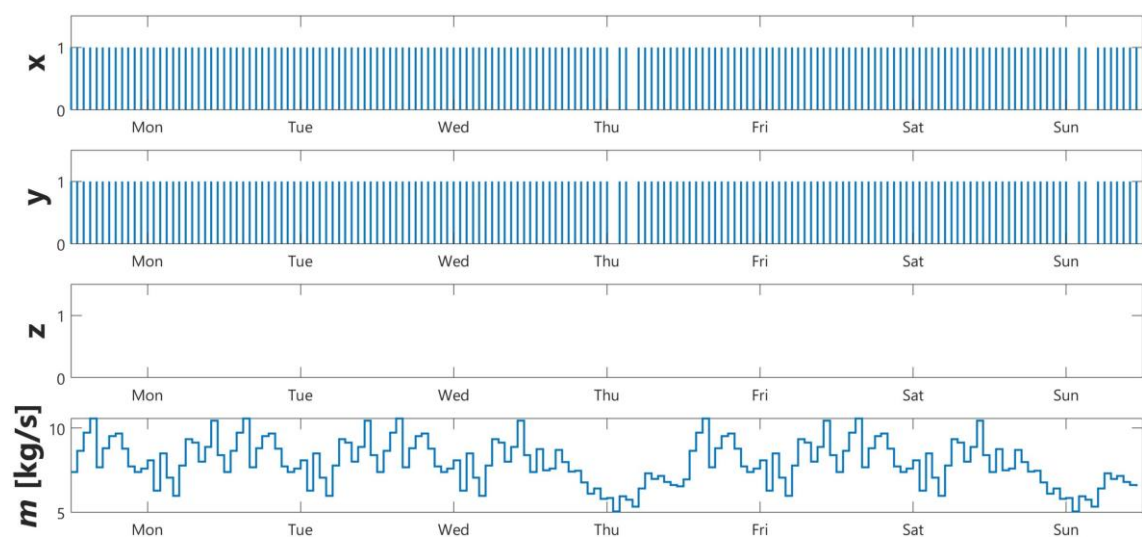


Figure 5.8: Profiles of the scheduling of technologies and mass flow rate for a winter week

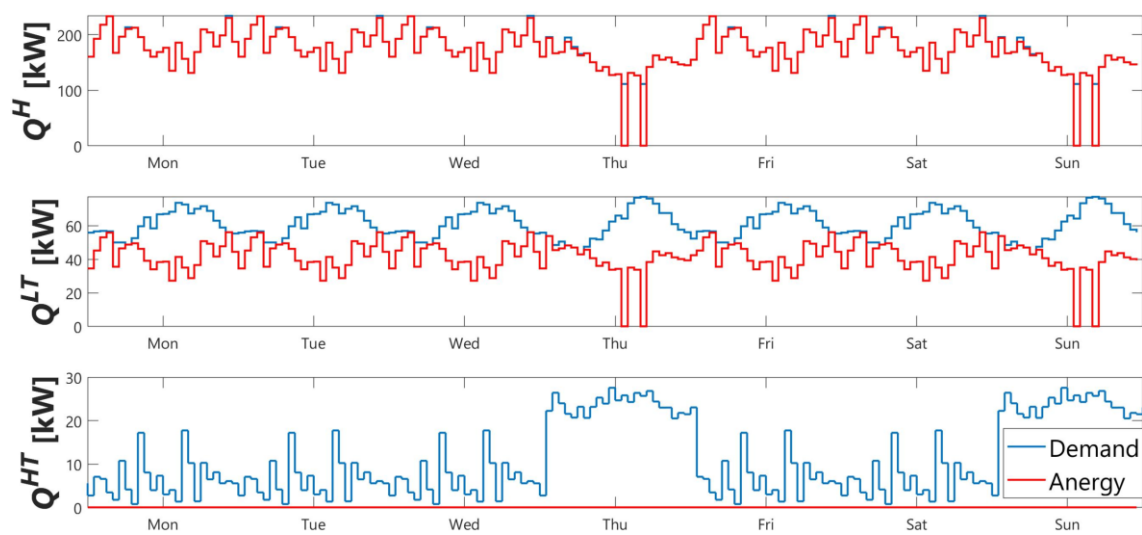


Figure 5.9: Profiles of the borehole temperature and geothermal flux for a winter week

Summer week

During the summer periods, there is a low cooling demand for the laboratories, while the heating and the high temperature cooling demands are high. The found solution of the optimization problem operates the technologies to meet mainly the cooling demand for the air conditioning system and to partially cover the thermal load. On the other hand, the low temperature heat exchanger is kept off for the whole period, leaving the corresponding electrical chiller to satisfy the demand.

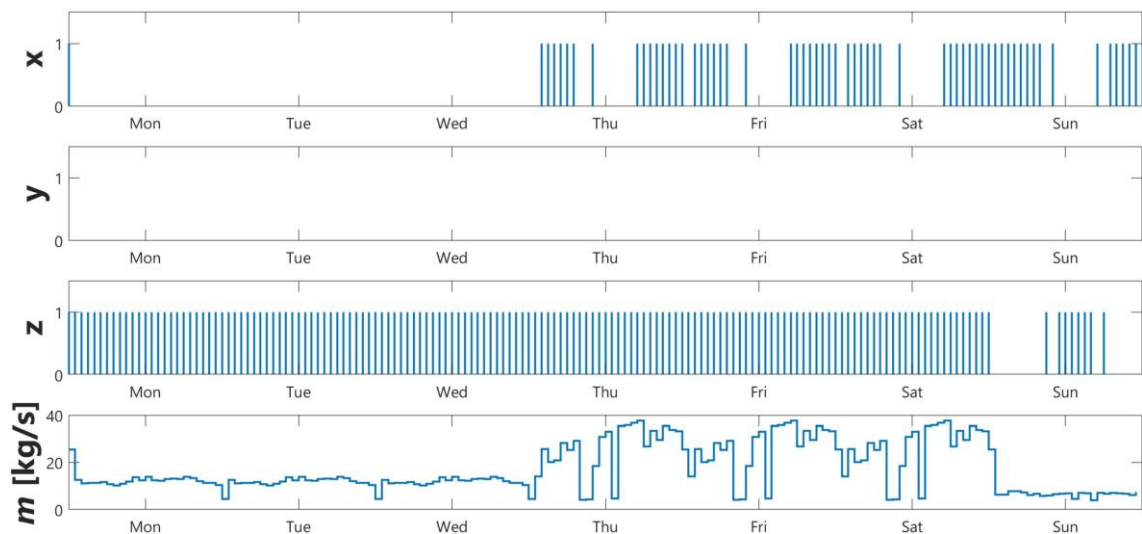


Figure 5.10: Profiles of the scheduling of technologies and mass flow rate for a summer week

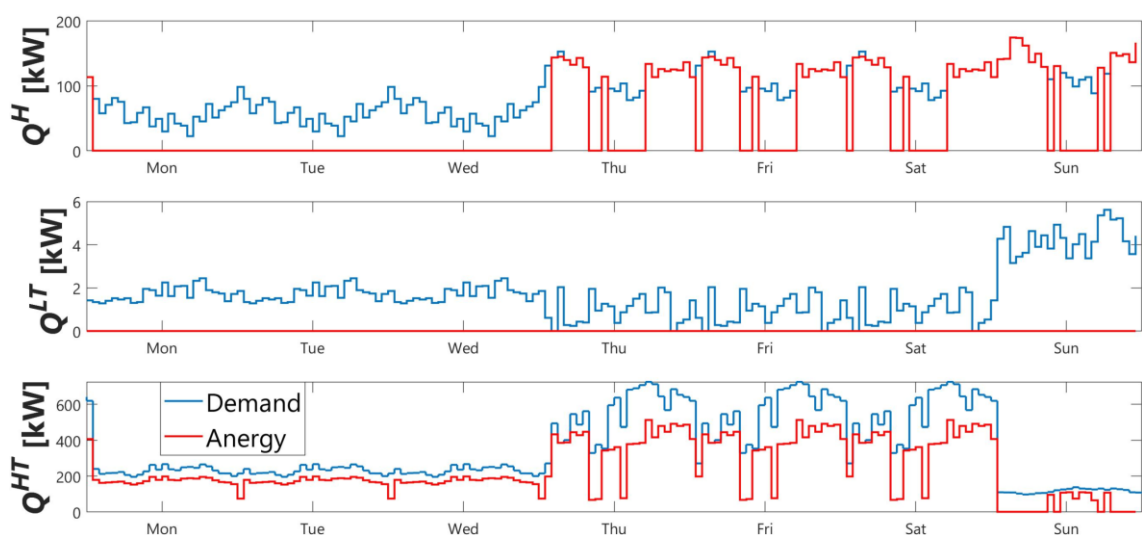


Figure 5.11: Profiles of the borehole temperature and geothermal flux for a summer week

5.1.4. Sensitivity on δ with and without HWTS

In this subchapter, a sensitivity analysis on the minimum load coefficient of the heat pump δ is performed in order to evaluate its impact on the total CO₂ emissions of the system (see Equation (4.32)). In the previous calculations, $\delta = 10\%$ is assumed, according to experimental data. Such analysis is conducted to assess the advantage of having a modular heat pump, consisting of multiple units of smaller size connected in series, thus with lower minimum load limit, in comparison with a unique technology, with higher minimum working point. The same analysis is performed in the case with and without the installation of a hot water thermal storage in the cluster. Results are illustrated in Figure 5.12.

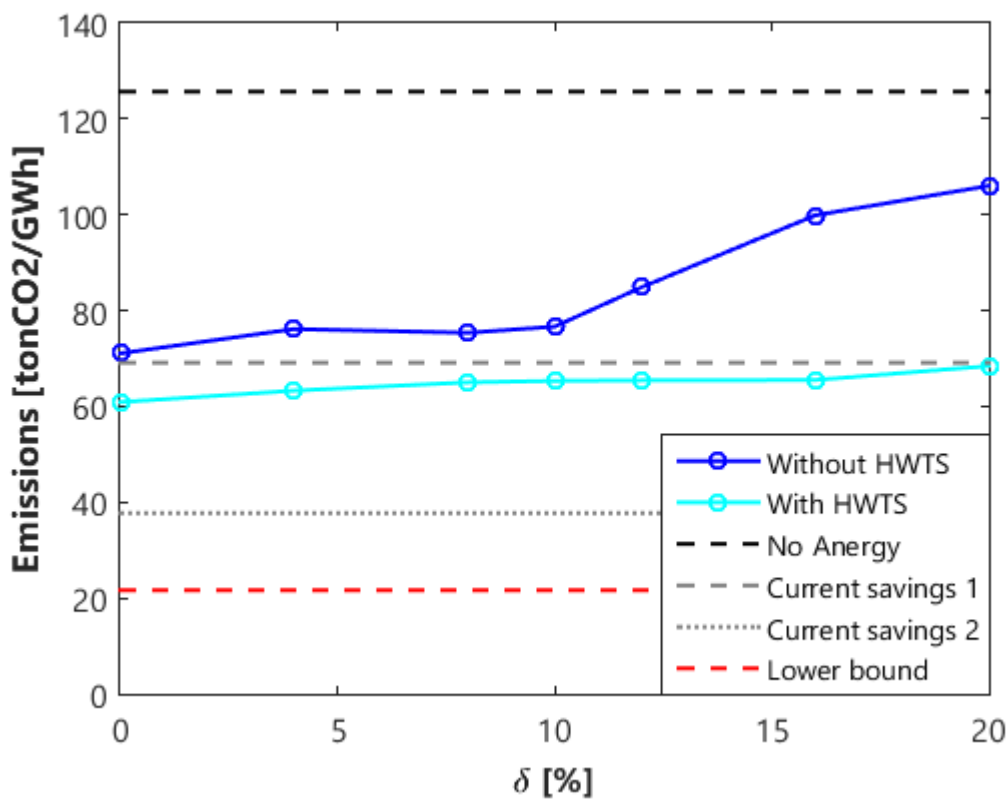


Figure 5.12: Sensitivity analysis on δ coefficient with and without HWTS

The results for the case without the hot water thermal storage show an emission increasing trend with a higher slope for $\delta > 10\%$. Instead, the curve of results for the

case with the hot water thermal storage presents a flat trend. This is due to the fact that the hot water thermal storage acts as a flexible short-term reservoir of thermal energy and allows the system to optimize the operation of the heat pump even in case of high minimum working point. It consequently permits to have a significant reduction on CO₂ emissions. This result indicates that a clever solution to remedy the problem of having a high value of δ is to install a hot water thermal storage of a suitable size for the particular application. It is a cheap technology that can guarantee considerable reductions in CO₂ emissions compared to the installation of a modular heat pump.

5.1.5. Sensitivity with temperature values at the outlet of the heat exchangers as decision variables

Another analysis is performed modifying the assumption of keeping constant the temperatures at the outlet of the two heat exchangers T^{LTHE} and T^{HTHE} . Such values are now set as decision variables of the optimization problem. The reference temperature values at the user are still 12 °C and 16 °C, but assuming that a counter-flow heat exchanger is installed, an outlet temperature of the heat transfer fluid until +4 °C with respect to the user reference value is allowed. Thus, the following constraints are added to the heat exchangers, substituting the constraints expressed by Equations (4.34) and (4.37):

$$T'_{i,t}y_{i,t} < 12 \text{ } ^\circ\text{C} \quad (5.3)$$

$$T''_{i,t} < 16 \text{ } ^\circ\text{C} \quad (5.4)$$

$$T''_{i,t}z_{i,t} < 16 \text{ } ^\circ\text{C} \quad (5.5)$$

$$T_{i,t}^{out} < 20 \text{ } ^\circ\text{C} \quad (5.6)$$

with $i \in I$ and $t = 1, \dots, T$.

This conceptual change in the formulation of the optimization problem introduces a higher flexibility of the plant to operate the conversion technologies. This allows an important reduction of the total annual emissions. For the same conditions of the optimal solution of Figure 5.4, the specific emission level is of $37.87 \text{ tonCO}_2/\text{GWh}$ with a higher utilization of the Anergy Grid, as reported in Table 5.2.

Table 5.2: Utilization coefficients of the Anergy Grid

Anergy Grid Coverage Fraction [%]	
Heating	70.0
Low temperature cooling	82.4
High temperature cooling	97.7
Global	82.5

Since the found solution allows a very strong reduction on the CO_2 emissions, a more detailed analysis is implemented. Applying the optimization strategy of Figure 4.10, an optimization applying the McCormick envelopes linearization method is performed for $D = 12$ with this new problem formulation. It provides indications about the yearly mass flow rate profile of the circuit. Different calculations are performed increasing the mass flow values with the multiplication factor as for the solution of Figure 5.4. Since the mass flow profile is scaled with the multiplication factor, the flow rate would reach very high peak levels, over 200 kg/s . Therefore, a maximum threshold value of 100 kg/s is imposed on the flow, in accordance with the experimental data.

Figure 5.13 shows the obtained results ($T HX_{var}$ curve). The curve containing the previous best solution of Figure 5.4 is reported as reference ($T HX_{fixed}$ curve).

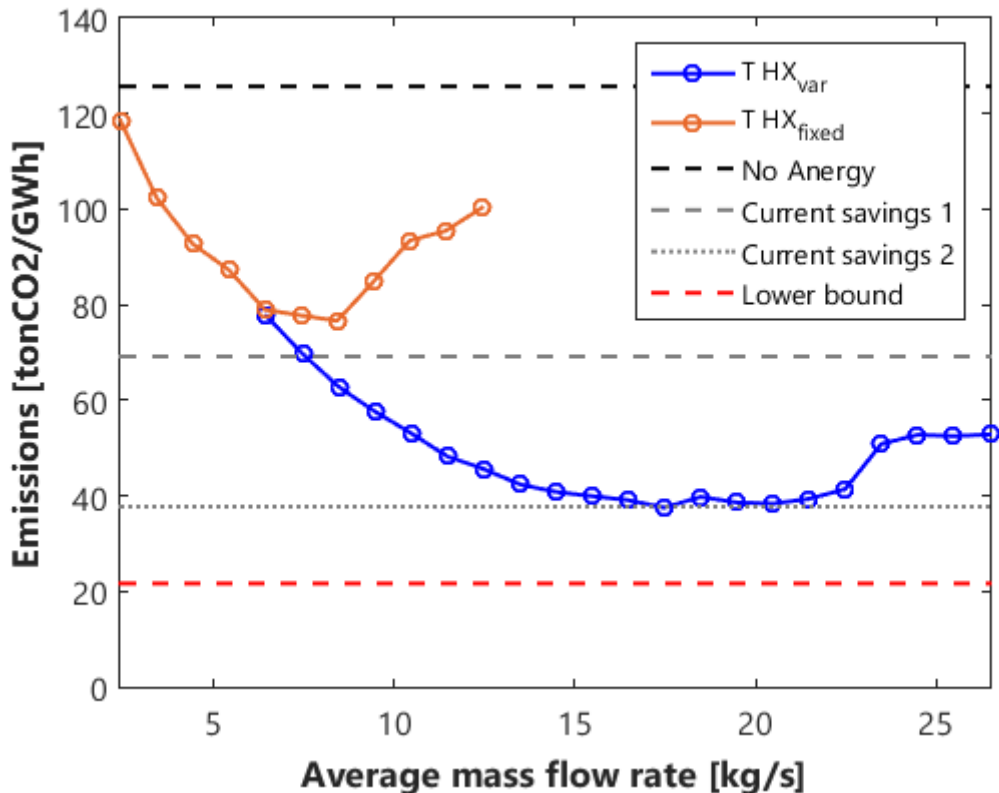


Figure 5.13: Sensitivity on the mass flow rate for the single node with the new set of constraints

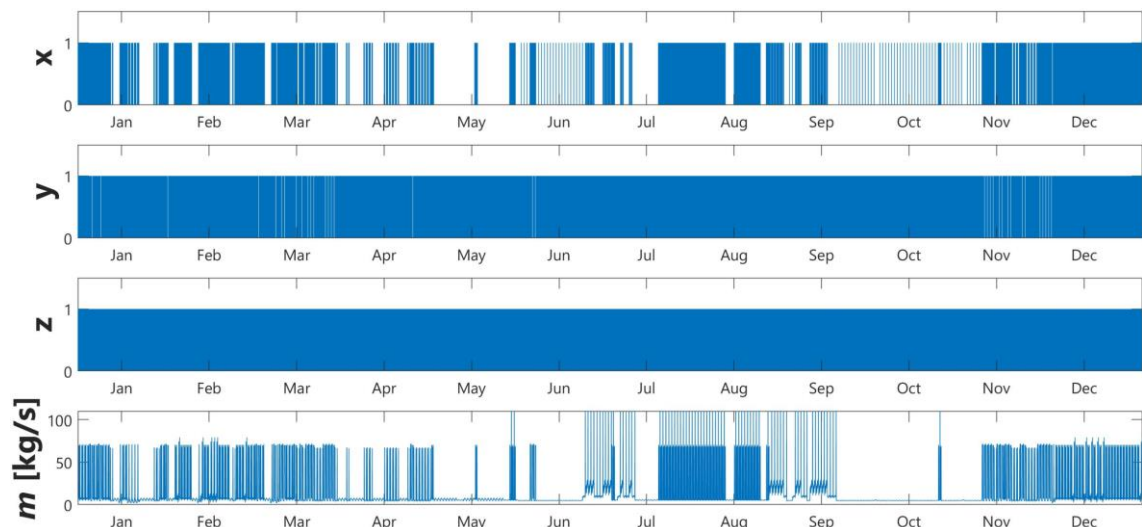
The results report a strong reduction in the levels of CO₂ emissions with respect to the previous formulation. The best solution is characterized by 37.50 tonCO₂/GWh, which corresponds to a CO₂ emissions saving of 70.2%, reaching the *Current Savings 2* value, associated with a system with hot water thermal storages in the clusters and with the possibility of dissipating heat and cooling in the environment. In Table 5.3 the percentages of demand covered by the Anergy Grid are reported. The high temperature cooling demand is totally satisfied and the low temperature one is covered by the Anergy Grid almost for the 80%. This allows to increase the thermal power provided by the heat pump still maintaining sustainable the operation at the end of the year.

Table 5.3: Utilization coefficients of the Anergy Grid

Anergy Grid Coverage Fraction [%]	
Heating	70.3
Low temperature cooling	79.8
High temperature cooling	100
Global	82.9

Results of the operation of the Anergy Grid for the found best solution are shown in

Figure 5.14, Figure 5.15 and Figure 5.16.

**Figure 5.14: Yearly profiles of the scheduling of technologies and mass flow rate**

The mass flow rate profile sets on higher values with an average of 16.3 kg/s and the heat exchangers are in operation throughout the year. When in operation, the heat pump is able to satisfy the thermal load profile even in the periods of highest demand. Given the increase in flow rate values, the temperature profile of the borehole experiences wider fluctuations, while maintaining the seasonal trend.

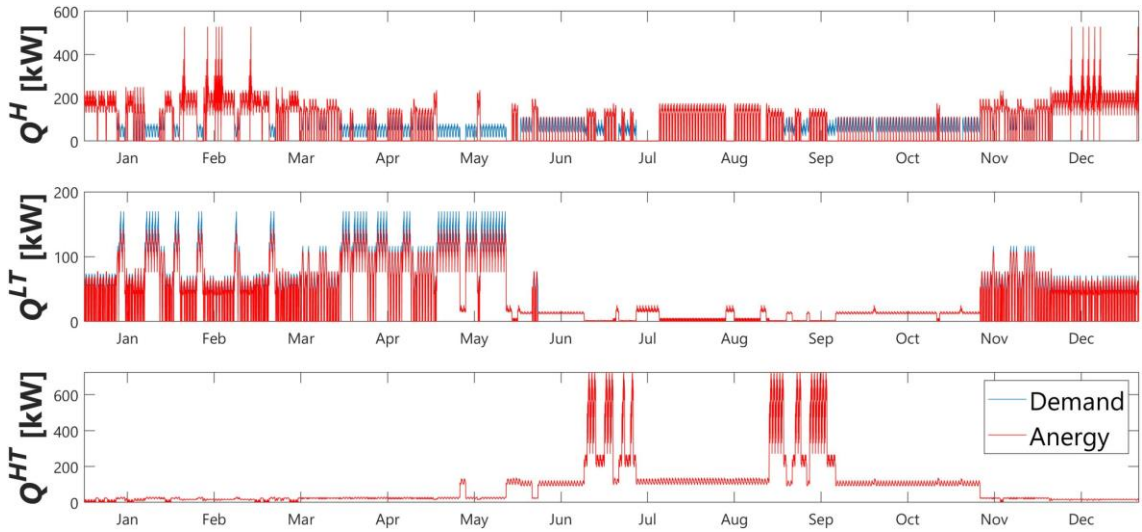


Figure 5.15: Heating and cooling fluxes requested (blue lines) and provided by the Anergy Grid (red lines)

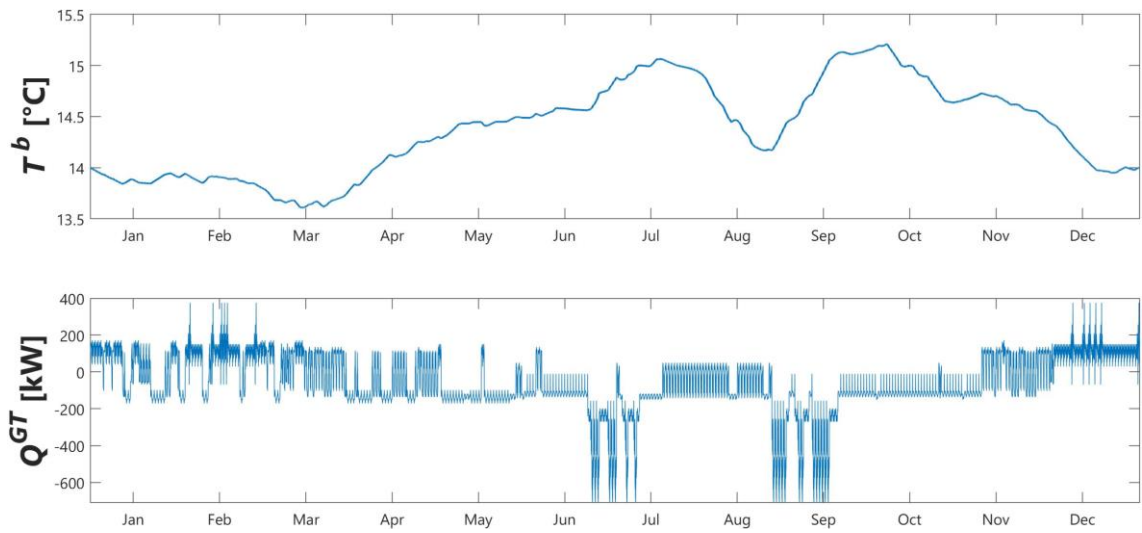


Figure 5.16: Yearly profiles of the borehole temperature and geothermal flux

In the light of the results obtained from the performed sensitivity analyzes, a study to investigate lower emission levels has been conducted. For the same conditions of the best found solution, a simulation with the installation of a hot water thermal storage is performed. Figure 5.17 illustrates the result of the lower bound obtained through the McCormick envelopes method (dashed green line) and the result obtained with the original equations (pink + marker). Such result is associated with a CO₂ emission saving value of 89.7%.

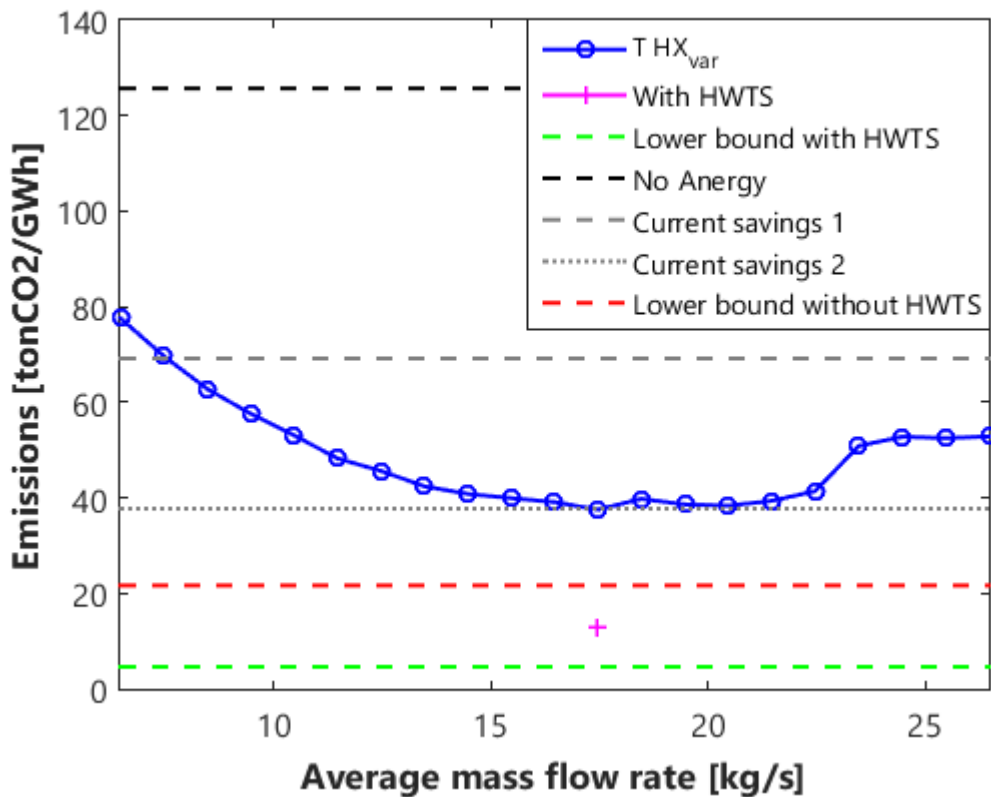


Figure 5.17: Emission level with new set of constraints with addition of HWTS

The corresponding percentages of demand covered by the Anergy Grid are listed in Table 5.4.

Table 5.4: Utilization coefficients of the Anergy Grid

Anergy Grid Coverage Fraction [%]	
Heating	92.6
Low temperature cooling	82.9
High temperature cooling	100
Global	93.4

The installation of the hot water thermal storage allows to further save important amounts of CO₂ emissions going below the lower bound of the previous case.

5.2. Simple network

In this subchapter, the simple network scheme of Figure 3.8 is analysed in order to understand the dynamic behaviour of the model with the introduction of the network constraints. It consists of the HPL and HPZ clusters connected to the GT HPL geothermal field and requires 2.64 GWh thermal, 1.68 GWh low temperature cooling and 1.16 GWh high temperature cooling annual demand. Each cluster has the temperature values at the outlet of the heat exchangers set as decision variables, as described in the subchapter 5.1.5, and no hot water thermal storages are installed.

5.2.1. Sensitivity on network directions

The simple network scheme leaves space for a few possible configurations of the hydraulic network. Three analysed paths, with directions chosen a priori, are considered in this study and are illustrated in Figure 5.18, Figure 5.19 and Figure 5.20.

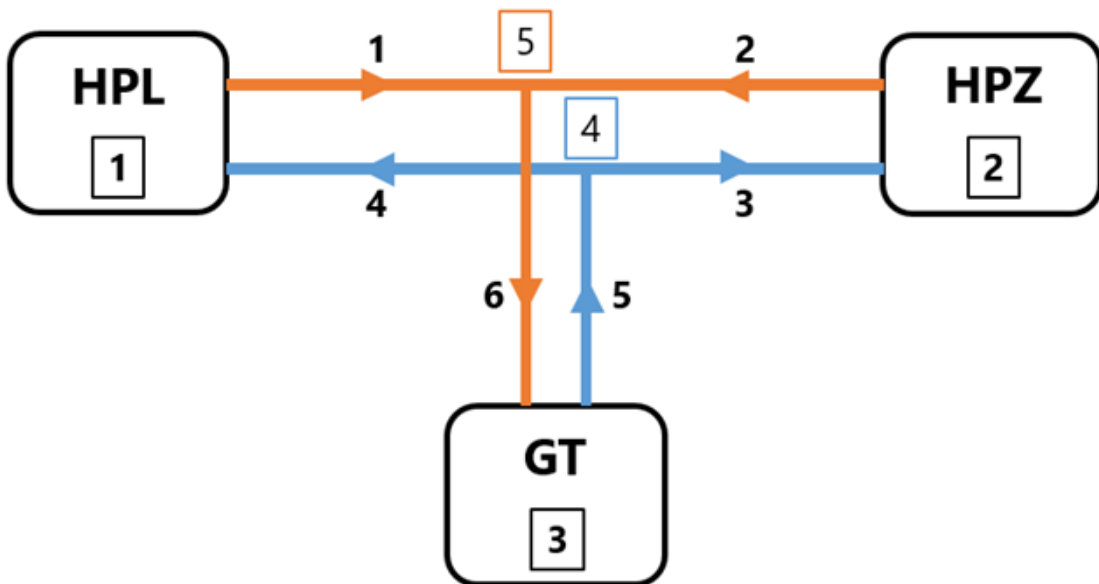


Figure 5.18: Simple network configuration 1

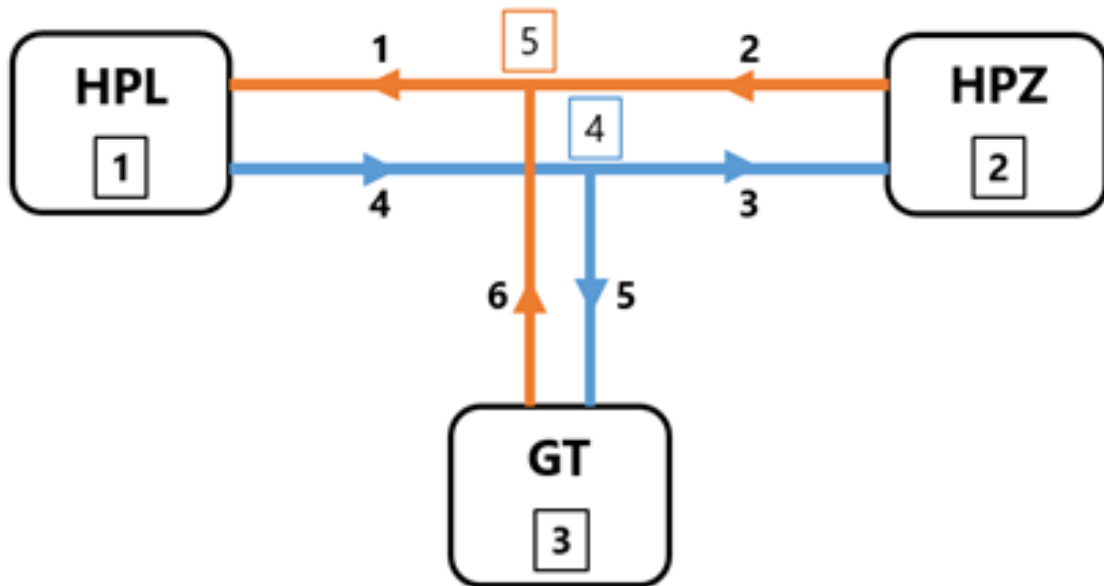


Figure 5.19: Simple network configuration 2

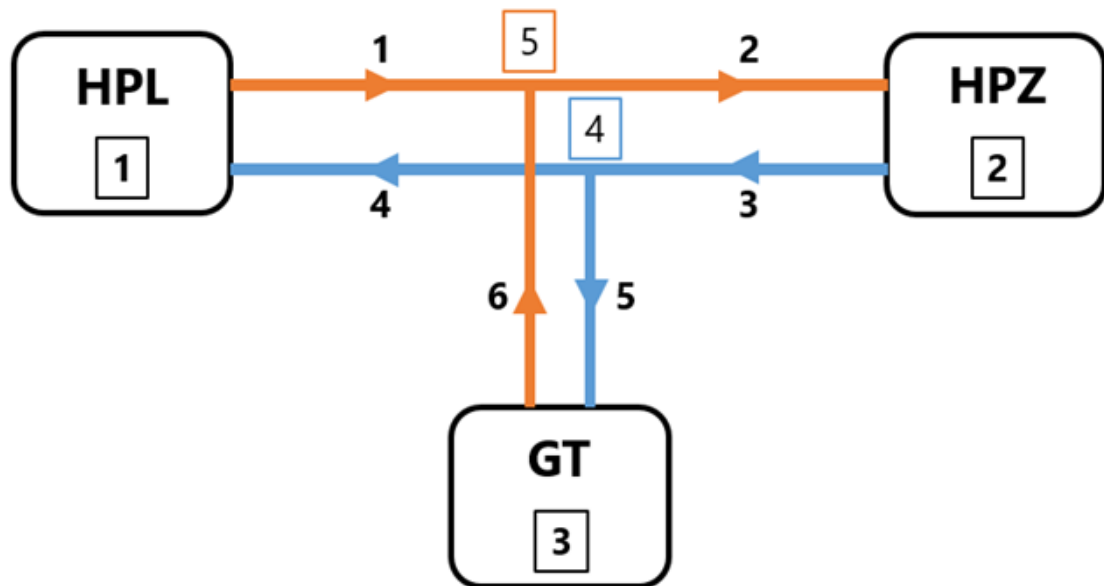


Figure 5.20: Simple network configuration 3

Three optimizations using the McCormick envelopes method are performed on the three paths in order to calculate the corresponding lower bounds. The lower CO₂ emission level is found for the Path 2, as illustrated in Figure 5.21. The general formulation of the optimization problem, described in the subchapter 4.5.8, also finds the Path 2 as the best one in terms of CO₂ emissions.

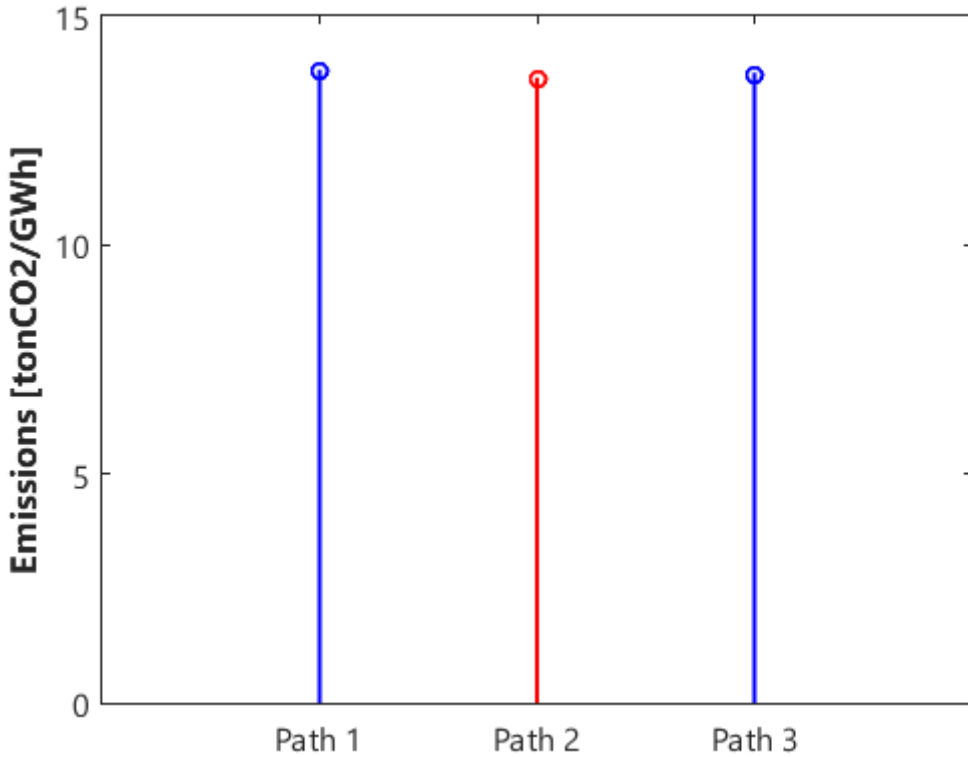


Figure 5.21: Path sensitivity on the simple network

Figure 5.21 shows a very small difference between the solutions, that are obtained for $D = 12$. This is due to the fact that they are solved by using the McCormick envelopes method, hence they are all lower bounds of the solution. McCormick envelopes method introduces a strong relaxation to the model, which is able to meet almost all the demands for all the chosen configurations.

5.2.2. Sensitivity on the mass flow rate

A sensitivity analysis on the mass flow rate for the three network configurations is performed on the linear model by using the input data of the mass flow derived from the solutions of the McCormick envelopes method. Results are found for the simple network configuration 1 (blue lines), 2 (pink lines) and 3 (green lines) for a variable mass flow rate profile that is increased by shifting (“o” marker) or scaling (“+” marker) the input values, as in Figure 5.4. It is important to note that the increase in the mass

flow profiles in the two clusters and in the geothermal field must respect the mass balances of the network. Such balances can be easily implemented in the simple network configuration. For the path 1, it is imposed that the mass flow profile flowing in the geothermal field has to be raised by the sum of the increases in the flow profiles of the two clusters. For the paths 2 and 3, it is imposed that the flow profile flowing in the cluster HPL and HPZ respectively has to be raised by the sum of the increases in the mass flow profiles of the geothermal field and of the other cluster. The obtained results are illustrated in Figure 5.22.

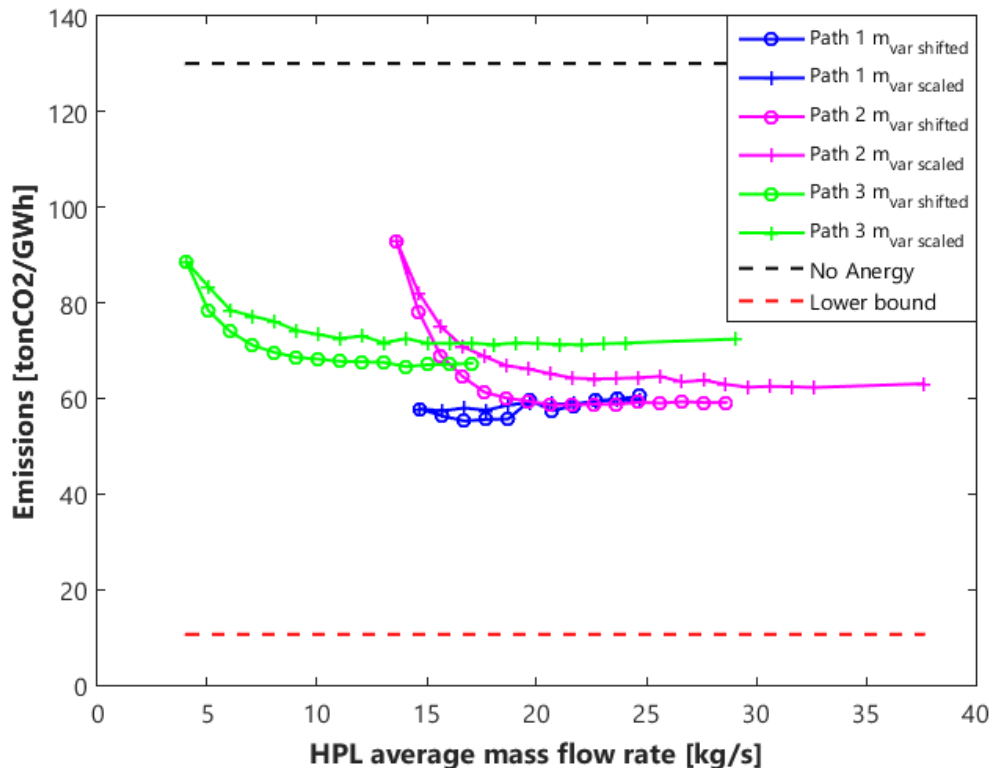


Figure 5.22: Sensitivity on the mass flow rate for the simple network

The dashed horizontal black line represents the full-scale emission level of the simple network, for which the technologies of the Anergy Grid are not employed and all the loads are satisfied by the auxiliary technologies. The dashed horizontal red line represents the lower bound of CO₂ emissions of the network configuration 2 found in

the subchapter 5.2.1. As shown in the Figure 5.22, the optimal network configuration chosen by the general formulation is not the optimal solution also for the implementation with the linear model. A difference of $3.36 \text{ tonCO}_2/\text{GWh}$ is found between the optimal solutions of path 1 and path 2, which corresponds to the 2.6% of the emission level without the installation of the Anergy Grid. However, the analysis of all possible network configurations in reasonable time is only possible for very simple networks. For more complicated networks, the loss of few percentage points of the objective function due to the implementation of a general method becomes a necessity.

The absolute best solution is relative to path 1. This is the configuration of the network in which the clusters draw independently from the geothermal field. It is worthy to point out that for the simple network scheme, the solutions found with a shifted mass flow are better than the ones with a scaled mass flow rate.

5.3. Anergy Grid

The whole plant scheme, as illustrated in Figure 3.12, is analysed in this subchapter. It consists of 5 clusters and 3 geothermal fields connected by two hydraulic rings and it is characterized by 9.07 GWh thermal, 2.47 GWh low temperature cooling and 1.31 GWh high temperature cooling annual demand. A procedure similar to that used for the single node is adopted. Clusters have the temperature values at the outlet of the heat exchangers set as decision variables, as described in the subchapter 5.1.5, and no hot water thermal storages are installed in the clusters.

5.3.1. Sensitivity on the number of typical days

Since the entire Anergy Grid consists in a bigger network, consequently with a bigger set of decision variables and constraints, a sensitivity analysis on the number of typical days is performed. Results are obtained implementing the general formulation of the

network, for which the flow directions in the branches are variables of the optimization problem and the McCormick envelopes method is applied. Also in this case, it is imposed that binary variables that determine the flow directions in the branches can assume only one value for the whole time horizon. Results are shown in Figure 5.23 (*McCormick* blue curve).

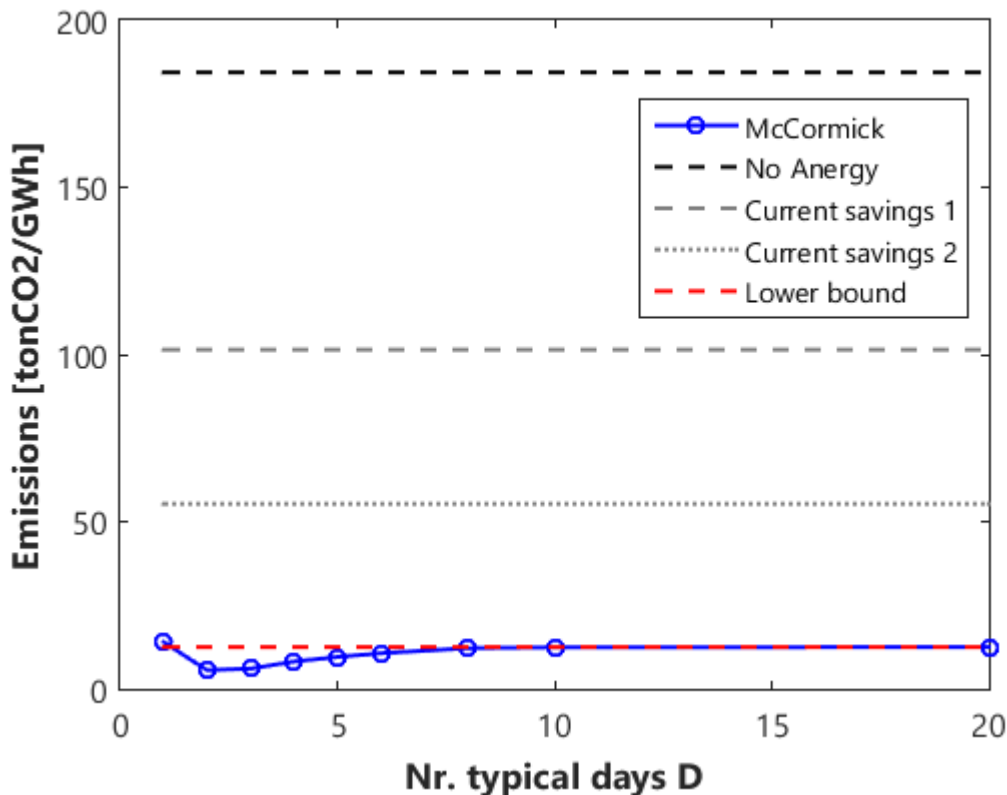


Figure 5.23: Sensitivity on typical days for the Anergy Grid with McCormick envelopes method

The dashed horizontal black line indicates the full-scale value of the CO₂ emissions for the Anergy Grid, in which all the demands are satisfied by the auxiliary technologies. The dashed and the dotted grey lines represent the emission levels with an associated CO₂ savings of 45% and 70% respectively, as reported in the subchapter 5.1.1. The dashed horizontal red line represents the lower bound found with the general formulation applying the McCormick envelopes linearization method for $D = 20$.

Results of Figure 5.23 show that for numbers of typical days $D = 6, 8, 10$, the emission levels are sufficiently close to the value found for $D = 20$.

5.3.2. Sensitivity on the network directions and on the mass flow rate

From the previous analysis, a number of typical days $D = 10$ is set, which describes the dynamics of the system with a very good approximation. Following the optimization strategy described in the subchapter 4.8.2, the network directions and the mass flow rate profiles obtained with the McCormick envelopes method are imposed as input values to the linear model. The network configuration chosen by the optimization tool for $D = 10$ is reported in Figure 5.24.

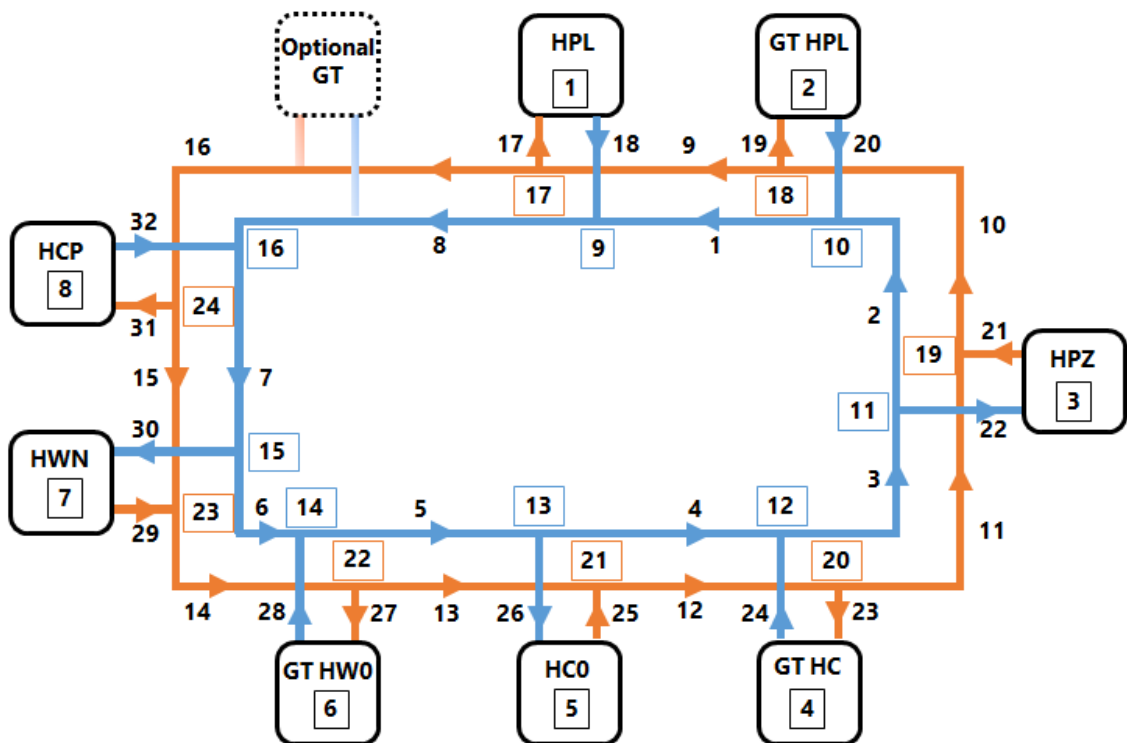


Figure 5.24: Selected network configuration

The solution found has a counter clockwise flow direction in both ring circuits. The clusters and the geothermal fields exchange the flow through the two rings.

The results obtained for the simple network in the subchapter 5.2 suggest to choose a network configuration in which the clusters operate independently of each other, exchanging the flow directly with the geothermal fields. Therefore, another configuration of the Anergy Grid is proposed, which is based on the analysis of the simple network. The Figure 5.25 illustrates the proposed educated solution for the network directions.

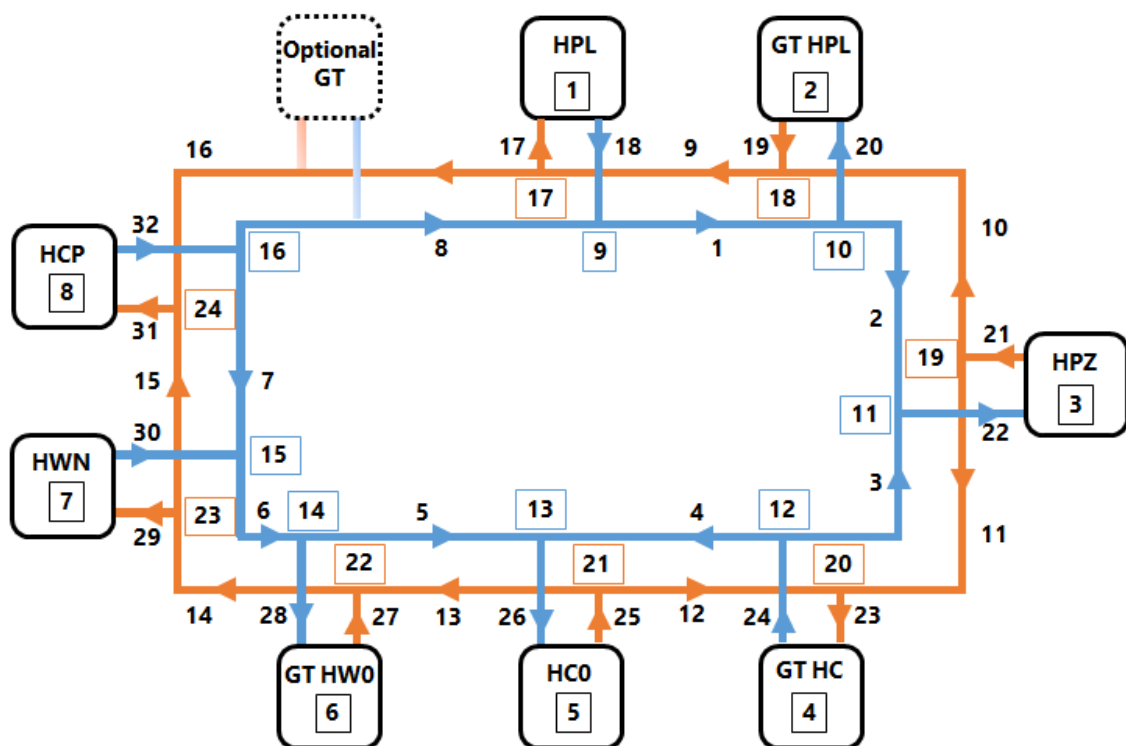


Figure 5.25: Educated solution of the network configuration

Given that there are 5 clusters and 3 geothermal fields, it is decided in principle that two pairs of clusters exchange the mass flow rates each other with one geothermal field and the remaining cluster and geothermal field exchange the flow directly. Since the geothermal field GT HPL is the smallest one, with 101 probes, it exchanges the mass flow directly with the cluster HPL. Given the layout of the network, it is chosen that the clusters HPZ and HC0 exchange the mass flow rate with the geothermal field GT HC and the clusters HCP and HWN exchange the mass flow with the geothermal field GT

HW0. Thus, a solution is obtained applying the McCormick envelopes method for this “educated” network configuration.

A sensitivity analysis on the mass flow rate for these two network configurations is performed. Results are obtained with the linear model, which takes as inputs the flow directions in the branches and the corresponding mass flow profiles, derived from the result of the McCormick envelopes method. Solutions are shown in Figure 5.26.

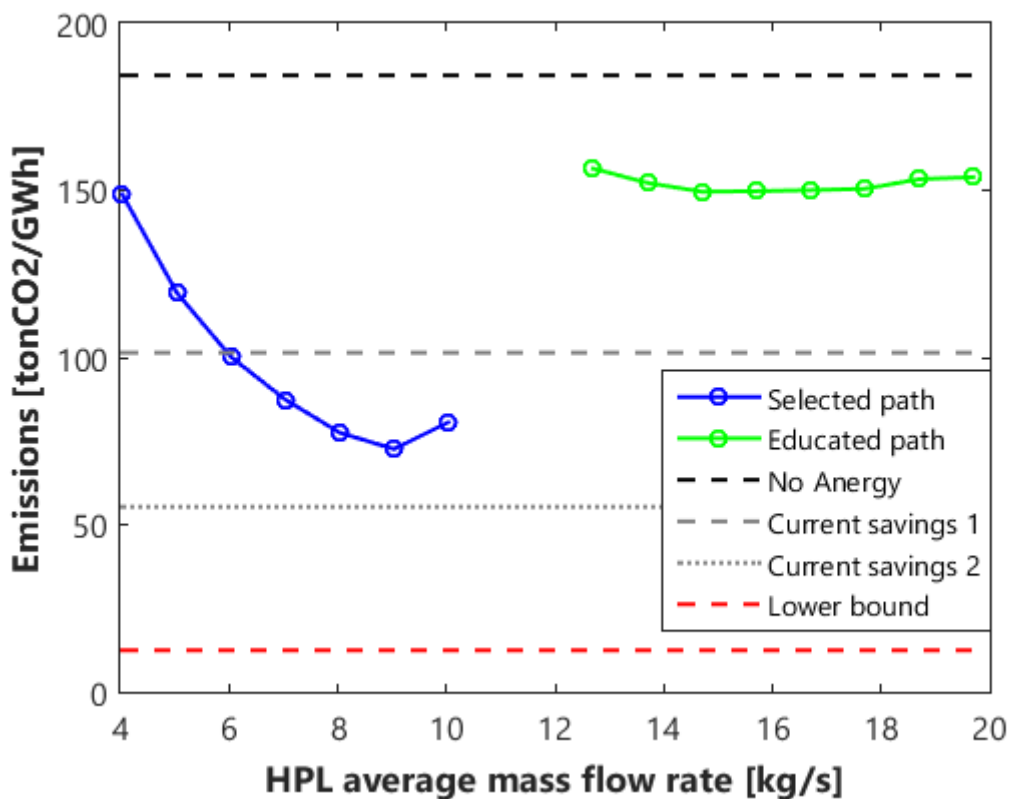


Figure 5.26: Sensitivity on the mass flow rate for the Anergy Grid

On the x -axis the average value of the mass flow rate profile flowing in the cluster HPL is reported. Solutions are obtained by increasing the mass flow profile derived by the McCormick envelopes solution through a translation, as suggested by the results of the simple network. Such translations have to respect the mass balance constraints of the network. For the selected path, this is imposed following the scheme of Figure 5.27, relative to a flow rate increase of \mathbf{k} [kg/s].

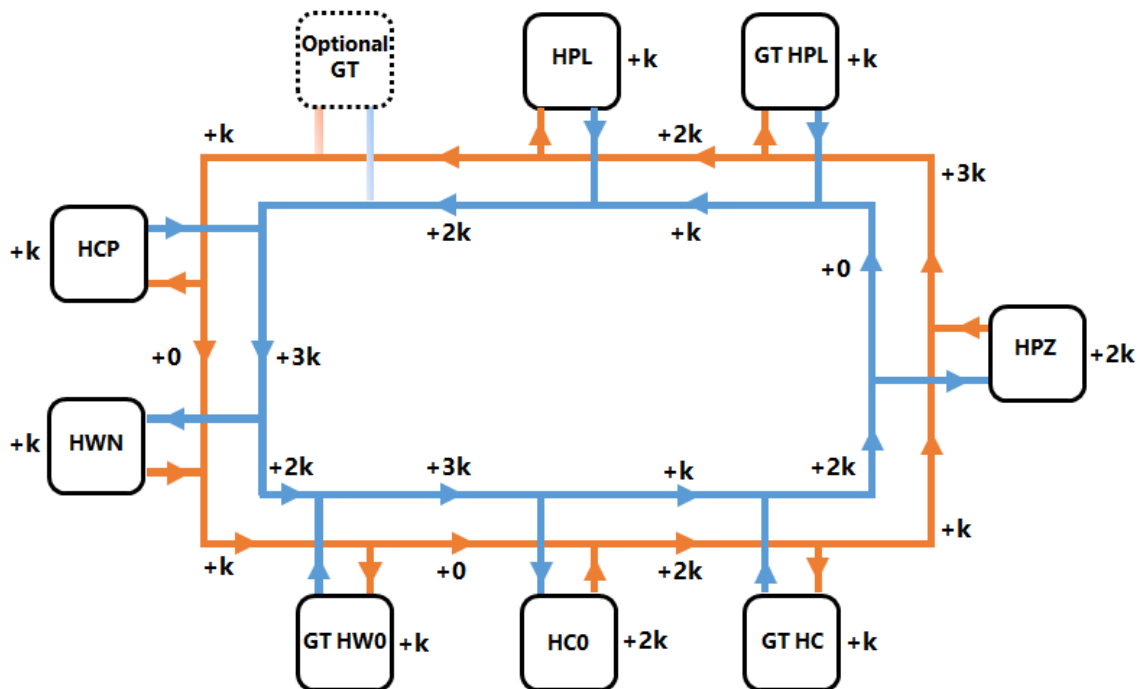


Figure 5.27: Strategy to increase the flow rate for the selected network configuration

For the educated path, the mass balances are imposed following the scheme of Figure 5.28, relative to a flow rate increase of k [kg/s].

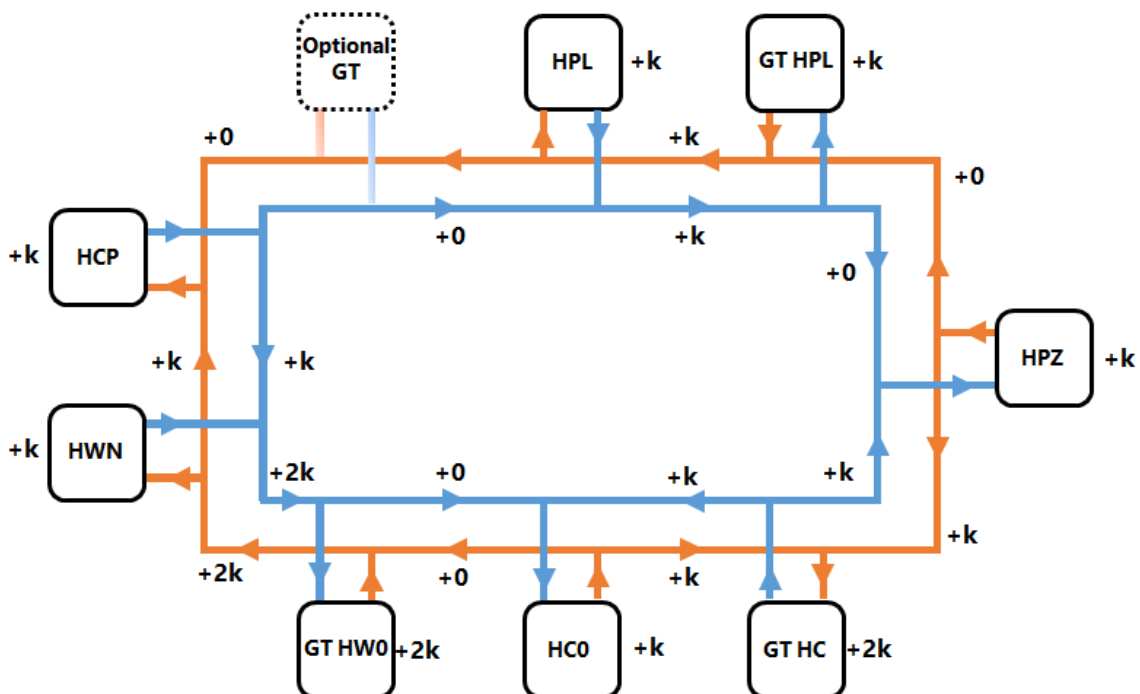


Figure 5.28: Strategy to increase the flow rate for the educated network configuration

Figure 5.26 shows that the results obtained with the “educated” network configuration have very high CO₂ emission levels, while the network directions and mass flow profiles identified by the optimization tool allow to achieve much better emission levels. This means that for a complex network like the Anergy Grid, a general formulation of the optimization model, which allows to set the directions of the flows in the branches as decision variables, is preferable.

The best solution found saves the 60.6% of CO₂ emissions. Table 5.5 indicates the corresponding percentages of demands covered by the Anergy Grid.

Table 5.5: Utilization coefficients of the Anergy Grid

Anergy Grid Coverage Fraction [%]	
Heating	64.8
Low temperature cooling	33.7
High temperature cooling	95.3
Global	61.9

5.3.3. Sensitivity on the number of hot water thermal storages and possibility of energy dissipation

A sensitivity analysis is performed on the number of hot water thermal storages installed in the Anergy Grid for the selected configuration and for the flow profiles of the best solution. In order to position the technologies to try to cover the whole network, results are found for the installation of:

- 1 hot water thermal storage installed in the HPL cluster
- 2 hot water thermal storages installed in the HPL and HWN clusters

- 3 hot water thermal storages installed in the HPL, HWN and HPZ clusters.

Results are illustrated in Figure 5.29:

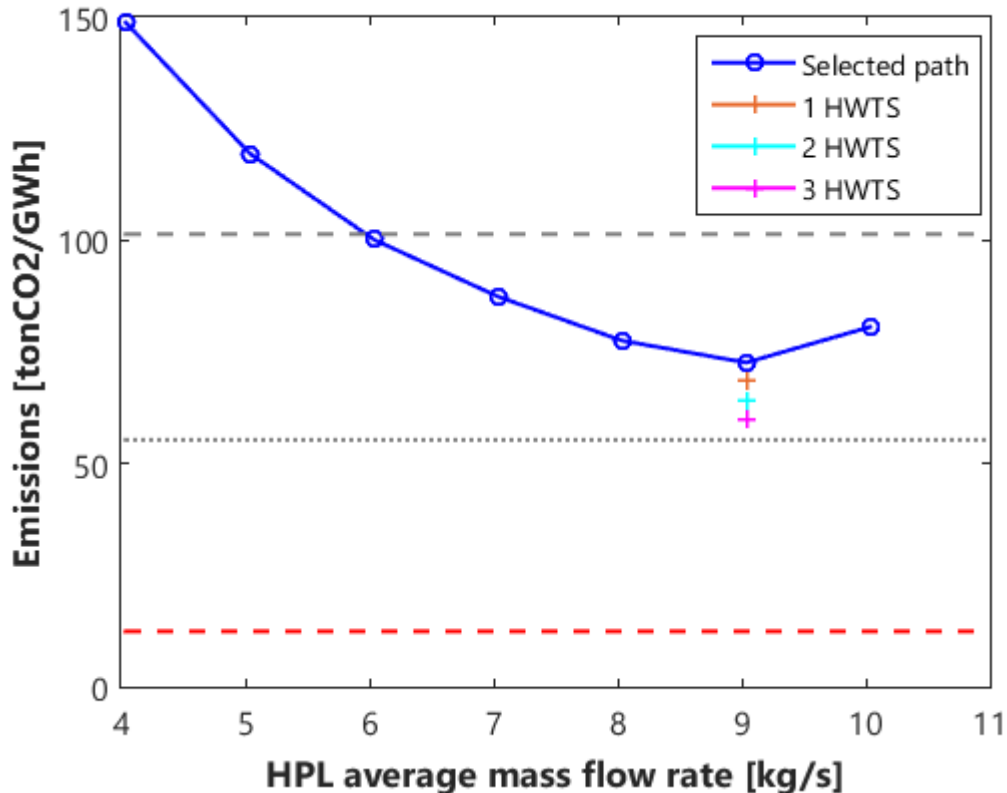


Figure 5.29: Sensitivity on the number of HWTS for the Anergy Grid

The solution obtained with the installation of 1 hot water thermal storage (orange + marker) allows a CO₂ emission saving of 62.8%, the one with 2 hot water thermal storages (cyan + marker) of 65.2%, while the solution for 3 installed hot water thermal storages (pink + marker) of 67.4%.

For the case with 3 installed hot water thermal storages, a simulation is performed by giving the possibility to the system to dissipate thermal, low temperature cooling and high temperature cooling energy into the environment, as suggested in [34]. This calculation is implemented to assess the impact of this plant solution on the value of

CO_2 emissions. Thus, the model constraints (4.51), (4.52) and (4.53) are substituted by the inequalities:

$$\dot{Q}_{i,t}^{HP} + \dot{Q}_{i,t}^B + \dot{Q}_{i,t}^{HWTS_out} \geq \dot{Q}_{i,t}^{H_D} + \dot{Q}_{i,t}^{HWTS_in} \quad (5.7)$$

$$\dot{Q}_{i,t}^{LT} + \dot{Q}_{i,t}^{CH_LT} \geq \dot{Q}_{i,t}^{LT_D} \quad (5.8)$$

$$\dot{Q}_{i,t}^{HT} + \dot{Q}_{i,t}^{CH_HT} \geq \dot{Q}_{i,t}^{HT_D} \quad (5.9)$$

with $i \in I$ and $t = 1, \dots, T$.

The obtained result is shown in Figure 5.30 with the black + marker.

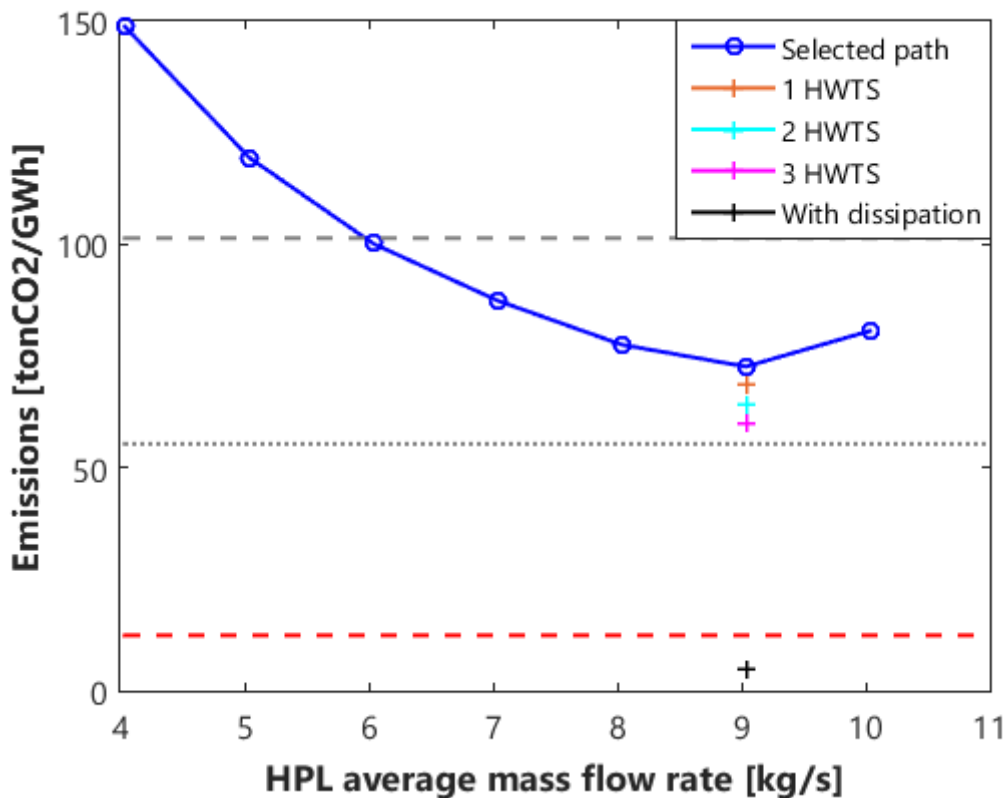


Figure 5.30: Anergy Grid emission level with dissipation

The solution found indicates that providing to the Anergy Grid the possibility of dissipating thermal or cooling energy in the environment allows a big reduction in CO_2 emission levels. The result is associated to an emission saving of 97.5%. However, no

restrictions on the amount of energy that can be dissipated are set to calculate this solution. The corresponding values of dissipated energy are the 27% of the thermal load, the 32% of the low temperature cooling demand and the 202% of the high temperature cooling load, for a total value of the 47% of the global demand. Future developments of the present study could perform a sensitivity analysis on the percentages of demand that can be dissipated into the environment.

CHAPTER 6: CONCLUSIONS

In this study, a very complex problem of multi-energy system optimization has been faced within a Mixed Integer Linear Programming framework to minimise the total annual CO₂ emissions. A solution strategy is proposed which makes use of the recurrent application of the McCormick envelopes method together with the other more known linearization techniques. Such strategy makes it possible to include in a MILP problem a general formulation of the configuration of a network in which a fluid circulates at different temperature levels by exchanging thermal and cooling power. Everything is analysed by managing a geothermal storage system with seasonal dynamics.

As proposed in the literature by Gabrielli et al. [5], a method of time discretization has been implemented to describe the seasonal dynamics of the storage simplifying the problem from the computational point of view.

The proposed strategy has a general validity and is therefore implemented to study the multi-energy system Anergy Grid installed at the ETH Science City Campus in Hönggerberg, Zurich.

Numerous sensitivity analyses on different parameters of the system are performed to assess the impact on the objective function. First, a single network node is analysed. Based on the obtained results, the model is extended to a simple network by integrating the general model that returns the optimal network configuration as an output. Finally, the entire Anergy Grid network is considered. The results obtained validate the choice to adopt a general strategy to select the network configuration and indicate a saving of CO₂ emissions far greater than that of the Anergy Grid current operation.

Interesting future developments of the present work can perform a sensitivity analysis for the case of the entire Anergy Grid on the percentage of energy demands that can be dissipated into the environment compared to the total loads. This would make it possible to better model the case study taking into account the most recent improvement works that have been done on the system.

REFERENCES

- [1] D. Brem *et al.*, “ETH Zurich,” *Grants Regist. 2019*, pp. 309–309, 2018.
- [2] I. Dincer, “Renewable energy and sustainable development: a crucial review,” *Renew. Sustain. Energy Rev.*, vol. 4, no. 1, pp. 157–175, 2000.
- [3] I. Dincer, M. A. Rosen, and P. Ahmadi, *Optimization of Energy Systems*, John Wiley, 2017.
- [4] P. Pinel, C. A. Cruickshank, I. Beausoleil-Morrison, and A. Wills, “A review of available methods for seasonal storage of solar thermal energy in residential applications,” *Renew. Sustain. Energy Rev.*, vol. 15, no. 7, pp. 3341–3359, 2011.
- [5] P. Gabrielli, M. Gazzani, E. Martelli, and M. Mazzotti, “Optimal design of multi-energy systems with seasonal storage,” *Appl. Energy*, vol. 219, no. June 2017, pp. 408–424, 2018.
- [6] S. Pfenniger, “Dealing with multiple decades of hourly wind and PV time series in energy models: A comparison of methods to reduce time resolution and the planning implications of inter-annual variability,” *Appl. Energy*, vol. 197, pp. 1–13, 2017.
- [7] C. Weber and N. Shah, “Optimisation based design of a district energy system for an eco-town in the United Kingdom,” *Energy*, vol. 36, no. 2, pp. 1292–1308, 2011.
- [8] S. Bracco, G. Dentici, and S. Siri, “DESOD : A mathematical programming tool to optimally design a distributed energy system,” *Energy*, vol. 100, pp. 298–309, 2016.
- [9] K. H. Williamson, R. P. Gunderson, G. M. Hamblin, D. L. Gallup, and K. Kitz, “Geothermal Power: Technology Brief,” *Proc. IEEE*, vol. 89, no. December, pp. 111–113, 2001.
- [10] F. Battistini, “Studio di fattibilità di un impianto di riscaldamento geotermico per un edificio pubblico e considerazioni economiche,” 2011.
- [11] J. W. Lund and T. L. Boyd, “Direct Utilization of Geothermal Energy 2015 Worldwide Review,” *Proc. World Geotherm. Congr.*, no. April, pp. 19–25, 2015.
- [12] D. Connolly, H. Lund, B. V. Mathiesen, and M. Leahy, “A review of computer tools for analysing the integration of renewable energy into various energy systems,” *Appl. Energy*, vol. 87, no. 4, pp. 1059–1082, 2010.
- [13] A. Alarcon-Rodriguez, G. Ault, and S. Galloway, “Multi-objective planning of distributed energy resources: A review of the state-of-the-art,” *Renew. Sustain. Energy Rev.*, vol. 14, no. 5, pp. 1353–1366, 2010.
- [14] P. Mancarella, “MES (multi-energy systems): An overview of concepts and evaluation models,” *Energy*, vol. 65, pp. 1–17, 2014.
- [15] J. Allegrini, V. Dorer, G. Mavromatidis, F. Ruesch, R. Evins, and K. Orehounig, “A review of modelling approaches and tools for the simulation of district-scale energy systems,” *Renew. Sustain. Energy Rev.*, vol. 52, pp. 1391–1404, 2015.
- [16] C. Elsido, A. Bischi, P. Silva, and E. Martelli, “Two-stage MINLP algorithm for the optimal synthesis and design of networks of CHP units,” *Energy*, vol. 121, pp. 403–426, 2017.
- [17] A. D. Hawkes and M. A. Leach, “Modelling high level system design and unit commitment for a microgrid,” *Appl. Energy*, vol. 86, no. 7–8, pp. 1253–1265, 2009.
- [18] P. Ahmadi, M. A. Rosen, and I. Dincer, “Multi-objective exergy-based optimization

- of a polygeneration energy system using an evolutionary algorithm,” *Energy*, vol. 46, no. 1, pp. 21–31, 2012.
- [19] E. D. Mehleri, H. Sarimveis, N. C. Markatos, and L. G. Papageorgiou, “A mathematical programming approach for optimal design of distributed energy systems at the neighbourhood level,” *Energy*, vol. 44, no. 1, pp. 96–104, 2012.
- [20] S. Bracco, G. Dentici, and S. Siri, “Economic and environmental optimization model for the design andthe operation of a combined heat and power distributed generation system in an urban area,” *Energy*, vol. 55, pp. 1014–1024, 2013.
- [21] P. Gabrielli, M. Gazzani, E. Martelli, and M. Mazzotti, “Optimal design of multi-energy systems with seasonal storage,” *Appl. Energy*, vol. 219, no. October 2017, pp. 408–424, 2018.
- [22] S.P. Lloyd, “Least squares quantization in {PCM}. Special issue on quantization,” *IEEE Trans. Inf. Theory*, vol. 28, no. 2, pp. 129–137, 1982.
- [23] MathWorks Inc., “Image Processing Toolbox™ User ’ s Guide R 2015 a,” 2015.
- [24] M. Yliruka, “Modelling and simulation of the Anergy Grid.” Research Project Report ETH Zurich, pp. 1–14, 2018.
- [25] F. You and L. Bounds, “McCormick envelopes Derivation for bilinear term Obtaining Upper and Lower Bounds Example : Convex Relaxation.” pp. 1–4, 2018.
- [26] C. Metz, “Optimization of a multi-node geothermal storage system for decarbonizing multi-energy systems.” Research Project Report ETH Zurich, pp. 1–14, 2019.
- [27] “The energy of tomorrow: Energy concept Anergy Grid ETH Hönggerberg,” *ETH Real Estate Manag.*, 2018.
- [28] M. Groissböck, N. DeForest, C. Marnay, G. Cardoso, M. Stadler, and D. Steen, “Modeling of thermal storage systems in MILP distributed energy resource models,” *Appl. Energy*, vol. 137, pp. 782–792, 2014.
- [29] A. Huber, H. E. Ag, and H. E. Ag, “Software Manual Program EWS Calculation of Borehole Heat Exchangers,” no. October, 2008.
- [30] S. Miglani, K. Orehounig, and J. Carmeliet, “Integrating a thermal model of ground source heat pumps and solar regeneration within building energy system optimization,” *Appl. Energy*, vol. 218, no. March, pp. 78–94, 2018.
- [31] J. Bisschop, *AIMMS Optimization Modeling*. 2015.
- [32] A. Messmer and R. Frischknecht, “Umweltbilanz Strommix Schweiz 2014 Bundesamtes für Umwelt (BAFU),” vol. 3, 2016.
- [33] R. Dutch, “Sustainability report,” 2016.
- [34] H. W. Seifert, M. Mast, and W. Seifert, “ETH Zürich - Hönggerberg Monitoring Energiekonzept Impressum,” 2017.

APPENDIX:

The reference profile of ambient temperature T^{air} used in this work as input data is reported in Figure 6.1.

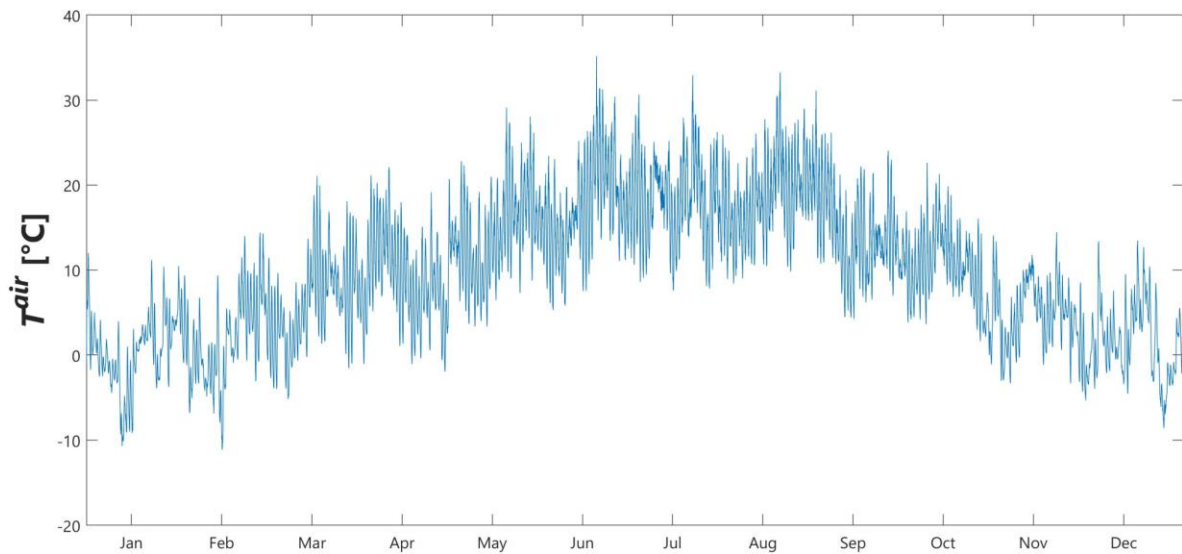


Figure 6.1: Ambient temperature profile